Oncogenic KSHV induces ALT to facilitate break-induced viral genome replication

Timothy P. Lippert

Thesis submission for:

Doctor of Philosophy in Clinical Sciences

Department of Haematology

Imperial College London

October 2019

Supervisors:

Dr Niklas Feldhahn
Department of Haematology
Imperial College London

Prof. Paul Farrell
Section of Virology
Imperial College London

Submission date:

31st October 2019

This work is dedicated to Freda Gladys Newcombe.

I hope she would have liked it.

DECLARATION

I, Timothy P. Lippert hereby confirm that this work is my own. Any text or data from other sources is referenced appropriately.

ACKNOWLEDGMENTS

I would like to thank Dr Niklas Feldhahn for accepting me in his lab and allowing me to continue the work which was started under Dr Grzegorz Sarek initially. Thank you for letting me participate in the Ssb project, although there was obviously some ups and downs working on this, I think we also had some really nice moment scientific curiosity and discovery together when discussing this work. Thank you for your mentorship throughout my time in Dept. Haematology.

I would like to thank Prof. Paul Farrell for his support and guidance. Your pragmatism and continuous, constructive challenge of the work has kept me on my toes. Also, thank you for teaching me many things about Epstein-Barr virus in the conversations we had while I was at St. Mary's especially.

I would like to thank Prof. Païvi Ojala. You were an incredible teacher to me and I learnt a lot about KSHV from you in our meetings. Also thank you for the invitation to Helsinki last year and sharing so many reagents with us over the years. You were essential for the success of this work.

I would like to thank Prof. Simon Boulton for the continued support and allowing me to finish the project at the laboratory in Francis Crick Institute. Your group is amazing, most of what I know about DNA damage responses and telomeres is from discussion with the many exceptionally talented people working in your lab on really cool things. I am excited to be part of this in the next year until we are finished with this work.

I would like to thank Dr Paulina Marzec for generous support and amazing collaborative work. You have been a great colleague in the lab and have taught me many techniques. I am truly thankful for that.

I would like to thank Prof. Mark Bower for providing us with such an exceptional collection of KS cases for the study and putting our work into clinical context in our meetings. Also thanks to Dr Alessia dalla Pria in this context.

I would like to thank Prof. Kikkeri Naresh for proving us with the PEL TMA. The ongoing collaboration with Mohamed and you has been stimulating.

I would like to thank Dr Grzegorz Sarek for recruiting me onto the project and sparking in me excitement for ambitious science.

I would like to thank Prof. Anastasios Karadimitris for being a true scientist and many nice discussions during my time at Dept. Haematology.

I would like to thank Dr Dirk Dorman, Mr Chad Whilding, Dr Donald Bell, and Dr Mark Renshaw for advice and help concerning microscopy.

I would like to thank Dr Rob White for ongoing collaboration and helpful discussion on EBV.

I would like to thank all colleagues in the Boulton group as well as Dept. Haematology and Section of Virology for stimulating discussions and advice along the way. I am grateful for especially interesting and ambitious scientific discussions with Dr Mark Robinson, Mr. Ondrej Belan, Mr. Jordan James, Dr Tohru Takai, and Dr Roopesh Anand.

Thanks to Nina for everything. None of this would have been possible without your support and love.

Most importantly, thanks to my loving family for always being there and believing in me.

ABBREVIATIONS

3C `	Chromosome conformation capture
AIDS	Acquired immunodeficiency syndrome
ALT	Alternative lengthening of telomeres
AP	Alkaline phosphatase
APB	ALT-associated PML body
ASF1A	Anti-Silencing Function 1A Histone Chaperone
ATM	Ataxia Telangiectasia Mutated
ATRX	Alpha Thalassemia/Mental Retardation Syndrome X-Linked
BIR	Break-induced replication
BLM	Bloom syndrome RecQ-like helicase
BrdU	5-bromo-2'-deoxyuridine
BSA	Bovine serum albumin
ChIP	Chromatin immunoprecipitation
CHOP	Cyclophosphamide, Hydroxydaunorubicin, Oncovin, Prednisone
CO-FISH	Chromosome-orientation FISH
cDNA	complementary DNA
cNHEJ	Classical non-homologous end-joining
d-loop	Displacement loop
DAPI	4′,6-diamidino-2-phenylindole
DDR	DNA damage response
DLBCL	Diffuse large B-cell lymphoma
dHJ	Double holiday junction
DNA	Deoxyribonucleic acid
dNTP	Nucleoside triphosphate
dsDNA	Double-stranded DNA
DTT	Dithiothreitol
EBV	Epstein-Barr virus

EDTA	Ethylenediaminetetraacetic acid
EdU	5-Ethynyl-2'-deoxyuridine
EGTA	Ethylene glycol tetra-acetic acid
EM	Electron microscopy
EMT	Endothelial to mesenchymal transition
FISH	Fluorescence *in situ* hybridisation
gDNA	genomic DNA
GFP	Green fluorescent protein
HCl	Hydrochloric acid
HIV	Human immunodeficiency virus
HR	Homologous recombination
HUVEC	Human umbilical vein endothelial cells
IHC	Immunohistochemistry
IP	Immunoprecipitation
IR	Ionising radiation
kb	kilobase
KCl	Potassium chloride
KS	Kaposi's sarcoma
KSHV	Kaposi's sarcoma herpesvirus
LANA	Latency-associated nuclear antigen
LCL	Lymphoblastoid cell line
LEC	Lymphatic endothelial cell
MCD	Multicentric Castleman's disease
MIP	Maximum intensity projection
miRNA	microRNA
MMEJ	Microhomology-mediated end-joining
mRNA	messenger RNA
MSM	Men who have sex with men
NaCl	Sodium chloride
NaOH	Sodium hydroxide

NHEJ	Non-homologous end-joining
NHL	Non-Hodgin's lymphoma
PAGE	Polyacrylamide gel elctrophoresis
PBS	Phosphate buffered saline
PCR	Polymerase chain reaction
PEL	Primary effusion lymphoma
PICh	Proteomics of isolated chromatin fragments
PNA	Peptide nucleic acid
PRC	Polycomb repressive complex
PolD3	DNA polymerase Δ3, accessory subunit
qFISH	Quantitative FISH
qPCR	Quantitative PCR
RAD51C	RAD51 paralogue C
RAD52	RAD52 homolog, DNA repair protein
RAP1	TRF2 interacting protein
RBC	Red blood cell
RNA	Ribonucleic acid
RNAi	RNA interference
RPA	Replication Protein A
RT-qPCR	Reverse transcription qPCR
scr	scrambled sequence
SDS	Sodium dodecyl sulfate
SDSA	Synthesis-dependent strand annealing
siRNA	small interfering RNA
SLX4	SLX4 structure-specific endonuclease subunit
ssDNA	Single-stranded DNA
SSA	Single-strand annealing
STORM	Stochastic optical reconstruction microscopy
STR	Short tandem repeat
siRNA	small interfering RNA

SSC	Saline-sodium citrate buffer
ssDNA	single-stranded DNA
T-SCE	Telomere sister-chromatid exchange
TBS	Tris buffered saline
TDP1	Tyrosyl-DNA Phosphodiesterase 1
TERRA	Telomere repeat-containing RNA
TIN2	TRF1 interacting nuclear factor 2
TPP1	Tripeptidyl peptidase 1
TR	Terminal repeat
TRAP	Telomere repeat amplification protocol
TRF	Telomere restriction fragment
TRF1/2	Telomere repeat binding factor 1/2
TRIS	Tris(hydroxymethyl) aminomethane
UV	Ultraviolet

LIST OF FIGURES

LIST OF TABLES

TABLE OF CONTENTS

ABSTRACT

Infection with Kaposi's Sarcoma herpesvirus (KSHV) has been linked to multiple cancers including Kaposi's sarcoma (KS), Primary effusion lymphoma (PEL), and Multicentric Castleman's disease (MCD). One of the hallmarks of transformed cancer cells is the activity of telomere maintenance mechanisms. The present study uncovers the onset of Alternative lengthening of telomeres (ALT) in response to KSHV infection from a proteomic screen of telomere-associated DNA damage response proteins by Proteomics of isolated chromatin fragments (PICh). In several initially telomerase$^+$ cell lines, features of ALT activation are present in response to KSHV infection including increased telomere sister-chromatid exchanges, C-circles, telomere clustering in interphase, ALT-associated proteins at telomere clusters, and telomere fragility. Binding of shelterin to telomeric DNA was increased upon infection with KSHV. Interestingly, cells which are latently infected with KSHV are dependent on ALT factors for their efficient proliferation in clonogenic assays and such factors may be essential for the maintenance of viral episomes in infected cells as shown by episome qPCR. Moreover, preliminary experiments by ChIP indicate an increase in heterochromatin marks at telomeres upon infection, similar to the marks documented on the KSHV episome. Analysis of primary tumour material from 8 KS and 7 PEL patients suggests that this not limited to the *in vitro* systems considered in this study. Taken together, this work demonstrates for the first time the capability of latent KSHV to trigger telomere maintenance via ALT and suggests a model in which KSHV episomes are replicated in tandem with telomeres by BIR in such cells. This provides a unique susceptibility of KSHV infected cancer cells to inhibition of ALT, which may be utilized for the trial of future treatment for KSHV-associated cancers.

INTRODUCTION

The experiments performed in this thesis are concerned with the study of telomeric chromatin in response to latent infection with oncogenic virus KSHV. Specifically, the work aims to address the hypothesis whether telomeres in KSHV-infected cells are elongated using a specialized telomere maintenance mechanism called ALT. This mechanism is based on carefully regulated activity of DNA damage response proteins at telomeres. I therefore start this thesis with a thorough introduction to key concepts, which will be covered in subsequent description of results and discussion thereof. The first section gives an overview of the key DNA repair pathways, which may be activated at the end of chromosomes, telomeres. In the interest of brevity, it does not aim to give information on the whole field of cellular responses to DNA damage and focusses on studies of double-strand break repair in human cells unless indicated otherwise. This is followed by an introduction to telomeres, how they usually inhibit the DNA damage response, and mechanisms of telomere maintenance. Special attention will be given to the molecular mechanism of ALT and how it is induced. Next, KSHV is introduced. Specifically, the viral life cycle, its clinical relevance, and published interactions with double-strand break repair proteins and host telomeres. The description of the virus life cycle will place additional focus on the mechanism of viral genome replication since this will be of particular relevance in the discussion of the results generated during the course of this work. Finally, the principle aims of the thesis are briefly summarised.

DNA double-strand breaks (dsDNA breaks)

The integrity of DNA, which makes up the human genome, is under challenge throughout the life span of every cell in our body. Even without additional insult, cells face a significant amount of endogenous DNA damage including approximately 10^5 oxidative lesions/day[1], more than 20,000 single-strand breaks/day[2], and 10-50 double-strand breaks per division[3,4]. The incidence of DNA damage is drastically higher when cells are subjected to genotoxic stress such as UV light, IR, or chemotherapy. DNA damage may result in genomic instability by loss or rearrangement of genetic material and this is a potential driver of malignant transformation if it confers cells with a proliferative advantage. In light of this danger, human cells have evolved mechanisms of DNA repair which are directed specifically to the site and type of DNA damage. The proteins involved in these repair pathways are collectively known as the DNA damage response.

Double-strand breaks present perhaps the most significant form of DNA damage. They arise endogenously upon chromosome breakage, replication fork collapse, and telomere deprotection[5]. In addition to this, somatic processes involve co-ordinated dsDNA breakage and re-joining by ds break repair pathways. Specifically, the dsDNA break response is used to generate combinatorial diversity of antigen and T-cell receptors during V(D)J recombination[6,7] in immature B- and T-lymphocytes, and functional diversity of secreted antibodies during class switch recombination[8] in mature B-lymphocytes. Double-strand breaks also occur upon genotoxic stress. Some processes cause dsDNA breaks *per se* such as ionising radiation, radiomimetic drugs[9] and topoisomerase inhibitors like etoposide[10]. Others generate DS breaks mainly by degeneration of other DNA lesions. For example, this occurs upon cisplatin treatment via replication fork collapse[11] or UV damage via endonuclease cleavage[12]. Taken together, dsDNA breaks in human cells may arise through normal cellular processes, accidental exposure or various cancer therapies.

Recognition of dsDNA breaks by the DDR

DDR signalling occurs through an extensive phosphorylation cascade, which results in expression, nuclear localization and modification of enzymes capable of triggering cell cycle arrest, apoptosis and DNA repair. Proteins involved in double-strand break repair are codsDNAmmonly inactivated by mutation in cancer cells and this contributes greatly to their genomic instability. In addition to this, cancer cells need to rely on backup ds break repair pathways (described below), which are more mutagenic and render them susceptible to genotoxic treatment such as chemotherapy. There are two main kinases which are responsible for the onset of the cascade in response to dsDNA breaks: DNAPk and ATM[13]. In addition to this, ATR contributes to signalling upon dsDNA break detection, although its main role is the initiation of the response to ssDNA breaks. Generally, the outcome of DDR signalling is dependent on the number and nature of dsDNA breaks[14], cell type[15], cell cycle stage[16,17], and genetic background[18] (possible outcomes summarised in Figure 1).

One effect of DDR signalling in response to dsDNA breaks is cell cycle arrest. Both activated DNAPk[19] and ATM[20] phosphorylate kinase Chk2 *in vivo* which induces its dimerization, extensive autophosphorylation, and activation[21]. Subsequently, downstream effectors are phosphorylated to induce arrest depending on cell cycle progression at the time of DNA damage. Activated Chk2 may signal for G1/S arrest via a P-Cdc25A, Cdk2 axis[22]. In addition to this, G2/M arrest may be triggered via sustained p-Cdc25C, and dephosphorylated Cdk1 [20,23]. Interestingly, it has been shown that Chk1 may also be activated by DNAPk[24] and ATM[25] which may provide another signal for G1/S or G2/M arrest in analogy to Chk2 activation. In addition to this, it is thought that DNAPk- or ATM-mediated stabilization of p53 and subsequent induction of p21 contributes to sustained cell cycle arrest[26,27] As a summary, activation of either DNAPk or ATM may signal for cell cycle arrest in response to dsDNA breaks by inhibition of Cdk1/2 through a signalling cascade

mediated by p-Chk1/2. This arrest is thought to serve as a pause, which allows DNA repair to take place efficiently.

If dsDNA breaks are too numerous or DNA repair fails despite cell cycle arrest, apoptosis may be triggered to prevent the propagation of cells with damaged DNA. Once phosphorylated, DNAPk, ATM and Chk2 are all capable of p53 activation[28,29]. In addition to this, both DNAPk and ATM may inactivate MDM2, the key inhibitor of p53 activity[30–32]. Apoptosis signalling via p53 may occur via multiple effectors. For example, active p53 induces transcription of pro-apoptotic proteins PUMA[33,34] and NOXA[35,36]. Taken together, detection of dsDNA breaks may trigger apoptosis via p53 signalling in protection of genomic integrity under circumstances where damage persists and repair has failed.

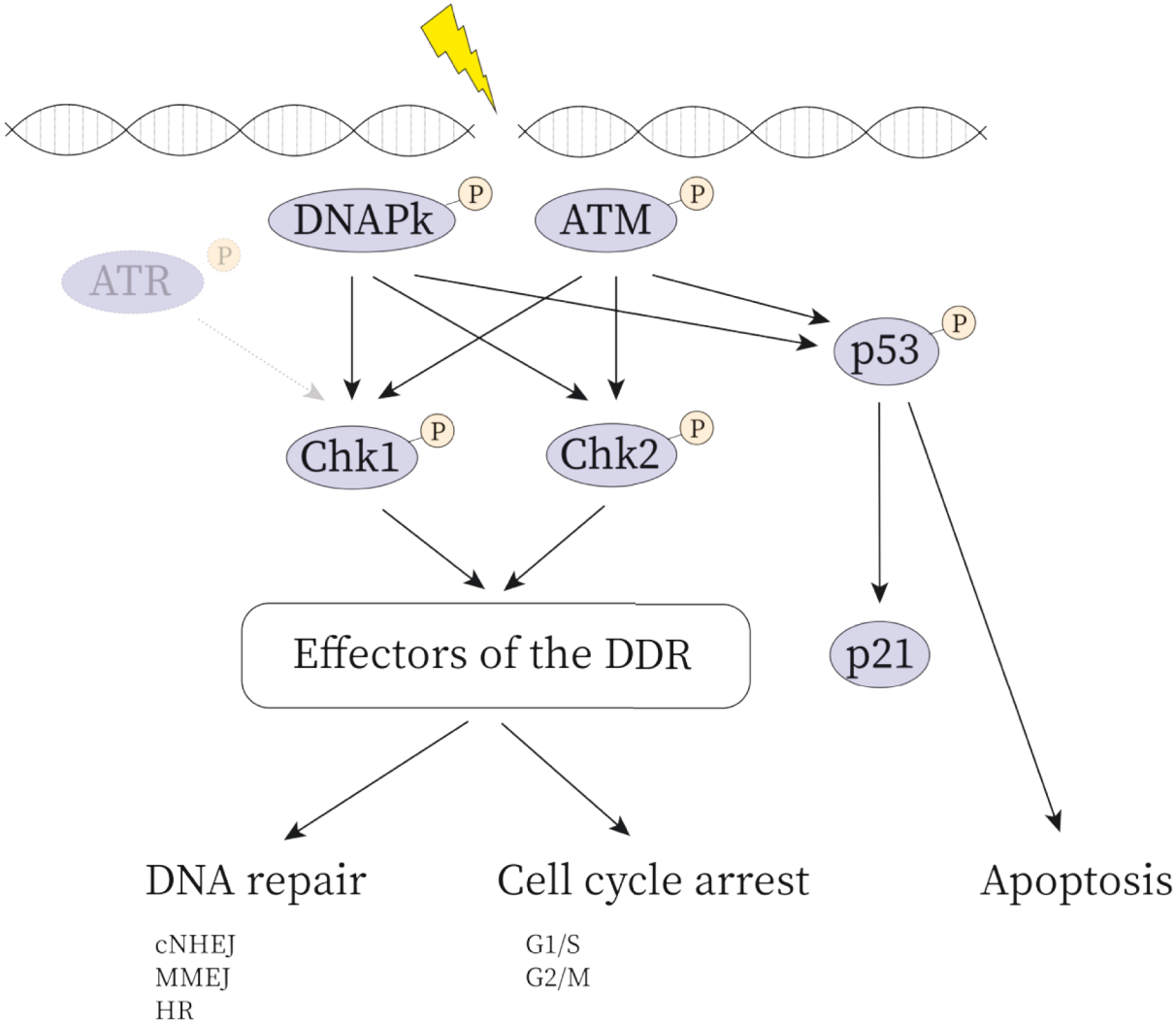

Figure 1: Possible outcomes of DDR signalling. Upon DNA double strand breakage, the cell may sense damage and trigger a phosphorylation cascade with considerable redundancy which may result in DNA repair, cell cycle arrest, or apoptosis of the cell exhibiting the damage.

Classical non-homologous end-joining (cNHEJ)

The default cellular response to repair of double-strand breaks with two blunt ends is cNHEJ[37] (Figure 2). It is predominantly used to repair dsDNA breaks during G1 phase of the cell cycle where no template for HR is present. It may also be active at dsDNA breaks in S and G2 phase[38], but not during mitosis[39]. In the first step of cNHEJ, each DNA end is bound by a single Ku70/Ku80 heterodimer[40,41]. Ku70/Ku80 then recruits numerous molecules of DNAPk which are activated by autophosphorylation[42,43]. Activated DNAPk then triggers an extensive signalling cascade and phosphorylates, amongst many others, double-strand break marker γH2AX[44]. Subsequently, recruitment of a scaffold consisting of XRCC4/Lig4[45], XLF/PAXX[46,47], and APLF[48] takes place between the Ku70/Ku80-capped ends. This likely serves as a means of bringing two ends into close proximity for efficient ligation[49]. APLF may also be the histone chaperone responsible for H2AX recruitment prior to phosphorylation by DNAPk and ATM[50]. Ligation of the double strand break is catalysed by Lig4[6]. Recent studies suggest that ligation is dependent on end-processing mediated by Artemis[51,52], PNKP[53], and TDP1[54]. This end processing prior to end joining. is one of the main factors which contribute to small nuclelotide insertions which have been documented at sites of cNHEJ[55]. In general, a pre-requisite for cNHEJ is inhibition of end resection and proteins which inhibit resection are crucial for pathway choice towards cNHEJ. This includes inhibition of resection by Ku70/Ku80[56] and 53bp1-RIF1 binding to free dsDNA break ends[57]. In summary, cNHEJ is a pathway, which can efficiently join together two blunt ends at a dsDNA break and involves a multistep process of detection, synapsis, and ligation (Figure 2).

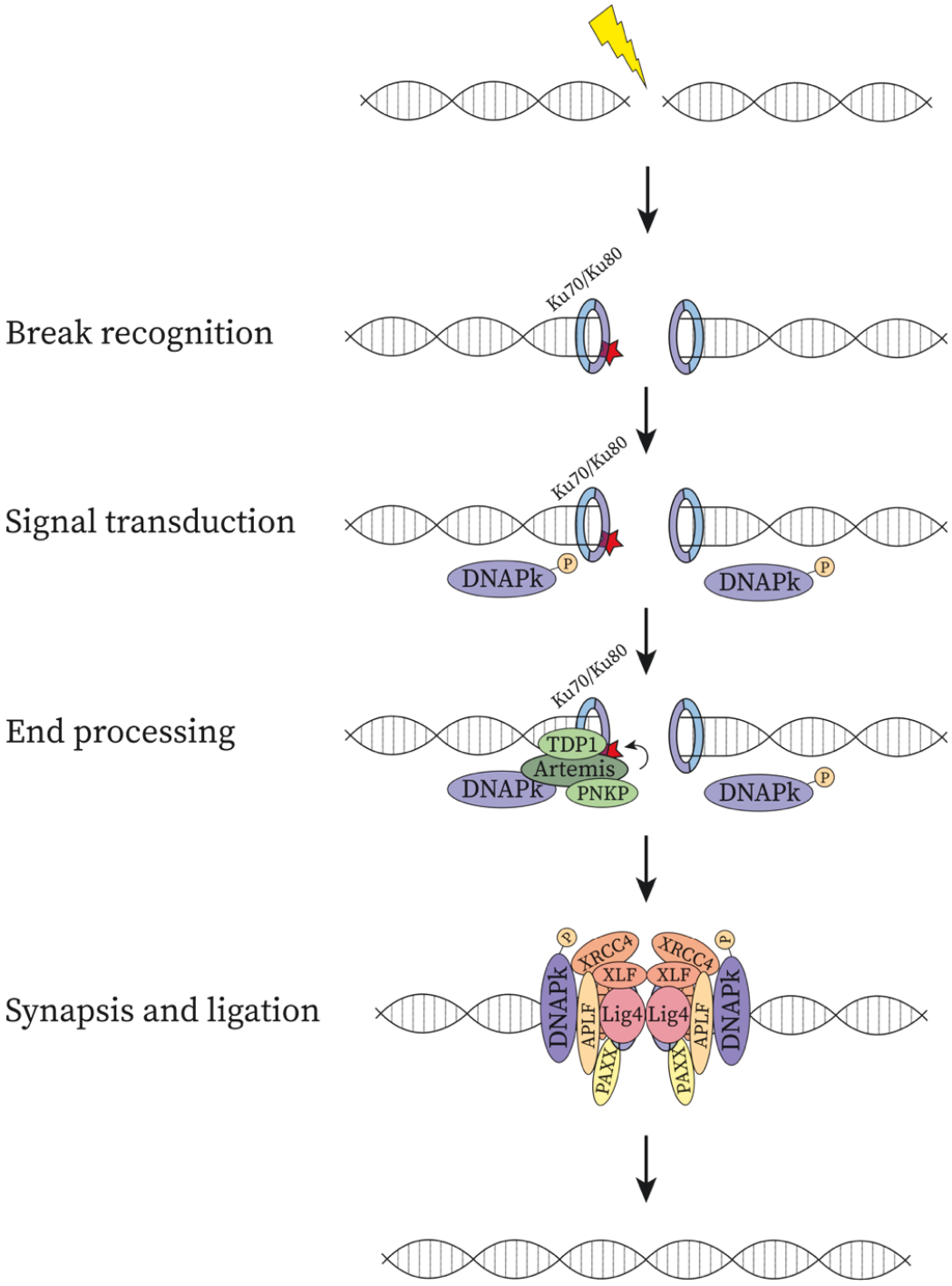

Figure 2: The mechanism of cNHEJ. Ku70/Ku80 recognise free double-strand DNA ends and trigger the recruitment and activation of DNAPk. This in turn allows the action of various end-processing enzymes such as Artemis which are essential for the ligation of the free ends. This is then mediated by the formation of a synapsis which brings the ends into close proximity to each other and ultimately ligation is carried out by Lig4 in complex with a number of co-factors.

Homologous recombination (HR)

HR involves a homologous dsDNA template corresponding to the region of the dsDNA break and is therefore restricted to S/G2 phase[58]. In contrast to cNHEJ, initial detection of free DNA ends is dependent on binding of the MRN complex consisting of Mre11, RAD50, and NBS1 (Figure 3). This complex is capable of displacing bound Ku70/Ku80[59]. MRN complex recruits ATM kinase to the break site via interaction with the C-terminal domain of NBS1[60,61]. This in turn stimulates ATM autophosphorylation and activity as well as phosphorylation of downstream effectors[62] as well as H2AX[63]. HR at double-strand breaks is crucially dependent on DNA end resection. This is also mediated by MRN. First, MRE11 introduces a SS nick in the duplex upstream of the dsDNA break[64] and recruits CtIP[65]. Both MRE11 itself and CtIP have 3' to 5' exonuclease activity and together generate a small SS gap.[66] This is then used to initiate full-blown resection up to the break site mediated by exonucleases Exo1, DNA2, and unwinding of the duplex by BLM helicase[67]. Together, these enzymes generate the 3' SS overhang which is essential for HR.

The resulting ssDNA is quickly bound by RPA heterotrimers which protects the ss end from interaction with other molecules[68]. Displacement of RPA is mediated by BRCA2[69] which, in complex with BRCA1-BARD1, competes for binding to the ss end[70]. In addition to this, BRCA2 also interacts with RAD51[71] and induces RAD51 deposition onto ssDNA, replacing RPA. The RAD51 filament mediates strand invasion into the homologous dsDNA template and this reaction is again facilitated by BRCA1-BARD1[72]. If sufficient base-pairing with the complementary strand is achieved, this results in the formation of a triplex DNA structure termed d-loop. This invasion may initiate different pathways of HR-dependent DNA synthesis (Figure 3). One of these is synthesis-dependent strand annealing (SDSA) in which one resected end of the dsDNA break invades a complementary duplex and is extended by Polδ[73]. Synthesis proceeds past the break site until the d-loop is disrupted. This disruption and subsequent dissolution of the d-loop is the trigger for SDSA and is mediated by helicases such as BLM[74] ,WRN[75], and RTEL1[76,77] as well as

Top3-Rmi complex[78] and FANCM[79]. Finally, there is a synthesis step, which fills in the resulting SS gap and therefore completes repair by SDSA. Another possibility is the formation of a double Holiday junction. This occurs by RAD51-mediated invasion of one resected end into the complimentary duplex, annealing of the other resected end with the ssDNA of the template, which arises from d-loop formation, and synthesis of a complementary strand (Figure 3). The resulting double Holliday junction is finally resolved either by BLM-Top3-Rmi1 complex or via nucleolytic cleavage by SLX4-SLX1[80] or Mus81-EME1/2[81,82] Resolution of this recombination intermediate may result in a crossing-over event at the site of the double-strand break if it occurs by endonuclease cleavage.

There are two other mechanisms of HR-mediated repair, which occur rarely at dsDNA breaks. The first one of these is single-strand annealing (SSA). In this pathway, RAD52 replaces RPA on the resected ssDNA end and mediates formation of a modified RAD51 filament which contains some RAD52[83,84]. In the context of SSA, strand annealing occurs between the two resected ends directly by XPF/ERCC1-dependent[85] flap removal and ligation (Figure 3). The polymerase and ligase involved in fill-in synthesis and completion of SSA respectively are not characterised to date[86]. Overall, SSA results in deletions and mutagenesis at the break site. The second pathway in this context is BIR. In this reaction, invasion of one resected end into the complementary duplex results in a d-loop as in SDSA or dHJ-mediated repair. However, in this process the d-loop replication bubble migrates unidirectionally and this can result in long extension of the invading ssDNA (Figure 3). This process is especially important in the context of collapsed replication forks[87]. The mechanism of BIR is described later in greater detail in the section on ALT telomere maintenance. In summary, HR encompasses a number of sub-pathways, which involve the generation of a resected, RPA coated ssDNA end intermediate and invasion of this end into a complementary dsDNA duplex. HR pathways are generally considered error-free, with the exception of SSA, since they allow accurate reproduction of nucleotide sequence from a homologous template.

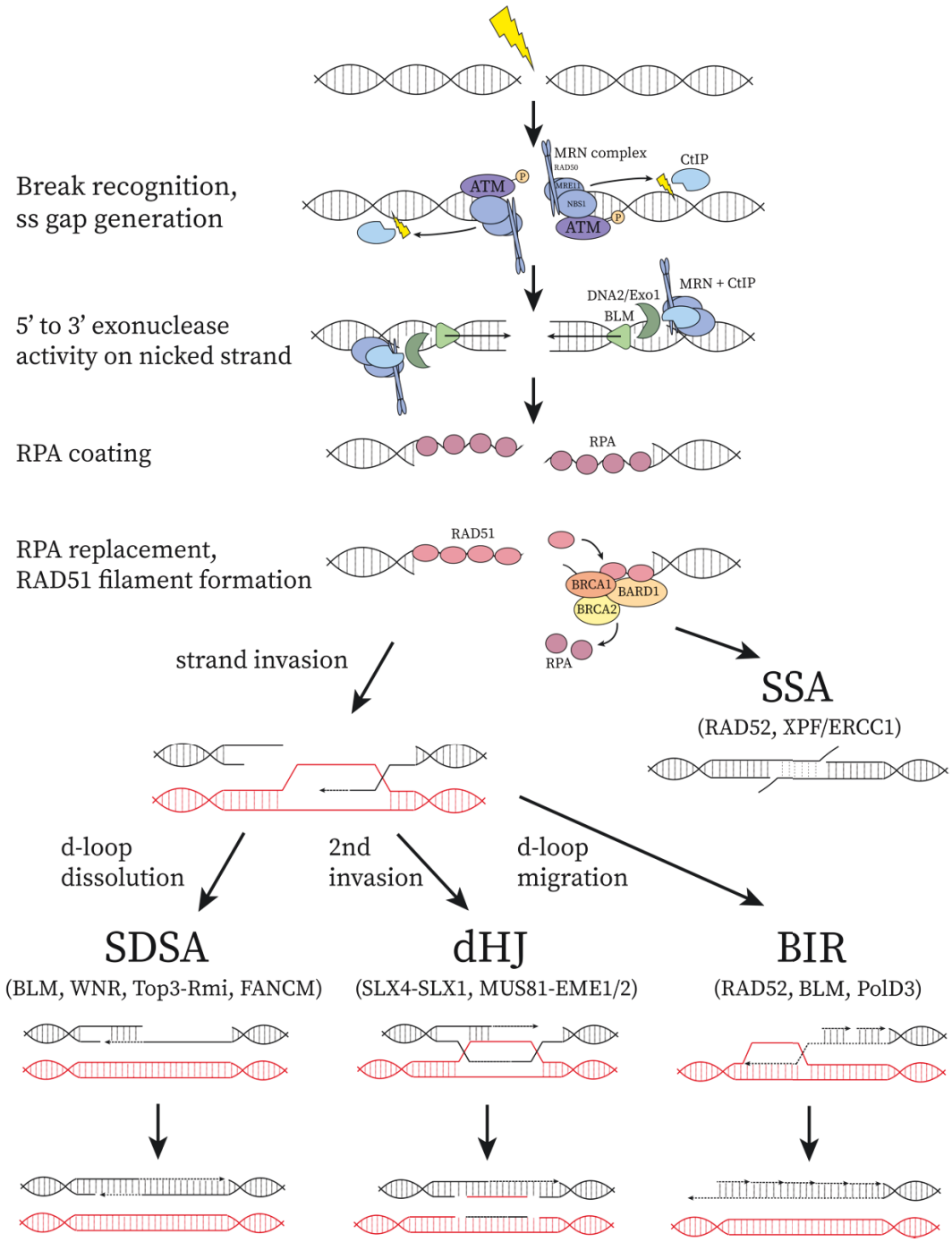

Figure 3: The mechanism of HR. MRN complex detects free dsDNA ends and this is accompanied by ATM activation and phosphorylation which triggers DDR signalling. MRN in complex with CtIP introduces a ss nick upstream of the break site which initiates resection and ss overhang generation by Exo1/DNA2 and BLM helicase. This is first coated with RPA which subsequently is replaced with RAD51 by the action of BRCA1/2 and BARD1. The resulting ss overhang is capable of invasion of a complementary duplex to form a d-loop which may trigger SDSA, dHJ formation, BIR, or SSA depending on several proteins (see text for details).

Microhomology-mediated end-joining (MMEJ)

Another dsDNA break repair pathway dependent on resection is MMEJ. Mechanistically, this pathway relies on the same machinery as HR to generate a resected ssDNA end coated by RPA catalysed by MRN complex, CtIP, Exo1/DN2, and BLM as described. Importantly, MMEJ is dependent on binding of PARP1 to dsDNA ends, which competes with Ku70/Ku80 and recruits MRN to the break site[88,89]. In contrast to HR, MMEJ does not require strand invasion into a complementary duplex and is therefore also potentially active outside of G2/S phase, analogous to cNHEJ. The key player of MMEJ repair is Polθ. This protein mediates annealing of elongated, resected ends and inhibits RAD51 binding and therefore HR[90]. In addition to this, Polθ-mediated DNA synthesis at the annealed portion of the resected ends stabilizes the bridging across the dsDNA break based on microhomology[91]. Finally, fill-in synthesis by an unknown factor, flap trimming by XPF/ERCC1[92] and ligation by Lig1 or Lig3[93,94] completes repair (Figure 4). The nature of resected ssDNA end pairing based on microhomology results in mutagenesis at the breakpoint (i.e. extended nucleotide sequence loss), an established feature of MMEJ. Generally, MMEJ is considered a backup end-joining pathway for cNHEJ and is more mutagenic. Cancer cells with inactivating mutations in cNHEJ often rely on MMEJ and this contributes to their genomic instability and susceptibility to chemotherapy.

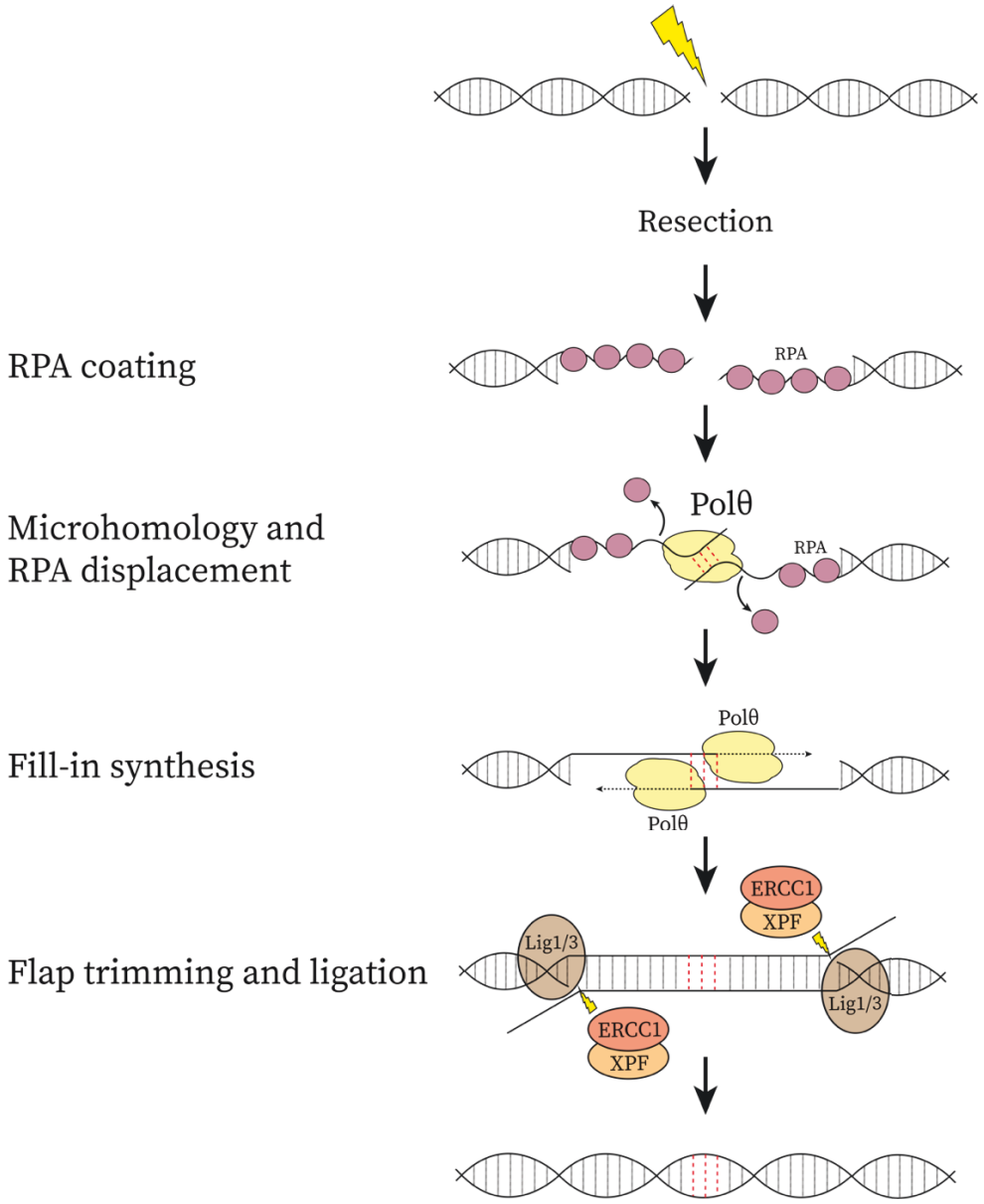

Figure 4: The mechanism of MMEJ. Repair proceed post-resection by replacement of RPA from ssDNA ends by Polθ. This enzyme then mediates annealing of ssDNA ends based on microhomology and subsequently performs fill-in synthesis in a bidirectional manner. Finally, resulting flaps are trimmed by ERCC1/XPF and any remaining ss gaps are repaired by ligation via Ligase 1 or 3. Resulting repaired region lacks sequences due to microhomology annealing.

The human telomere, a constitutive dsDNA break

The human genome is made up of linear pieces of DNA, the ends of which are in theory identical with DNA breaks. Usually, such breaks trigger cell cycle arrest through checkpoint activation and DNA repair or apoptosis by the DDR as discussed. In a sense, telomeres are the only double-strand breaks that persist throughout many cell cycles without detrimental consequences. This is achieved by tight interaction with many DDR proteins, resulting in modulation of all major DNA repair pathways. Defects in the regulation of the DDR at telomeres result in genomic instability or cell death. Another key feature of telomeres, which greatly impacts on their functionality, is the length of telomeric DNA. This is especially modulated in cancer and involves interaction with DDR proteins in the case of ALT telomere maintenance. The following section describes these phenomena in detail.

The molecular structure of telomeres inhibits DDR activation

The human telomere is comprised of a 5-15kb TTAGGG repeat sequence at chromosome ends. This is paired with a complementary C-rich, hexameric repeat to form a duplex for all but the final 50-400 nucleotides which make up a single stranded G-rich overhang. The main protein complex at human telomeres is called shelterin, as defined in seminal publications by Titia de Lange[95]. It is composed of TRF1, TRF2, TPP1, TIN2, RAP1, and POT1 (Figure 5). Both TRF1 and TRF2 bind directly to telomeric dsDNA with high affinity via their Myb/SANT domains[96]. In addition to this, POT1 is capable of binding directly to ss telomeric DNA via two OB-fold domains[97,98]. However, its affinity to telomeric ssDNA alone is not sufficient for its specific recruitment to telomeres[99]. Rather, POT1 is recruited to telomeres by interaction with TPP1[100]. Overall, human shelterin assembles at telomeres via the high affinity binding of TRF1 and TRF2 to the 5-15kb of telomeric repeat DNA at the end of chromosomes Together, this regulates many telomeric functions including formation of the t-loop, telomere replication/elongation, and interaction with the DDR.

Analysis of telomeric DNA by electron[101] and STORM super-resolution microscopy[102] revealed a lariat-like loop conformation termed t-loop. Further analysis showed that this takes place by invasion of the upstream duplex by the G-rich ssDNA overhang, which forms a d-loop (Figure 5). The t-loop and masking of the SS overhang by strand invasion are thought to be one of the main ways in which telomere structure inhibits DDR activation. In line with this, TRF2 has been shown to be a crucial for t-loop formation and TRF2 knockout leads to rapid chromosome end-to-end fusions by NHEJ[103,104]. Another challenge to t-loop formation is the fact that telomeres end in a blunt end or with a minimal 3' overhang after each round of DNA replication depending on strand orientation[105]. This indicates that there must be resection after telomere replication to generate the 50-400 nucleotide ssDNA overhang. Initial 5' to 3' exonuclease activity at the leading strand of telomeres may be performed by Apollo. This has been confirmed in mice[106,107] and is likely the case in humans based on a recorded telomeropathy due to Apollo mutation[108]. CtIP has been implicated as an exonuclease which contributes to G-overhang generation in human cell lines[109]. Interestingly, a notion of excessive resection followed by fill-in synthesis for effective generation of the overhang has been raised by several recent reports in mouse models[110–112]. Based on these reports, resection is followed and counteracted by fill-in synthesis. This is thought to occur by Cst binding to the ss overhang post-resection and synthesis of DNA by Polα/primase. Given that both Cst and Polα have a confirmed role in regulating G-overhang in human cell lines[113,114], it is sensible to suspect an orthologous mechanism in humans. Taken together, the formation of the t-loop is a multistep process, which is dependent on synthesis of a G-overhang mediated by a partially characterised set of DDR factors and upstream invasion of the duplex mediated by TRF2. Overall, this provides the first layer of protection by which telomeres are shielded from aberrant detection as a dsDNA break by the DDR.

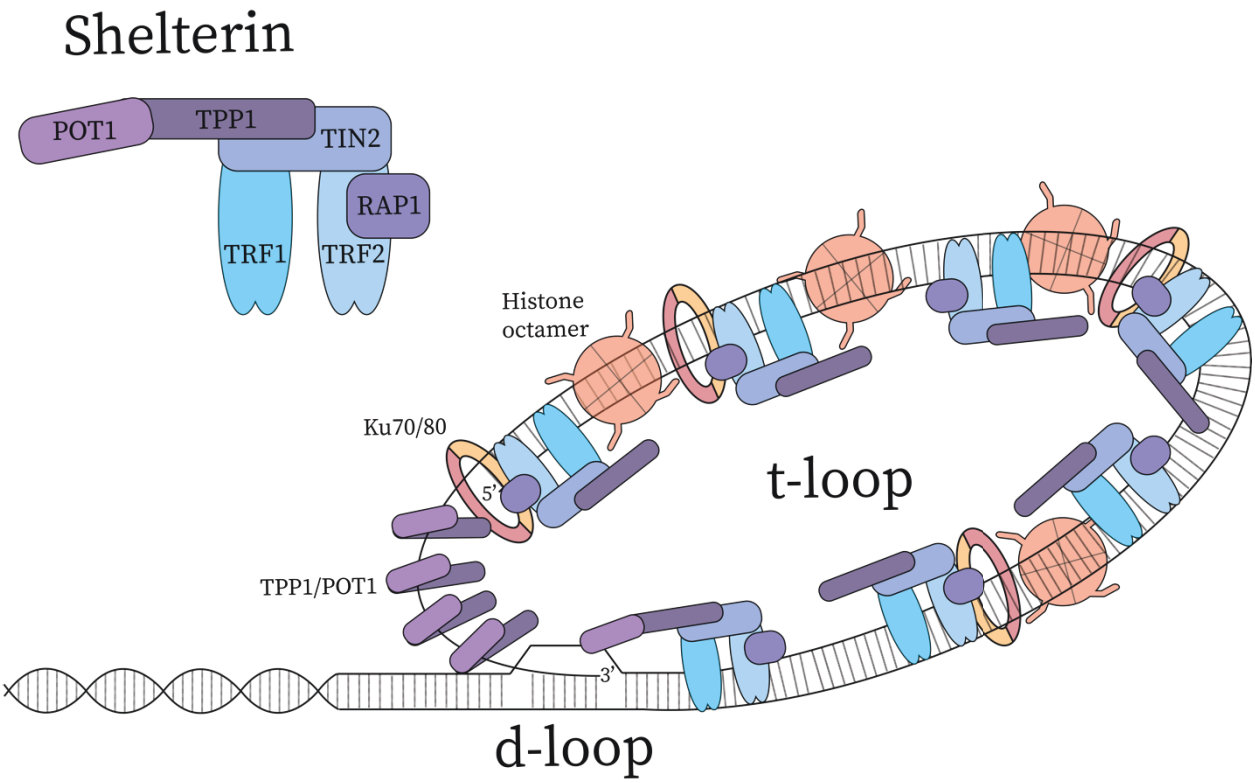

Figure 5: Overview of telomeric structure. Shelterin is the main telomere-associated complex and catalyses the formation of an overall t-loop structure. 3' overhang is generated by a yet incompletely characterised mechanism. POT1/TPP1 is thought to mediate invasion into the upstream duplex which leads to the formation of the d-loop. Other ubiquitously telomere-associated proteins include histone octamers which commonly show repressive post-translational modifications such as H3K9me3 as well as Ku70/Ku80 which in complex with TRF2 persists in a repressed form that shields telomeres from aberrant DDR activation.

In addition to this, shelterin proteins directly inhibit the DDR in a redundant manner. TRF2 directly inhibits recruitment of 53bp1, a crucial step in cNHEJ, via multiple domains[115]. Ku70/Ku80 is found constitutively bound to telomeres, seemingly at odds with cNHEJ repression. However, TRF2 interacts strongly with telomere-bound Ku70 α-helix 5 and prevents Ku70/Ku80 hetero-tetramerization necessary for cNHEJ[116]. RAP1 may also be involved in direct inhibition of cNHEJ based on its ability to ameliorate fusions observed upon TRF2 knockout[117] and its ability to bind Ku70 α-helix 5 via an uncharacterised domain[116]. TPP1-POT1 and/or TRF1 directly inhibit ATR-mediated DDR at the G-rich overhang or stalled replication forks at telomeres[118,119]. MMEJ is also inhibited at telomeres by TRF2 in

analogy to cNHEJ as well as via RNF8-TPP1 interaction[120]. In addition to this, HR is inhibited at telomeres. One key protein at telomeres which mediates this repression is Ku70 which is highlighted by increased HR at dysfunctional telomeres in Ku70 knockout cells[121,122]. Inhibition of HR at telomeres is especially important at the d-loop where nucleolytic resolution would lead to t-loop excision and loss. TRF2 basic domain directly inhibits XRCC3-dependent t-loop excision[123]. In summary, direct inhibition of the DDR is mediated by shelterin proteins as well as constitutive binding and inactivation of Ku70/Ku80 at telomeres.

Despite the redundant suppression of DDR signalling at telomeres, several factors involved in DNA repair pathways are utilized for telomere maintenance. For example, TRF2-mediated recruitment of RTEL1 helicase is crucial for t-loop unwinding prior to replication during S-phase[124,125]. SLX4-mediated recruitment of nucleases is used to trim very long telomeres rapidly via t-loop excision under normal conditions[126,127]. Overall, the relationship between telomeres and the DDR is complex. On the one hand, redundant mechanisms are in place to inhibit a dsDNA break response, which would lead to cell cycle arrest or apoptosis. On the other hand, concerted action of shelterin and DNA damage proteins is required for telomere replication.

Telomere maintenance in cancer cells

Shelterin in complex with several kb of repetitive telomeric DNA is at the basis of effective DDR inhibition which allows cellular proliferation. However, a considerable challenge to this situation is given by the semi-conservative nature of DNA replication. The last Okazaki fragment on the lagging strand of a linear piece of DNA (such as a chromosome) will be preceded by a small gap due to primer removal. This is a constitutive source of end-shortening over many divisions which is known as the end-replication problem[128]. If telomere shortening is unopposed, critically short telomere length leads to telomere crisis, a failure of DDR inhibition, which triggers double strand break responses resulting in senescence and/or apoptosis. This progressive shortening of telomeres is an intrinsic barrier to unlimited cellular proliferation and therefore an anti-tumour mechanism. In cancer cells, two pathways of telomere maintenance have been described to circumvent this problem: Activity of Telomerase[129] or Alternative Lengthening of telomeres (ALT)[130]. Both of these exhibit distinct characteristics and occur independently of each other for the most part (discussed below). Analysis of tumour tissue has indicated that 85-90% of cancers maintain their telomeres with telomerase, while 10-15% use ALT[131]. The following will briefly describe telomerase activity in the context of cancer followed by a detailed description of ALT. The latter pathway relies heavily on the activity of DDR factors at telomeres, which were introduced in previous chapters.

Telomerase

Telomerase was initially described in the ciliate *Tetrahymena* by Carol Greider and Elizabeth Blackburn in 1984[129] as an enzyme capable of elongating primers which contained telomeric repeat sequences. Considerable subsequent work by their research groups and others showed that telomerase was in fact widely conserved and maintained telomeres in the majority of human cancers (reviewed in[132]). Telomerase is made up of an RNA essential for the complementarity to telomeric repeats termed TERC[133] and a large reverse transcriptase called TERT. Expression of

TERT is strongly suppressed in human somatic cells and TERT expression alone is a sufficient trigger for cell immortalization *in vitro*[134]. Indeed, gain-of-function mutations in the TERT locus are very common in cancers which use telomerase as their telomere maintenance mechanism[135]. In addition to this, stem cells extend their telomeres with telomerase (reviewed in [136]). Therapeutic inhibition of telomerase is pursued by multiple companies with varying drug design. Perhaps the most promising of these so far clinically is Imetelstat, a nucleolipid which competes with and inhibits TERC. This drug has been successful as single-agent therapy in Phase II trials for myelofibrosis[137], myelodysplastic syndrome[138], multiple myeloma[139], and essential thrombocythemia[140]. The latter of these applications showed promising efficacy in a recent combined Phase II/III trial with 29% of patients showing a prolonged response[141]. Although there are obvious challenges to clinical translation of telomerase inhibition based on its importance for stem cells, knowledge and characterisation of this telomere maintenance mechanism has yielded promising clinical trials in selected haematological cancers.

ALT

In 1995, the dogma that telomerase is solely responsible for elongation of telomeric DNA in cancer was challenged by the realization that some cancer-derived cell lines maintained telomeres in the absence of telomerase activity[142]. Seminal follow-up work by Roger Reddel showed clearly that this also occurs in tumour tissue samples[143,144] and in the absence of TERT gain-of-function mutations[145] via a yet-uncharacterised process which he termed alternative lengthening of telomeres (ALT). This pathway has been defined in much detail since its discovery, partly due to the fact that it may present a vulnerability specific to cancer cells. It is now appreciated that approximately 10-15% of cancers maintain their telomeres via ALT[146]. It is most common in cancers where immortalized cells are of mesenchymal origin such as osteosarcomas (64%), Leiomyosarcomas (58%), or astrocytoma (42%)[131,147].

ALT in based on HR at telomeres. This was first elegantly shown by insertion of a sub-telomeric tag sequence on a single chromosome and subsequent monitoring of the tag location by metaphase FISH[148]. Only ALT cell lines were capable of spreading such a tag to other chromosomes over subsequent divisions which sparked the notion of HR at telomeres in the context of ALT. Importantly, it was later shown that this could not be explained by a global increase in HR due to ALT[149]. Distinguishing features (other than lack of telomerase activity) for cells which utilize ALT as their primary telomere maintenance mechanism have been defined by detailed subsequent study of ALT cell lines and tumour tissue. These features are discussed in detail below since taken together, they are sufficient to conclude the activation of telomere maintenance via ALT.

ALT-associated PML bodies (APBs)

PML bodies consist of PML/TRIM19 and form large membrane-less organelles in the nucleus based on protein phase transition[150]. They are observed in unperturbed cells as well as many biologically and clinically significant contexts such as responses to viral infection (reviewed in [151]). However, unique to cells using ALT, a subset of PML bodies co-localizes with telomeric DNA (APBs)[152]. The formation of APBs is restricted to late S/G_2 phase of the cell cycle[153,154]. They are thought to be the site of ALT-specific telomere recombination based on several lines of evidence. Firstly, the composition of PML bodies differs if they are APBs at telomeres. APBs are characterised by the presence of HR proteins such as RPA[155], NBS1[153], RAD51[152,156], RAD52[152], MUS81[157] as well as shelterin proteins including TRF2 (reviewed in [158]). Secondly, APBs coincide with the brightest telomeric signals in telomere FISH experiments within a given nucleus of an ALT cell line. Multiple studies have shown that such clustered ALT telomeres incorporate BrdU/EdU in G_2 phase specifically and this is an event specific to HR (for example[154,159–161]). Conversely, knockdown of PML reduces telomere clustering[162] and abrogates EdU incorporation at telomeres[163]. Taken together, it is likely that APBs present the site of telomere synthesis by HR in

the context of ALT and present a robust marker for ALT activity in scenarios where no significant global changes in PML protein are detected.

Heterogeneous and increased telomere length

In studies of ALT cell lines, telomere length is distributed in a manner, which is markedly different from other cells. It is recognised that ALT telomere maintenance results in a heterogeneous distribution of telomere length, usually ranging widely from 5-50kb within a single cell line or tumour sample[142,164]. Human somatic cells have an average telomere length of 12kb (+/- 2kb)[165] which decreases with age to about 9kb[166]. Cancers which maintain their telomeres with telomerase usually have an average telomere length of approximately 9kb (+/-5kb)[167,168]. In general, ALT cell lines show a mean increased and heterogeneous absolute telomere length which distinguishes them from telomerase$^+$ and mortal cells[169]. Therefore, measurement of telomere length may be taken as an indicator of ALT and this characteristically includes the presence a mean increase as well as very long and short telomeres.

Telomere sister-chromatid exchange (T-SCE)

As discussed, HJ resolution by nucleolytic activity may result in a crossing-over event between chromatids. T-SCE is measured by a specialized FISH protocol known as CO-FISH[170] (described in detail later). In line with HR-based mechanism of telomere elongation, ALT cell lines have higher incidence of T-SCE than telomerase$^+$ cell lines[171]. However, T-SCE alone is not sufficient to conclude ALT activity as it may also occur in the absence of telomere length heterogeneity and APBs[127,172]. Nevertheless, as increased HR at telomeres resulting in T-SCE occurs mostly in cells using ALT, this may be taken as evidence for the activity of this pathway if presented with complementary analysis.

C-circles and other complex telomeric DNA

Another characteristic of ALT is the occurrence of non-linear, extrachromosomal telomeric DNA. Such molecules are often circular as shown by EM and 2D gel

electrophoresis[173] and depend on HR factors such as NBS1, RAD51 paralogue XRCC3[174]. They may be in the conformation of a largely ds circular DNA (t-circle), or a largely ss circle with fragmented complementary stretches (G- or C-circle depending on continuous strand)[175]. T-circles are not specific to ALT since they also occur upon t-loop excision. For example, they are also observed in conditions of shelterin dysfunction[123] or DNA damage generally[176,177]. However, C- and G-circles are specific markers of ALT cells and the former has been used extensively to diagnose ALT in cell lines and tumours[175,178]. In addition to this, other complex branched telomeric DNA may be present in ALT cells[179]. Such complex DNA may be extrachromosomal or chromatin bound and may include HR intermediates as well as collapsed forks[180]. However, there is currently no convenient experimental way to detect such molecules. Thus, C-circles are a widely assayed and convenient marker of excised telomeric HR intermediates, which are exclusively reported in cells which utilize ALT for telomere maintenance.

ALT-associated changes in chromatin

Telomeric DNA is organised as chromatin, and this likely extends to the very end of telomeres[181]. The loading and dissociation of core histones is slow[182] in comparison to shelterin and DDR factors which bind telomeric DNA more dynamically based on single-molecule experiments[183]. Therefore, it is perhaps not surprising that ALT, which requires homology search between telomeres, is associated with changes in chromatin composition. Histone octamers differ in their composition in ALT$^+$ cells. Variant H3.3 is displaced[184,185] and macroH2A1.2 is deposited[186], in both cases due to the absence of histone remodelling enzyme ATRX at ALT telomeres. In addition to changes in histone variants, telomeric chromatin is differentially modified (epigenetically) in ALT cells. ALT chromatin may be enriched for heterochromatic histone marks. Increased H3K9me3 and H4K20me3 have been reported in ALT cells, a reaction which is dependent on HP1α[187] and potentially SETDB1 based on a recent study in mice[188]. Key to the activity of HP1α and generation of H3K9me3 at telomeres is the presence of telomeric RNA, TERRA[189]. TERRA may be present at

elevated levels in ALT cells[190]. However, this could simply be due to the fact that longer telomeres result in higher levels of TERRA regardless of active telomere maintenance mechanism as reported[189]. Generally, controversy over the level of heterochromatin at ALT telomeres relative to other/no active telomere maintenance exists in the literature. Similar conclusions may be drawn for the induction of TERRA, which may also simply be a non-specific by-product of the relative elongation of telomeres, which is observed upon induction of ALT. On the other hand, the changes in variant histones H3.3 and macroH2A1.2 described are consistently observed in ALT thus far and may be regarded as a marker for the activity of this telomere maintenance mechanism.

Model of the ALT mechanism

Previous paragraphs have outlined how cells which maintain their telomeres via ALT show a number of defining features: i) The presence of select HR factors and APBs at clustered telomeres; ii) Active HR-based telomere synthesis in late S/G_2 phase of the cell cycle; iii) The presence of telomeric HR-intermediate or resolution products such as C-circles; iv) Relative changes in the makeup of telomeric chromatin and the length of telomeric DNA. Based on these observations, the question arises as to what the precise mechanism of ALT telomere elongation entails.

Based on initial work on telomerase-independent survival of yeast[191], it was confirmed that HR in ALT synthesizes DNA by BIR, specifically by activity of PolD3 as part of Polδ[160]. Subsequent extension of traditional CO-FISH analysis indicated that ALT BIR telomere synthesis may proceed either in a conservative or semi-conservative manner[192]. This distinction is strengthened by subsequent studies and based on these new data it was proposed that ALT proceeds as a bifurcated pathway (Figure 6). The first distinction between the two pathways was the realisation that BLM and SLX4 have opposing and selective effects on certain aspects of ALT[164]. SLX4 overexpression exacerbates T-SCE as detected by CO-FISH, while BLM suppresses these hallmarks in ALT cells. However, this was opposed with their effect

on telomere extension, which was promoted by BLM and inhibited by SLX4. In line with this, a recent study showed that co-factor SLX4IP regulates exacerbation of such ALT hallmarks in the context of SLX4 knockout by direct inhibition of BLM[193]. Another distinction between the two arms of the ALT pathway is their dependency on RAD52. RAD52 and SLX4 act non-epistatically in terms of their effect on ALT hallmarks upon knockout[194] and are therefore likely separated mechanistically. In addition to this, RAD51 seems to be dispensable for BIR DNA synthesis in a recent study, while RAD52 is essential for this[163]. On the other hand, it has been shown that long-range homology searching in ALT is dependent on RAD51-Hop2[156]. This search is most likely aided by telomere clustering, a process which is dependent on binding of nuclear orphan receptors to sub-telomeric variant repeats[195].

Based on the studies described above, I suggest that ALT acts in two ways mechanistically which are likely to be interlinked and occur in tandem in a given cell. Both mechanisms use PolD3 for DNA synthesis. One of these involves inter-chromosomal homology search in a RAD51-Hop2 and nuclear orphan receptor-dependent manner. This is followed by abortive semi-conservative BIR, which ends with SLX4-mediated HJ resolution. The other one is long-range, conservative BIR stimulated by RAD52-RAD51 strand invasion and BLM activity (Figure 6).

Induction of ALT

The first insight into the relationship of telomerase and ALT comes from studies of hybrid cell lines[196]. ALT$^+$ cells were fused with telomerase$^+$ fibroblasts and surviving clones were analysed. In all cases, the resulting cell line used telomerase for telomere maintenance which suggested that there is an intrinsic inhibitor of ALT. Initially, it was proposed that ATRX may be this inhibitor based on its loss of expression in ALT cell lines and common mutation in ALT$^+$ tumours[197]. In agreement with this notion, knockout of ATRX in mortal or telomerase$^+$ cell lines induced features of ALT transiently[198]. However, these experiments did not result in a persistently ALT$^+$ cell line and it was later shown by systematic analysis of ALT cell

lines that not all of them had lost ATRX expression[199]. Therefore, although alterations in telomeric chromatin were certainly suggested as an underlying mechanism of ALT induction due to ATRX well-documented role as a histone remodelling enzyme, loss of this protein alone is excluded as a pioneering event. The only documented incidence of sustained ALT induction in a telomerase$^+$ background is upon knockdown of chromatin remodelling factor Asf1[200]. Interestingly, this study showed that ALT induction was dependent on replicative stress at telomeres and required an initial telomere length of approximately 20kb. This latter observation casts the physiological relevance of this mechanism into doubt somewhat given that 20kb is well above the length of telomeres observed in mortal cells, including telomerase$^+$ stem cells. Therefore, it seems that it is possible to induce ALT by modulation of telomeric chromatin in telomerase$^+$ cells experimentally and this may involve loss of Asf1.

Another important aspect of the putative switch from telomerase to ALT is the presence of replicative stress and DNA damage at telomeres. This is highlighted by the fact that proteins which resolve replicative stress also counteract ALT activity including SMARCAL1[201] and FANCM[161,202]. In line with this, increased replicative stress markers were confirmed upon Asf1 knockdown[200]. It is possible to transiently induce many of the hallmarks of ALT in human cells by creating conditions of replicative stress at telomeres. An example of this is ATRX knockdown, DAXX knockout, and telomere DNA damage which was reported to trigger APBs and C-circles in telomerase$^+$ cells[203]. However, this report does not present a permanent switch to ALT since cells are also undergoing apoptosis under these conditions and there is no telomere length heterogeneity, clustering, or T-SCEs[203]. Other examples of selected ALT hallmarks induced by replicative stress and DNA damage at telomeres are found in studies of mice. For instance, RTEL1 knockout MEFs show T-SCEs, t-circles, and length heterogeneity[124]. These and other studies demonstrating replicative stress and damage at ALT telomeres have led to attempts to abrogate ALT altogether by chemical inhibition of ATR. One study showed that hallmarks of

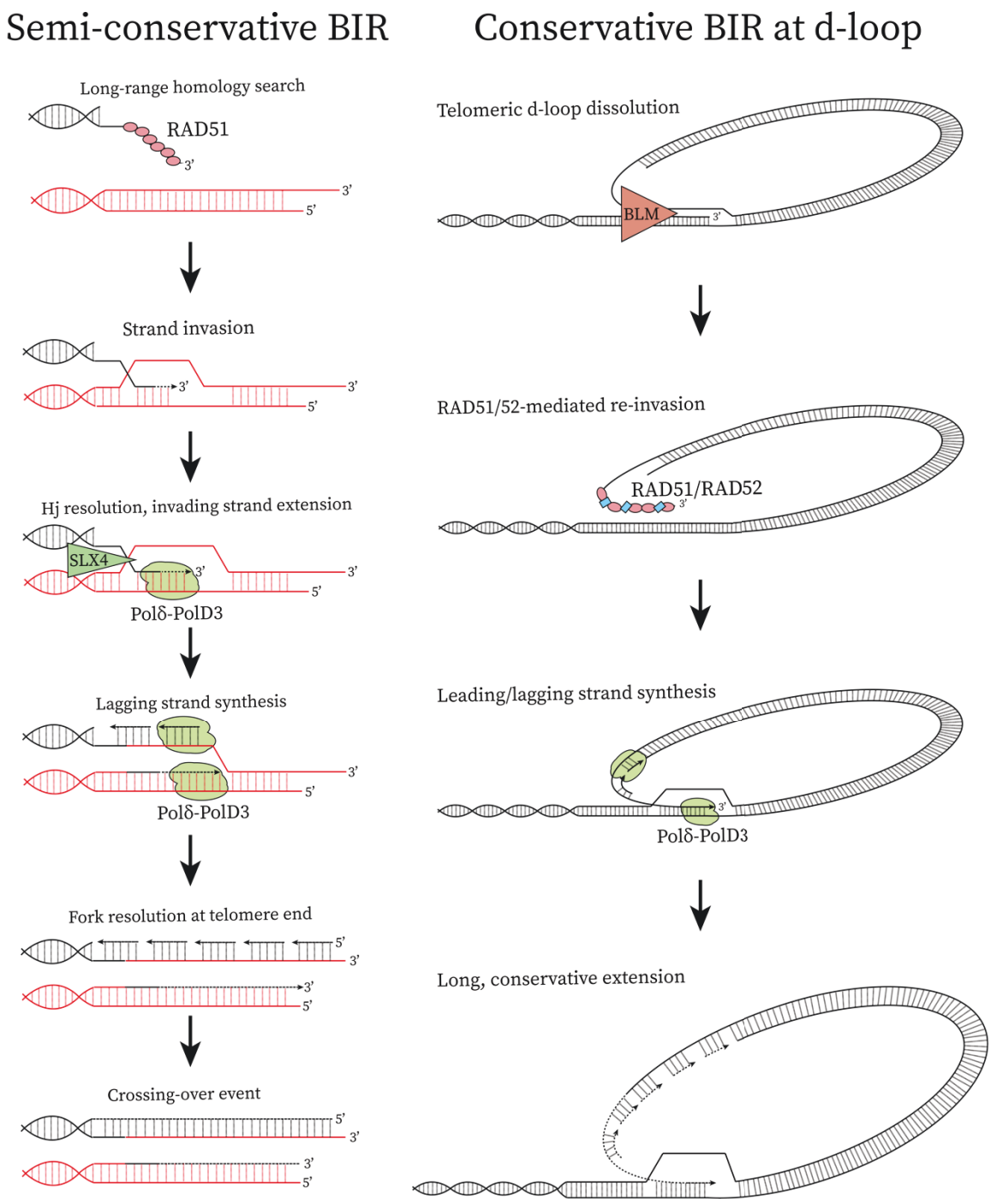

Figure 6: Model of ALT mechanism. Semi-conservative BIR mediated by RAD51 filament formation resulting in long-range homology search triggers inter-chromosomal invasion. SLX4 cleaves resulting holiday junction and DNA synthesis by Pold3/Polδ. Conservative BIR may be initiated within a given telomere or between adjacent chromatids This is mediated by formation of RAD51/RAD52 mixed filament and strand invasion followed by conservative DNA synthesis on both leading and lagging strand. D-loop migration proceeds by BLM activity until conservative synthesis has been completed to the end of the telomere.

ALT were decreased and cells were killed upon inhibition of ATR-mediated repair of DNA damage resulting from the replicative stress at ALT telomeres[204]. However, subsequent systematic analysis of this effect in other ALT cells lines later cast this into doubt and no selective killing was achieved overall[205]. In summary, while replicative stress and DNA damage has been widely reported at telomeres of ALT cells, it is not possible to induce ALT by these means and ALT cannot be abrogated by inhibition of the DDR.

Overall, only Asf1 knockdown in cells with long telomeres is known to induce ALT in initially telomerase$^+$ cells to date. Factors which impact the induction of cellular phenotypes associated with the activity of ALT are replicative stress at telomeres and the composition of telomeric chromatin. Generally, crosstalk between telomerase and ALT is likely to be extensive and any changes in active telomere maintenance mechanism are complex. In support of the challenging nature of these studies, no experiment so far has been able to demonstrate *de novo* induction of ALT in mortal cells or loss of ALT and re-activation of telomerase.

ALT as a therapeutic target

Inhibition of ALT presents an attractive strategy for future therapy of cancer. This is based on the fact that in contrast to telomerase activity, ALT has not been recorded to occur in normal somatic or stem cells. Additional incentive for the development of such inhibitors is given by reports in mice which suggest that telomeres inhibition drives evolution towards telomere elongation by ALT[206]. Future therapeutic approaches may include combinatorial inhibition of both ALT and telomerase to minimise the emergence of resistance. Currently, pre-clinical studies to derive a specific inhibitor of ALT are the subject of active investigation by several groups.

Kaposi's Sarcoma Herpesvirus (KSHV)

During the AIDS epidemic in the 1980s, clinicians commonly encountered patients who presented with disseminated dermal angiosarcomas. This cancer was known as Kaposi's Sarcoma (KS), named after the Hungarian dermatologist Moritz Kaposi who initially described them in 1872[207]. Neither Moritz Kaposi nor clinicians in the 1980s knew what the etiological agent behind this disease was. However, this changed with the discovery of herpesvirus-like sequences by representative difference PCR analysis of AIDS-KS performed by Yuang Chang and Patrick Moore in 1994[208]. In the following year, the same viral sequences were found in HIV-related cancers PEL[209] and MCD[210]. The virus was named KSHV, human herpesvirus 8 (HHV8) and classified as an oncogenic γ-herpesvirus, based on sequence similarity with closely related EBV[211]. Since these events, considerable research has been dedicated to understanding this oncogenic virus with the aim of devising targeted therapy against some of its associated cancers.

KSHV-associated cancer

KS occurs commonly in immunocompromised patients and may be treated effectively upon reconstitution of normal immune function. The WHO-GLOBOCAN survey determined that 41,799 new cases were diagnosed globally in 2018 and 19,902 cases of KS-associated lethality were recorded[212]. Most of these cases occur in Africa and this reflects the uneven distribution of KSHV globally. While 5-15% of individuals are infected in Europe, the virus is endemic in sub-Saharan Africa where >70% of the population carry the virus[213]. KS is commonly associated with productive HIV infection. In line with this, AIDS-KS is the most common tumours in some sub-Saharan countries where KSHV is endemic and HIV is still epidemic[214,215]. In Europe, AIDS-KS is a rare disease due to the wide availability of antiretroviral therapy. However, KS risk is still elevated in HIV^+ individuals upon antiretroviral treatment in comparison to the general population[216]. AIDS-KS is curable with combined chemotherapy/antiretroviral treatment or antiretroviral treatment

alone[217]. Endemic KS has been reported in HIV$^-$ individuals in sub-Saharan with high KSHV prevalence. This is mainly a disease of young children and is thought to involve immunosuppression due to malnutrition. Endemic KS often progresses to systemic lymphadenopathy and death[218]. KS also occurs as an iatrogenic disease. It may develop upon immunosuppressive therapy as administered post-transplantation[219] and in autoimmune disease such as Crohn's[220,221]. Generally, the treatment of KS in this setting includes the lowering of the dose of existing drug treatment in an attempt to balance KS progression with the therapeutic purpose of immunosuppression (such as preventing organ rejection)[222]. Classic KS, as described by Moritz Kaposi, is a largely indolent disease, which develops in elderly KSHV$^+$ individuals. As a summary, KS presents as a diverse group of diseases with varying clinical outcome. Histologically, KS is made up of a 3D meshwork of spindle cells which are thought to be the immortalized cancer cells within lesions. The tumours are highly angiogenic and there is a number of infiltrating lymphocytes in lesions (see Chapter 3 of results for histology examples).

KSHV infection has also been linked to the onset of several lymphoproliferative malignancies that are often present in conjunction with KS. Multicentric Castleman's disease (MCD) is a disease characterised by abnormally proliferating, KSHV$^+$ plasmablast-like B-lymphocytes within lymphoid follicles or the mantle zone[223]. Symptoms of MCD include flares of acute inflammation, lymphadenopathy, and effusions[224]. If left untreated, MCD results in secondary NHL such KSHV$^+$ DLBCL[225] and is ultimately associated with very poor prognosis due to evolution towards multiple organ failure and haemophagocytic syndrome[226]. Treatment with Rituximab has been successfully employed for the treatment of MCD, with >90% patients showing remission of the disease and no secondary NHL[227,228]. However, some reports indicate that this regimen may result in significant flare-up of pre-existing KS and potent re-activation of the KSHV productive life cycle, which may render it unsuitable for some patients[229]. The second lymphoproliferative disorder associated with KSHV is Primary Effusion Lymphoma (PEL). This malignancy is

characterised by common EBV co-infection (85%)[230] and immunosuppression. Its clinical presentation includes effusions of abnormally proliferating lymphocytes into body cavities and sometimes also solid extracavitary tumours[231,232]. Prognosis for patients diagnosed with PEL is extremely poor with median survival of 6.2 months[233]. No efficient therapy has been established and standard CHOP chemotherapy is commonly applied in the clinic[234]. In summary, KSHV may cause a number of different lymphoproliferative disorders with varying clinical prognosis.

Overall, there is a varied spectrum of cancers associated with KSHV infection. There are considerable differences in the aggressiveness and clinical outcome of these diseases. Most KS cases are treatable whereas some of the blood cancers associated with the virus are usually fatal. There are several potential therapies that are being considered for the treatment of PEL and MCD specifically. These include monoclonal antibody treatments other than Rituximab (Elsheikh, Lippert, *et al.* in preparation). However, all targeted therapy against KSHV-associated cancers is currently only in pre-clinical development and there is the need to develop a new approach for the remaining patients where existing therapy is ineffective.

KSHV life cycle

As a γ-herpesvirus, the life cycle of KSHV is characterised by three key events; i) Initial infection of the host, ii) Establishment of latency; iii) Productive, lytic infection. This section will describe the molecular biology underlying these aspects of the KSHV life cycle in more detail. This will be following by an evaluation of the interface between the DDR and KSHV and ultimately a description of the existing reports on host telomeres and KSHV infection.

Initial infection of host cells

The infectious KSHV virion consists of an icosahedral capsid with a diameter of 125nm[235], an intermediate tegument layer, and one copy of the approximately 170kb[211] dsDNA genome. Transmission of KSHV may be either horizontal in high risk groups such as MSM though sexual intercourse[236,237] or vertical in endemic areas through saliva[238]. KSHV displays broad tropism and may infect a variety of different cell types including B- and T-lymphocytes, endothelial cells, and neurons[239]. Initial binding of the virion to host cells occurs by interaction of KSHV with membrane heparan sulfate[240] Subsequent entry is mediated by binding of KSHV capsid protein gB to host integrins α3β1, αVβ1, and αVβ5[241,242]. This triggers a complex signalling cascade which ultimately leads to engulfment of the capsid into the cell via clathrin-mediated endocytosis[243] or directly into the cytoplasm by nuclear envelope fusion with the plasma membrane[244]. Recent studies have implicated interaction with host EphrinA2 in the initiation of KSHV entry via lipid raft formation and uptake in a process resembling macropinocytosis[245,246]. Subsequently, virions are released into the cytoplasm and travel along the cellular microtubular cytoskeleton toward the nucleus by interaction with dynein motor proteins[247]. The capsid docks to the nuclear pore and the KSHV genome is released into the nucleoplasm in a linear conformation[244].

Latency

During latency, KSHV persists as a circular episome in the nucleus of infected cells without production of infectious virions. In latently infected cells, the KSHV genome persists as >50 copies within the nucleus[248]. There is some variation in terms of copy number and it has been documented that PEL cells in particular have an increased number of episomes per cell (see results chapter 4). Viral gene expression is restricted to enable long-term persistence while avoiding immune detection. The key latency-associated genes vFLIP (ORF71), vCyclin (ORF72), and LANA (ORF73) are co-transcribed from the same locus[249]. This transcription is autoregulated by LANA[250]. In addition to these proteins, the latency locus encodes 12 viral miRNAs. KSHV vFLIP acts as an direct inhibitor of apoptosis by mimicry of cellular cFLIP and induction of cFLIP expression through NF-κB activation[251]. It has been shown that some PEL cell lines are addicted to vFLIP[252] and based on these findings, inhibitory peptides against vFLIP are under development[253]. In primary endothelial cells such as HUVECs, vFLIP expression alone is sufficient to trigger cell elongation reminiscent of endothelial to mesenchymal transition (EMT) and spindle cell morphology[254,255]. EMT is thought to be an important step in metastasis and progression of cancer[256]. KSHV vCyclin is a viral homologue of cyclin D1 and counteracts vFLIP-mediated senescence and cell cycle arrest[257]. It triggers entry into S-phase by interaction with cell cycle regulators including Cdc25a[258], Cdc6[259], and Bcl2[260]. LANA acts as a molecular tether which attaches the viral episome to host chromatin (Figure 7). It is essential for maintenance of viral episomes during latency[261]. On the KSHV genome, LANA binds two distinct sites found within the viral terminal repeat region with its C-terminal DNA binding domain[262]. On host chromatin, LANA does not bind DNA but rather interacts with nucleosomes to achieve episome tethering. Specifically, crystallography studies have shown that the N-terminus of LANA binds to histone variants H2A and H2B[263]. Interestingly, LANA has also been shown to bind directly to DDR-associated variant γH2AX[264]. Taken together, the key KSHV gene products which are expressed during latency are concerned primarily with sustaining continuous proliferation of infected cells by

inhibition of apoptosis and cell cycle arrest as well as the establishment of episome clusters, which reside in a favourable chromatin niche within the host genome.

The KSHV episome is also fully chromatinized and exhibits specific loop conformation and histone modification. Study of KSHV episomes by 3C has revealed loop formation involving the latency promoter region in a CTCF-mediated manner[265]. Disruption of the sites involved in loop formation resulted in de-regulation of latent transcription, indicating that this episome loop is important for the maintenance of latency. In addition to this, analysis of histone modifications on the KSHV episome chromatin revealed the presence of both active and repressive histone marks. H3K27me3 has been detected throughout latent viral genomes, although the incidence of these marks is highest at lytic promoters[266,267]. In these studies, LANA was shown to catalyse these modifications by recruitment of PRC2 and DAXX. LANA has also been shown to interact and recruit HP1α to viral genomes for putative deposition of further repressive marks[268]. In line with this, H3K9me3 has been detected on both the TR and lytic promoters of a KSHV BAC in 293T cells265. However, a subsequent study examining the same mark on KSHV episomes in BCBL1 PEL cells showed no H3K9me3 association with viral sequences266. Histone marks associated with active chromatin such as H3K4me3 and H3ac have been reported at the KSHV TR[265,269]. As a summary, the chromatin of KSHV episomes in infected cells exhibits an overall loop structure as well as features of both hetero- and euchromatin, which may be mediated by LANA. Disruption of this conformation impacts on the maintenance of latency and it is therefore likely to be important for the persistence and establishment of latent infection.

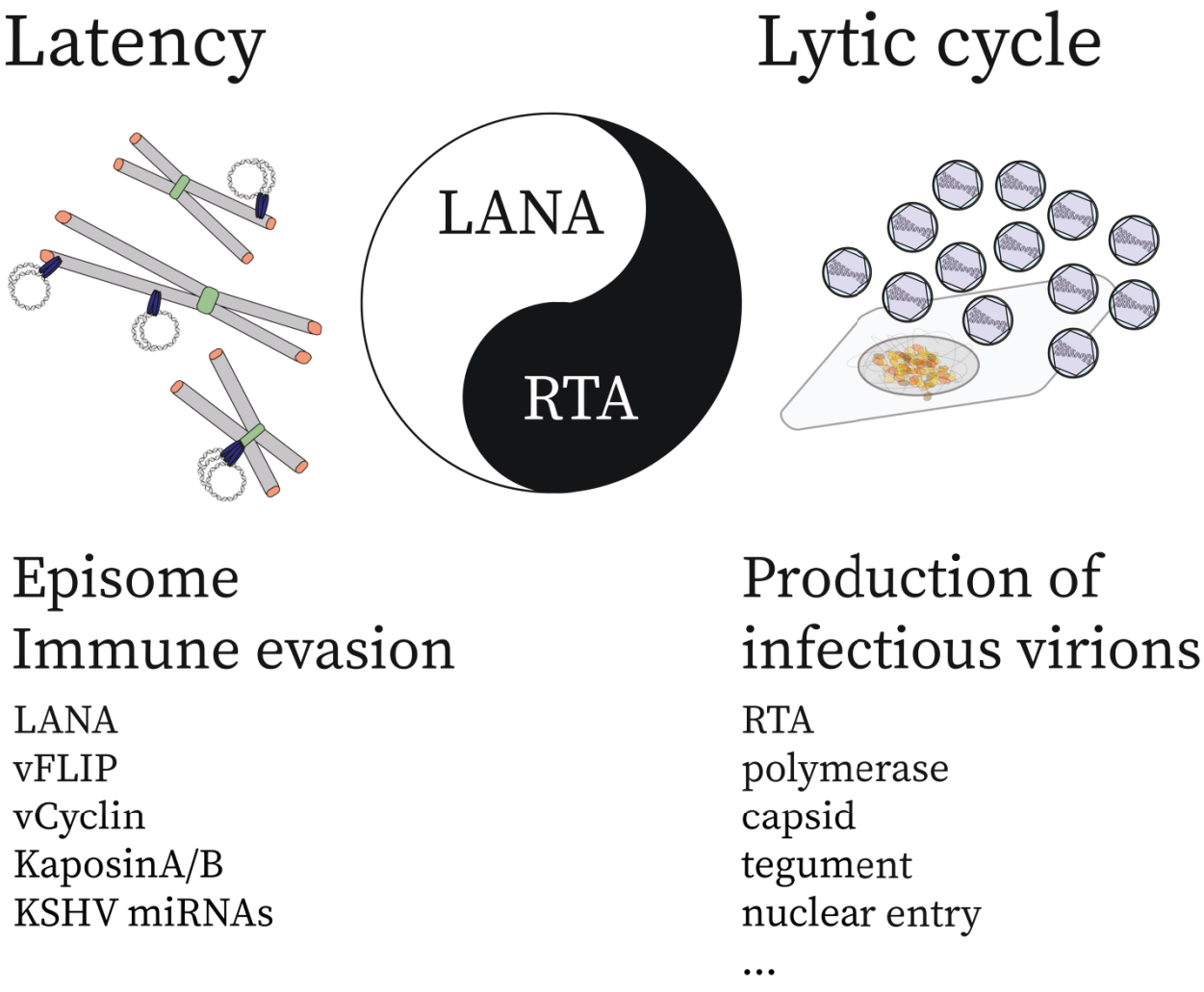

Figure 7: The life cycle of KSHV. Viral infection is biphasic and the choice between latency as an episome tethered to host chromatin or the production of infectious virions is mediated by LANA (which also acts as an episome tether, shown in dark blue) and RTA transcription factor activity respectively. Latent episomes are maintained in the presence of limited viral gene products and rely on hijacking of the cellular replication and/or DNA repair machinery to maintain viral genomes. On the other hand, the lytic replication program includes a viral replication factory and many factors which make up the structure of KSHV virions and mediate cell exit.

LANA mediates replication of KSHV episomes in infected cells. This is illustrated well by reports which indicate that a plasmid containing more than two KSHV TRs (the binding sites of LANA) can be replicated and maintained by ectopic expression of LANA alone in both B-cells[262] and endothelial cells[270]. Interestingly, recent studies have shown that tethering and replication of latent episomes is highly dependent on LANA oligomerization and clustering[271]. Mechanistically, it has been shown that the C-terminal domain of LANA interacts with a number of factors which are associated with the initiation of replication including ORC2[272], PCNA/RFC[273], and MCM complex[274]. However, the dynamics of these interaction are somewhat unusual in these reports and may indicate replication uncoupled from bulk S-phase synthesis. For example, interaction of LANA with several subunits of the MCM complex was not restricted to S-phase and persisted in mitosis[274]. Similarly, ChIP/qPCR experiments showed that ORC2 binding to the KSHV TR still occurred in mitotic cells[272,275] and Polδ binding persisted throughout G2 and M phase of the cell cycle[276]. This is in contrast to normal DNA replication, where neither ORC nor MCM complex are bound to DNA during G2/M phase[277,278]. Meselson-Stahl experiments in the same self-replicating KSHV TR plasmid system mentioned above indicate that whatever the mechanism of latent episome replication, it occurs in a semi-conservative manner[279]. In summary, KSHV episomes are likely to replicate in an atypical manner during latency dependent on the oligomerisation of LANA and activity of the replisome outside of S-phase.

Lytic reactivation

Lytic replication stands in contrast to viral latency and is aimed at the production of infectious virions rather than the avoidance of immune detection. In fact, lytic replication is highly immunogenic. This is highlighted by the occurrence of T-cells reactive to KSHV antigens upon lytic induction specifically[280,281]. RTA (ORF50) is the master regulator of lytic replication and its expression alone is sufficient to trigger the productive lytic cycle in infected cells[282,283]. This is balanced by activity of LANA which competes with RTA in latently infected cells[284]. RTA alone or in conjunction

with cellular transcription factors such as RBP-Jκ[285] activates expression of the full KSHV gene program to allow efficient production of virions. In analogy with other herpesviruses, these genes have been classified into IE (immediate early), E (early), and L (late) genes[244]. In contrast to the latent gene program, lytic genes encode a viral replication machinery which is highly conserved across all herpesviruses. This includes a viral DNA polymerase (ORF9), polymerase co-factors (ORF59), helicase (ORF44), primase (ORF56) and primase co-factors (ORF40, 41)[244]. Additional genes expressed during lytic replication are concerned with the generation of capsids within the nucleus[286], the nuclear egress complex formed by ORF67, ORF69[287], transport to the cell membrane by exocytosis[288], and tegumentation of the virion[289,290]. Therefore, the lytic KSHV cycle differs from latency in several key aspects, specifically the extensive expression of viral genes resulting in a host immune reaction, and the production of infectious virions through expression of many viral genes (Figure 7).

The mechanism of viral genome replication during the lytic cycle is also significantly different from latency. It is thought to occur in a multi-step process that, in analogy to other viruses, results in the production of long linear concatemers via a rolling circle amplification mechanism. Lytic replication is initiated by RTA and K8 binding to one of two replication origins, OriLyt-L/-R[291]. There are eight C/EBP motifs within these origins and specificity of RTA/K8 binding to this region is mediated by association with host C/EBPα[292]. The binding of these proteins then recruits the viral replication machinery outlined in the previous section including KSHV polymerase, helicase, and primase. Several host proteins are also implicated in efficient lytic replication as their knockdown impairs the production of virions by the lytic cycle. This includes Topoisomerase I/II[293], REQL, PARP, and DNAPk[291]. In summary, both virus and host factors have been shown to be important for effective production of viral genomes for incorporation into virions. Together with the observation that herpesvirus genomes are found to be present in a linear conformation upon lytic induction by Gardella gel

electrophoresis[294], this has led to the ubiquitous suggestion in the literature that lytic replication may occur via a rolling circle-like mechanism. However, direct demonstration of this mechanism and characterisation of the precise factors involved in it remains elusive to date.

KSHV life cycle in cancer cells

The stage of KSHV life cycle within tumour biopsies and cell lines varies greatly depending on the tissue of origin. Viruses within KS lesions are largely latent with low levels of lytic cycle and reinfection[295] and this is also the case for KSHV-infected primary LECs[296]. In endothelial-like cell line models of KS, there is no lytic reactivation at all and the virus is strictly latent[282,297]. In contrast, PEL and MCD show significant reactivation of the virus as observed by IHC for KSHV lytic proteins in patient sections[298]. However, in contrast to closely related γ-herpesvirus EBV, establishment of latent KSHV infection is not sufficient to trigger immortalization of primary human lymphocytes or endothelial cells *in vitro*. Therefore, latency seems to be the default program in adherent cell lines and KS whereas lytic replication is commonly observed in lymphocyte cell lines and tumours.

KSHV interaction with the DDR

Incoming and replicating KSHV genomes present an exogenous piece of DNA, which may be potent substrate for DDR activation. A number of reports, which are in support of a complex interaction between KSHV infection and the DDR, indicate that such interactions have varying consequences for the virus. Evidence for this model is based on both direct study of interaction between the DDR and KSHV proteins, as well as possible further viral modulation of the DDR through effects on innate immune sensing upon infection.

The consequences of DDR activation differ depending on the stage of the KSHV life cycle *in vitro*. During latency establishment, the incoming KSHV genome is thought to be in a circular conformation upon nuclear entry in analogy to other herpesvirus infections. In one report, detection of BrdU-labelled KSHV genomes immediately after entry showed that these co-localize with DNA damage marker γH2AX[299]. ATM inhibition resulted in a decrease in KSHV copy number in this setting, which suggests that activation of an ATM-mediated DDR may be beneficial for the virus at this stage of the life cycle. During the lytic cycle, however, the opposite effect is observed. Several studies indicate that induction of lytic replication is accompanied by a strong induction of γH2AX and dsDNA breaks[300,301]. Follow-up work showed that lytic replication of KSHV triggers cell cycle arrest via checkpoint signalling and inhibition of this response led to increased viral titre[302]. On the one hand, the DDR machinery may be used by the virus for latency establishment whereas on the other hand DDR activation suppresses the production of viral genomes during lytic replication. It is tempting to speculate that host cNHEJ or MMEJ machinery may be used for herpesvirus genome re-circularization upon nuclear entry. The mechanism of this process is uncharacterised to date.

Proteomic screening approaches, which analyse the KSHV-host interactome have further indicated association with the DDR. For example, systematic expression and pulldown of the complete KSHV ORFome in HEK293T cells coupled to mass spectrometry has been carried out. In this data set, all three subunits of RPA heterotrimer are detected with high confidence as potential interactors of LANA[303]. In addition to this, the screen identified Lig3, ERCC1, PARP2, and TDP1 as further candidate interactors of LANA. Interaction between lytic proteins and the DDR was also indicated by this study, namely K8-SMARCAL1 as well as K10-BLM/ERCC6L. Another study was performed to analyse the interactome of recombinant LANA specifically by GST pulldown and mass spectrometry. Again, RPA1/2 were detected as well as RAD51C, ZRANB2, and Lig1[304]. Finally, DNA affinity purification mass spectrometry for OriLyt in lytically active BCBL1 cells was carried out. This approach detected PARP1, DNAPk, Ku70, and Lig3 at KSHV OriLyt[291]. Overall, the nature of these experiments necessitates confirmation of interactions by additional experiments for validation. Nevertheless, in summary, proteomic interactor screens have indicated a number of additional candidate host DDR factors, which may associate with KSHV throughout the virus life cycle.

There are intriguing parallels between the DNA damage response and innate immune sensing of viral infection and this field of research has received considerable attention recently. Modulation of innate immune sensing has been extensively documented in the context of KSHV infection. Therefore, taken together with increasing knowledge of the involvement of innate immunity in the DDR, another interface between KSHV infection and the DDR has been described. Perhaps the best example of this is innate immune sensing by the cGAS/STING pathway[305]. It is established that detection of exogenous KSHV DNA by the cGAS and induction of type I interferon is an innate immune response which restricts infection[306]. However, a number of recent reports have shown that a similar cellular response is initiated against endogenous cytoplasmic DNA such as micronuclei resulting from DNA damage or segregation errors during mitosis[307–309]. cGAS/STING signalling is

potently inhibited during KSHV infection[310]. Therefore, modulation of this pathway by viral gene products is bound to influence their role in sensing damaged self-DNA and clearance of cells with genomic instability. Similarly, IFI16 has been shown to sense self-DNA upon induction of dsDNA breaks by etoposide treatment to trigger type I interferon response[311]. IFI16 is degraded in cells during KSHV lytic reactivation and utilized for maintenance of viral latency[312]. It is thus likely that innate immune responses which survey the cell for potentially recombinogenic and damaged self-DNA in the cytoplasm are modulated upon KSHV infection.

As a summary, the current knowledge on the interface between KSHV infection and the DDR suggests that there is extensive crosstalk and modulation. The outcome of this modulation for the virus may be both restrictive or permissive, depending on the stage of the KSHV life cycle. Generally, evidence suggests that latency utilizes DDR factors for viral episome maintenance, whereas DNA sensors may restrict the generation of viral genomes during lytic replication.

KSHV interaction with host telomeres

Reports of interactions between host telomeres and KSHV have been limited. No endogenous interaction between telomeric DNA or shelterin and the virus has been documented. However, the LANA interactor screen indicated potential association with TRF1[304]. The result of this interaction was suggested to be displacement of TRF1 from telomeres and shortening of telomeric DNA. However, TRF Southern blot analysis was only partially conclusive and used a system in which LANA was expressed ectopically and individually. In contrast to this study, LANA has also been shown to activate expression of a transfected construct containing one of the main promoters of telomerase[313]. This study did not attempt to measure the effect of LANA on telomere length. So far, the impact of KSHV infection on telomeric chromatin remains virtually unexplored with some indication by one report of interaction between LANA and TRF1[304].

Aims of the study

The present investigation aims for a systematic examination of the telomere-associated proteome in response to latent KSHV infection. Interest in this is based on the fact that changes in proteins bound to telomeres may indicate biological phenomena, which are important for KSHV oncogenesis. Firstly, dysfunctional telomeres are a source of significant genomic instability via aberrant DDR activation. This may take place via cNHEJ, MMEJ, or HR as discussed. Secondly, protein markers of the activity of telomere maintenance mechanisms may be enriched at telomeres of infected cells specifically. As mentioned, telomere maintenance is a pre-requisite for cancer cell proliferation. In analogy with other published virus-host interactions, interaction with the DDR at telomeres may be co-opted by KSHV to promote infection or persistence and this possibility will be examined. Finally, the relevance of any such interaction for KSHV-associated cancers will be interrogated by examination of primary samples of KS and PEL, two of the main instances of such malignancy.

To investigate changes in protein bound to telomere upon infection systematically, comparative PICh/mass spectrometry is performed in a BJAB cell line model, in the presence and absence of latent KSHV infection. Key changes in the telomeric proteome are confirmed by telomere IF-FISH. Next, the activity of telomere maintenance mechanisms in cells harbouring latent KSHV infection is examined in detail. To this end, two initially telomerase^{+} cell lines are infected in biological triplicate and analysed for key features of active telomere maintenance. First, telomere length is determined by telomere qFISH and TRF Southern blotting. Subsequently, the activity of both known telomere maintenance mechanisms, telomerase and ALT, is examined directly. This includes the measurement of telomerase activity by TRAP assay and *hTERT* expression by RT-qPCR. All known criteria for ALT activity are examined as outlined in the introductory text of the thesis. This includes quantification of T-SCEs by telomere qFISH, telomere fragility,

and C-circles. Finally, IHC/FISH is performed on paraffin-embedded sections of KS and PEL tumours to determine the physiological relevance of findings made using the abovementioned cell line models. This study presents the first thorough evaluation of the impact that latent KSHV infection has on the DDR at telomeres and telomere maintenance mechanisms, with the aim of identifying potential novel therapeutic avenues for intervention in KSHV-associated cancer.

MATERIALS & METHODS

Cell culture

All cell lines were cultured in humidified incubators at 5% CO_2, 37°C. Medium used for cell culture was either RPMI (BJAB) or DMEM (SLK, U2OS, EA.hy926) supplemented with 10% FBS and 1% Penicillin/Streptomycin. Cells harbouring latent KSHV were maintained under selection with 4μg/mL Puromycin. All cell lines in the study were tested for Mycoplasma by PCR as described[314] at various stages of the project and were found to be negative throughout. STR profiling was performed on all cell lines used in the study by the Cell Services science technology platform (STP) of the Francis Crick Institute which confirmed their identity. Details on cell lines included in the study may be found in Table 1.

Cell line	Source	EBV/KSHV status	Comments	Reference
SLK	Dr Grzegorz Sarek	-/-	Commonly mischaracterised cell line, identified as clear cell renal carcinoma cell line Caki1	[315]
EA.hy926	ATCC	-/-	Fusion cell line created from HUVECs and A549 lung carcinoma cell line. Retains many properties of an endothelial cell in culture.	[316]
BJAB	Dr Grzegorz Sarek	-/-	Burkitt's lymphoma cell line	[317]
iSLK.219	Dr Grzegorz Sarek	-/+	Modified KSHV producer cell line based on SLK cell line. Contains recombinanat KSHV (rKSHV.219) and doxycyclin-inducible RTA.	[282]
U2OS	Crick Institute Cell Services STP	-/-	Osteosarcoma cell line, ALT+	[318]

Table 1: Summary of cell lines used in the study

Isolation of RNA/DNA

Genomic DNA for KSHV episome qPCR and TRF Southern blotting was obtained by Phenol-Chloroform extraction. Briefly, cells were resuspended in proteinase K buffer (100mM TRIS-HCl pH 8, 0.2% SDS, 200mM NaCl, 5mM EDTA) and 0.2mg/mL proteinase K was added for overnight digestion at 55°C. An equal volume of Phenol:Chloroform:isoamyl alcohol (ratio 25:24:1) was added, mixed vigorously and phase separation was achieved by centrifugation at 10,000 x g for 20min. The aqueous upper phase was collected and DNA was precipitated by addition of >2.5x volume of ice-cold 100% ethanol and gentle mixing of the resulting solution by inversion of tube. DNA was pelleted by centrifugation at 10,000 x g for 15min and washed with 70% ethanol to remove residual salt from proteinase K buffer. Material was again pelleted by centrifugation and all ethanol was removed by aspiration. The resulting pellet was air dried prior to resuspension in TE buffer and quality control of resulting genomic DNA by analysis of A260/280 absorbance ratio. In the case of TRF Southern blotting and C-circle assay, RNA was removed by treatment with RNAse A in PBS (50μg/mL) for 3h at 37°C and a second Phenol-Chloroform extraction.

RNA for RT-qPCR was isolated from cells which were homogenized by serial aspiration through a fine needle (27G) for approximately 2min in resuspension buffer supplied with RNA isolation kit (RNeasy Mini kit Qiagen #74104). The resulting suspension was processed according to manufacturer's protocol. RNA was converted into cDNA for PCR using the RevertAid First Strand cDNA Synthesis Kit (ThermoFisher #K1621) according to manufacturer's protocol.

qPCR/RT-qPCR

For the episomal maintenance assay, a standard curve of fixed number of molecules obtained by PCR using primers specific to KSHV TR region (Table 1) was calculated with Avogadro's constant. The same primers were used for qPCR of the standard curve together with 100ng of isolated DNA per condition. Signal was generated by amplification with SYBR Green JumpStart Taq ReadyMix (Sigma #S4438). In the case of qPCR using cDNA for RT-qPCR expression analysis, equivalent cDNA from 25ng of isolated RNA was amplified using SsoAdvanced SYBR Green Supermix (BioRad #172-5260). Origin of all primer sequences is indicated in Table 1[276,319].

siRNA transfection

Cells were grown to 60% confluency as judged by brightfield microscopy prior to transfection. Pools of siRNA for knockdown of target proteins were obtained from Dharmacon. For each pool, 1/1,000 final volume DharmaFECT 1 (Dharmacon #T-2001) was added to 1/200 final volume OptiMEM. The solution was incubated at room temperature for 5min to allow for formation of lipid transfection complexes. Subsequently, siRNA was added at a final concentration of 40nM and incubated together with DharmaFECT 1/OptiMEM for 20-40min at room temperature. Finally, the active transfection mix was applied to cells for 12-18h. Cells were washed with PBS and recovered in regular complete growth medium for two days prior to analysis to allow for loss of any residual protein within cells. Analysis by Western blot was carried out at day 3 post-transfection.

Primer pair	Sequence (5'-3')	Source
Telomere repeat	TTAGGGTTAGGGTTAGGGTTAGGG AATCCCAATCCCAATCCCAATCCC	This study
KSHV OriA	CAAGCACGCGCATATAACCC GGGATATGCTTCCGCCTCAT	Prof. Paivi Ojala (Univerity of Helsinki)
GAPDH	GTCTCCTCTGACTTCAACAGCG ACCACCCTGTTGCTGTAGCCAA	OriGENE #HP205798
KSHV OriLyt	CTGTCCCAGCATAGGCTC CCTGTGCCCAAATCTGTCCT	Prof. Paivi Ojala (Univerity of Helsinki)
KSHV TR1	GGGCGCCCTCTCTCTACTG CCCAAACAGGCTCACACACA	Ref. [271]
KSHV TR2	CATAAATATTCCGGATACAAGGCTCG GACTCCTCGCACAGTAGAGAGAG	Prof. Paivi Ojala (Univerity of Helsinki)
hTERT	CGGAAGAGTGTCTGGAGCAA GGATGAAGCGGAGTCTGGA	Ref. [311]

Table 2: List of PCR primers used during the course of this project

Blotting techniques

To perform dot blotting on to Nylon membrane, each sample was made up to a total volume of 80μL by addition of 2X SSC. Positively charged nylon membrane (Hybond-N+ Amersham #RPN203B) was soaked in 2X SSC for 5min. The dot blot apparatus was assembled according to the manufacturer's instructions (Bio-Dot BioRad #1706545). Vacuum was applied and wells were washed twice by addition of 200μL of 2X SSC to all wells. Samples were loaded into the desired wells and subsequently 200μL of 2X SSC was again added twice to ensure complete transfer of samples. The resulting membrane was removed from the apparatus and subjected to 365nm UV light for additional binding (120 mJ/cm^2 UV) prior to probe hybridisation.

For slot blotting, all components of the manifold (Hoefer #PR648) were stripped of any ssDNA by submersion in 0.4M NaOH for at least 3h. Each sample (<50μL) was denatured by addition of 300μL 0.4M NaOH, 10mM EDTA and incubation at 99°C for 10min. Positively charged Nylon membrane was briefly activated in water and the slot blot manifold was assembled according to the manufacturer's instructions. Wells were washed twice by addition of 300μL water. Samples were applied and subsequently wells were washed again by addition of 0.4M NaOH. The membrane was removed from the apparatus and subjected to 365nm UV light (120 mJ/cm^2 UV) followed by probe hybridisation.

Western blotting was performed essentially as described[320]. For high molecular weight transfer, 0.1% SDS was added to transfer. After blocking for 30min in TBST (0.05% v/v Tween-20) containing 5% w/v milk, antibodies were applied in the same buffer. Full list of antibodies used in this study is found in Table 2. Images of chemiluminescent signal were obtained using a BioRad ChemiDoc imager #17001402.

TRF Southern blotting was performed as follows: 5μg of gDNA was incubated overnight at 37°C with RsaI/HinfI, 15U each per reaction. The enzymes were then heat inactivated at 80°C for 20mins and the sample loaded onto a large (length >25cm) 1.5% w/v agarose/TAE gel using loading dye which contained Bromophenol Blue and Xylene Cyanol. Electrophoresis was performed overnight at 4°C, 50V until the desired separation was achieved. The gel was stained with Ethidium Bromide (5μg/mL in TAE) for 20min and imaged prior to capillary transfer. The gel was removed from the electrophoresis tray and subjected to the following washes in preparation for transfer. Depurination of DNA in the gel was achieved by a 30min wash in 0.25M HCl. Denaturation was performed with two 30min washes in 1.5M NaCl, 0.5M NaOH followed by neutralization in two 30min washes in 3M NaCl, 0.5M Tris-HCl pH 7.5. Subsequently, DNA in the gel was transferred on to positively charged Nylon membrane by capillary action. Briefly, a shallow bath of 20X SSC was

Antibody	Manufacturer	Catalogue number	Dilution
α-LANA	Millipore	MABE1109	1:250 (IF), 1:1,000 (WB)
α-PML	Santa Cruz	sc-966	1:500 (IF)
α-BLM	Abcam	ab2179	1:500 (IF), 1:1,000 (WB)
α-RAD52	Abcam	ab124971	1:2,000 (WB)
α-PolD3	Abcam	ab182564	1:5,000 (WB)
α-β-Actin	Biolegend	664802	1:2,000 (WB)
α-SLX4	Prof. John Rousse	Homemade	1:5,000 (WB)
α-H3	Abcam	ab10799	5µg/IP (ChIP), 1:1,000 (WB)
α-H3K9me3	Abcam	ab8898	5µg/IP (ChIP)
α-H3K27me3	Abcam	ab6002	5µg/IP (ChIP)
α-H4K20me3	Abcam	ab9033	5µg/IP (ChIP)
α-TRF2	Millipore	4A794	5µg/IP (ChIP), 1:1,000 (WB)
α-DAXX	Santa Cruz	sc-7152	1:1,000 (WB)
α-ATRX	Bethyl	A301-045A	1:500 (WB)
α-ASF1a	Cell Signalling	2990	1:1,000 (WB)
α-rat (HRP)	Abcam	ab97057	1:2,000 (WB)
α-mouse (HRP)	Dako	P0447	1:2,000 (WB)
α-rabbit (HRP)	Dako	P0399	1:2,000 (WB)
α-rat (Alexa 488)	Invitrogen	A1106	1:500 (IF)
α-mouse (Alexa 488)	Invitrogen	A11001	1:500 (IF)
α-mouse (Alexa 647)	Invitrogen	A21236	1:500 (IF)
α-rabbit (Alexa 488)	Invitrogen	A1108	1:500 (IF)
α-rabbit (Alexa 647)	Invitrogen	A21245	1:500 (IF)

Table 3: List of antibodies used in experiments performed for this project

used as a reservoir for electrolytes which were drawn through several layers of Whatman paper, the gel and membrane by capillary action to enable transfer of nucleic acid. A weight of approximately 3kg was placed onto the setup and transfer was allowed to proceed for two days. Subsequently, membrane was removed from transfer setup and crosslinked by exposure to UV light (120 mJ/cm^2 UV) prior to hybridization.

Alkaline phosphatase-labelled chemiluminescent probes were used for detection of telomeric DNA in C-circle assay and TRF Southern blotting. To generate these probes, telomere primer-dimer PCR was performed (primers in Table 1) followed by PCR purification (Qiagen #28104) and labelling reaction using AlkPhos Direct Labelling reagents (Amersham RPN3680). The manufacturer's protocol was followed throughout except for the labelling reaction which was allowed to proceed for 45min at 37°C. Probe was hybridized in buffer supplied with the kit overnight and washes with buffers outlined in the manufacturer's protocol were performed at 55°C. Chemiluminescent signal was generated by addition of CDP-Star substrate (Roche #12 041 677 001).

PICh

Experiment was performed essentially as described[321], in collaboration with Dr Paulina Marzec (Francis Crick Institute). $1x10^{10}$ BJAB cells were grown in suspension, harvested, and crosslinked in 1% w/v Formaldehyde for 30min at room temperature. The cells were pelleted by centrifugation at 3,200 x g for 15min or until supernatant was completely clear. These centrifugation conditions were used throughout to pellet cells between washing steps. The cells were washed twice with PBS containing 1mM PMSF. The pellets were harvested sequentially owing to the large number of material needed for the assay and frozen at -80°C for storage between harvests. The thawed pellet was washed in sucrose wash buffer (0.3M sucrose, 10mM HEPES-NaOH pH 7.9, 1% Triton X-100, 2mM MgOAc). RNA was removed by re-suspension of pellet in 0.5% Triton X-100 and incubation overnight at 4°C with 1.5 mg/mL RNase A. Subsequently, the resulting chromatin was pelleted by centrifugation as described above and washed six times with PBS containing 1mM PMSF. Finally, chromatin was re-suspended in high salt buffer (10mM HEPES-NaOH pH 7.9, 100mM NaCl, 2mM EDTA pH 8, 1mM EGTA pH 8, 0.2% SDS, 0.1% sodium sarkosyl, 1mM PMSF) prior to chromatin shearing by sonication with a Qsonica Q700. The resulting solution was warmed up to 58°C, added to Streptavidin

resin (ThermoFisher #20361), and incubated overnight at room temperature on a rotator. The pre-cleared chromatin was further purified by centrifugation at 16,000 x g through a Sephacryl S-400 column (GE #17060901). Next, SDS was added to a final concentration of 0.2% prior to hybridization with either scrambled or telomere-specific capture probes. These probes were desthibiotin-coupled, 2'flourinated LNA as described[188,195]. Hybridisation was achieved by the following temperature cycle: 3min at 25°C, 7min at 71°C, 3h at 37°C, 3min at 25°C. The resulting chromatin was pelleted by centrifugation at 16,000 x g for 15min. Magnetic streptavidin beads (ThermoFisher #65001) were washed twice in low salt wash buffer (10mM HEPES-NaOH pH 7.9, 30mM NaCl, 2mM EDTA pH 8, 1mM EGTA pH 8, 0.2% SDS, 0.1% sodium sarkosyl, 1mM PMSF) before addition to chromatin resuspended in H_2O and capture overnight at room temperature. The next day, beads were washed six times in high salt wash and once in low salt wash with the same composition as described. Beads were transferred to a low protein binding 15mL tube and washed twice 5min with high salt wash at 42°C, 1000rpm for 5min. Elution of material from beads was achieved by re-suspension in 75% high salt wash, 25% D-biotin (ThermoFisher #1595) and incubation at room temperature, shaking at 1000rpm followed by incubation for 10min at 65°C. The supernatant containing the eluted DNA-protein hybrids was transferred three times into new tubes with intermittent immobilization of any remaining magnetic beads to remove them completely. Protein in the resulting solution was precipitated with 15-20% TCA for 10min at 4°C followed by centrifugation at 16,000 x g for 15min. Supernatant was removed from pellet and tubes filled with pre-chilled 100% acetone. Protein was re-suspended by vortexing tubes and again pelleted by centrifugation as in previous step. Wash with 100% acetone was repeated once. The protein pellet was resuspended in crosslink reversal solution (50mM Tris-HCl pH 8.8, 2% SDS, 0.5M 2-mercaptoethanol) and analysed by PAGE/silver staining using SilverQuest kit (ThermoFisher #LC6070) following manufacturer's protocol. Bands were excised and sent for analysis by mass spectrometry to Taplin group, Harvard.

Chromatin Immunoprecipitation (ChIP)

Cell were grown on 15cm dishes (one per pulldown) to a confluency of 80% and fixed in 10mL 1% Formaldehyde/PBS for 10mins at room temperature. Reaction was quenched by addition of 500µL of 2.5M Glycine to each plate. The cells were harvested by scraping in 3mL of 0.05% Tween-20/PBS. Cells were pelleted by centrifugation at 1,200 x g for 10min and washed once with PBS. Pellets for each condition were pooled, resuspended in 10mL Lysis buffer 1 (50mM HEPES-KOH pH 7.9, 140mM NaCl, 1mM EDTA pH 8, 10% Glycerol, 0.5% NP-40, 0.25% Triton X-100, supplemented with complete protease inhibitor cocktail (ROCHE #4693159001) and incubated at 4°C on a platform rocker for 10min. The cells were pelleted by centrifugation at 1,350 x g for 5min at 4°C. The resulting pellet was re-suspended in Lysis buffer 2 (10mM HEPES-KOH pH 7.9, 200mM NaCl, 1mM EDTA pH 8, 0.5mM EGTA, and protease inhibitors as in previous buffer) and incubated at room temperature for 10min, gently rocking. Solution was gently homogenised using a dounce homogeniser with tight pestle on ice 20x. The resulting isolated nuclei were pelleted by centrifugation at 1,350 x g for 10min. The pellet was resuspended in Lysis buffer 3 (10mM HEPES-KOH pH 7.9, 100mM NaCl, 1mM EDTA, 0.5mM EGTA, 0.1% sodium deoxycholate, 0.5% sodium lauroylsarcosine, and protease inhibitors as before) and sonicated using QSonica as in PICh (Amplitude 70, 3min, pulse ON 15sec, pulse OFF 45sec). The samples were transferred to 1.5mL tubes and spun down at 16,200 x g for 10min at 4°C. Supernatant containing chromatin was transferred to a new tube and 1/10 total volume 10% Triton X-100 was added by gentle inversion. DNA concentration was determined in the resulting chromatin solution and normalized between conditions. Magnetic Protein A/G (at ratio of 1:1) beads were washed three time with 0.5% BSA/1mM PMSF/PBS and 100µL of washed beads were added to each sample for preclearing at 4°C for 1h in an overhead rotator. Beads were removed with magnetic stand and primary antibodies were added overnight at 4°C, gently rotating (see Table 2 for antibodies). On the next day, 100µL of blocked beads was added to each sample for 2h at 4°C for capture of

antibodies in solution. The beads were collected on the magnetic stand and washed with the following buffers, 1mL per tube: five washes with RIPA buffer (50mM HEPES-KOH pH 7.55, 250mM LiCl, 1mM EDTA, 1% NP-40, 0.7% sodium deoxycholate) and one wash with TE/50mM NaCl. Residual TE was removed by pelleting beads by centrifugation at 950 x g for 3min. 210µL of elution buffer (50mM Tris-HCl pH 8, 10mM EDTA, 1% SDS) was added and beads were incubated at 65°C, 1500rpm for 30min. Finally, beads were spun down briefly in a microcentrifuge and supernatant containing eluted material was collected. Crosslink was reversed by incubation at 65°C overnight and DNA was purified by Phenol:Chloroform extraction as described in previous section.

TRAP assay

2,000 cells were lysed on ice in 1X CHAPS buffer (10mM Tris-HCl pH 7.5, 1mM $MgCl_2$, 1mM EGTA, 0.1mM Benzamidine, 5mM β-mercaptoethanol, 0.5% CHAPS, 10% Glycerol) for 30min. Lysate was cleared by centrifugation at 15,000 x g for 15min. TRAP reactions were set up as described in the manufacturer's protocol (Millipore #S7700) with the following modifications: i) Lysate was incubated with substrate for 1h at 25°C prior to PCR; ii) Samples were electrophoretically fractionated in 1X TBE on a pre-cast non-denaturing TBE 10% polyacrylamide gel; iii) Gel was stained with 1X SYBR Gold (Invitrogen #S11494)/1X TAE for 30min in the dark followed by triple de-stain in 1X TAE, 5min each.

C-circle assay

For C-circle assay, varying amounts of isolated DNA were added to a total volume of 50μL Φ29 reaction buffer (8mM DTT, 1mM dNTPs, 2X Φ29 reaction mix (NEB #M0269), 0.2mg/mL BSA, 0.1% Tween-20) in the presence or absence of 7.5U Φ29 polymerase (NEB #M0269). Rolling circle amplification of circular DNA was allowed to proceed for 8h at 30°C. Subsequently, the reaction was terminated by denaturation for 20mins at 80°C. Dot blot onto Nylon membrane and Southern blotting for telomeric DNA was performed as described above for slot blotting.

BIR foci assay

Cells were enriched in G2/M phase of cell cycle by sequential treatment with 2mM Thymidine (Sigma #T9250) for 16h, recovery in normal medium for 6h, and treatment with Cdk1 inhibitor RO-3306 (Sellekchem #S7747) for 12h. During the final 1h of the RO-3306 treatment, medium was supplemented with 10μM EdU to pulse-label DNA synthesis. For flow cytometry, cells were harvested by trypsinisation and fixed in 4% Formaldehyde/PBS for 15min at room temperature. The fixed cells were washed three times with PBS followed by permeabilization via gentle addition of pre-chilled 100% Methanol and incubation overnight at -20°C. The cells were pelleted and washed once with PBS prior to Click-iT reaction. Alexa488 was covalently coupled to incorporated EdU by Click-iT chemistry using Click-iT Plus imaging kit (ThermoFisher #C10637) following the manufacturer's protocol. Finally, cells were counterstained with DAPI at 0.2μg/mL for 10min at room temperature prior to flow cytometry. For cells grown on cover slips, the procedure outlined above was followed essentially as described by incubation/washing cover slips in a 12-well plate with the solutions described. This was followed by standard IF-FISH procedure as described in detail below which was fully compatible with the Alexa488 label coupled to EdU by Click-iT chemistry. The resulting cover slips were finally mounted on to slides using ProLong Gold prior to analysis by microscopy.

Telomere FISH

Cells were arrested in metaphase by addition of 0.1μg/mL (final concentration) colcemid into complete growth medium for 2h. After dissociation of cells by trypsinization and washing with PBS, cells were treated with hypotonic solution (0.075M KCl) for 10min at 37°C. Fixation was carried out by dropwise addition of ice-cold methanol:acetic acid (3:1) to the pellet, which was resuspended under gentle agitation. Resulting metaphase preparation was stored at -20°C. Frosted slides were submerged briefly in 45-50% acetic acid and the suspension of fixed cells was dropped evenly across slide from a height of about 70cm. Slides were drained immediately from all remaining solution and air dried for at least 1h.

Rehydration was carried out with PBS for 5min followed by re-fixation in PBS containing 4% Formaldehyde for 2min. Formaldehyde was removed by three washes with PBS and slides were treated with 1mg/mL Pepsin in 10mM Glycine pH 2.0 for 17min at 37°C. Slides were washed twice briefly in PBS and fixed again with 4% Formaldehyde in PBS for 4min. Formaldehyde was again washed out with PBS and subsequently slides were de-hydrated in an ethanol series (70%, 85%, 100%). Slides were allowed to air dry completely. Telomere PNA probe (TelC-Cy3, PANAGENE #F2001) was applied at a final concentration of 4nM in hybridization buffer (10mM Tris-HCl pH 7.5, 70% deionized formamide, 0.5% ROCHE Blocking reagent #11096176001) and denatured on slide at 75°C for 1min. Hybridization was carried out at room temperature for 1h 30min or overnight at 4°C. Slides were washed with Wash #1 (10mM Tris-HCl pH 7.5, 1mg/mL BSA, 70% Formamide) twice for 15min followed by Wash #2 (100mM Tris-HCl pH 7.5, 150mM NaCl, 0.08% Tween-20) three times for 5min. Slides were de-hydrated with the ethanol series as before and air dried. Cover glass was mounted using ProLong Gold with DAPI (ThermoFisher #P36931).

Telomere Chromosome-orientation (CO)-FISH

Incorporation of nucleoside analogues was achieved by addition of 7.5μM BrdU/2.5μM BrdC to complete growth medium for 18h (SLK and EaHy.926 cell lines) which corresponds to roughly 3h below population doubling time to avoid double labelling. Cells were harvested and Metaphase spreads were obtained as described in the Telomere FISH method above. However, slides were air dried for at least 12h for CO-FISH.

Slides were treated with 0.5μg/mL RNAse A in PBS for 30min at 37°C and subsequently stained with 10μg/mL Hoechst 33258 in 2XSSC for 15min. Single-stranded nicks were introduced by exposure of slides in a shallow bath of 2X SSC to UV light (365nm) for 1h. 10U/μL of Exonuclease III (Promega #M1811) was applied in buffer supplied with the kit at 37°C twice for 1h. The slides were dipped briefly in PBS, H_2O, and then left to dry completely overnight. The first probe (TelG-Alexa488, PANAGENE #F1008) was applied at 4nM in hybridization buffer (10% Dextran Sulfate, 50% deionized Formamide, 2X SSC) for 1h 30min. Slides were briefly washed in modified Wash #1 (10mM Tris-HCl pH 7.5, 1mg/mL BSA, 70% Formamide) and second probe was applied (TelC-Cy5, PANAGENE #F1003) at 4nM in the same hybridization buffer for 1h 30min. Slides were washed twice in Wash #1 (10mM Tris-HCl pH 7.5, 1mg/mL BSA, 70% Formamide) for 10min followed by two washes in 2XSSC at 37°C for 10min. Finally, slides were three times in Wash #2 (100mM Tris-HCl pH 7.5, 150mM NaCl, 0.08% Tween-20) for 5min, dipped in H_2O, air dried, and a cover slip was mounted using ProLong Gold with DAPI.

Immunoflourescence (IF)-FISH

Cells were grown on glass cover slips (diameter 13mm, thickness 0) in 12-well plates to 80% confluency. Cytoplasm was pre-extracted by placing coverslips on ice in pre-chilled 0.5% Triton X-100/PBS for 5min. This solution was removed, and the cells were fixed with 2% Methanol-free Formaldehyde in PBS for 15min. Formaldehyde

was washed out with PBS and the coverslips were stored in 0.1% Sodium Azide/PBS at 4°C prior to staining.

Cover slips were blocked in antibody dilution buffer (ADB; 10% Goat Serum, 0.1% Triton X-100, 0.1% Saponin, 1X PBS) for 30min. Primary antibodies were applied at dilutions indicated in Table 3 for 1h followed by three washes in PBST (0.05% Tween-20, 1X PBS) for 5min. Corresponding goat secondary antibodies from Table 2 were applied for 1h. Previous and all subsequent steps were carried out on cover slip in the dark. Two washes with PBST and one wash with PBS of 5min each were carried out followed by re-fixation in 2% Methanol-free Formaldehyde for 5min. Cover slips were dipped in H_2O and air dried. Telomere PNA probe (TelC-Cy3, PANAGENE #F2001) was applied at a final concentration of 4nM in hybridization buffer (10mM Tris-HCl pH 7.5, 70% deionized Formamide, 0.5% ROCHE Blocking reagent #11096176001) and denatured on slide at 85°C for 1min 30sec. Hybridization was carried out at room temperature for 1h. Cover slips were washed twice in Wash #2 (TdL recipe, no BSA) for 15min followed by three washes of 5min with PBS. Cover slips were briefly dipped in H_2O, air dried and mounted in pairs on to a frosted slide using ProLong Gold with DAPI.

IHC-FISH

Slides were heated at 65°C for 10min to melt paraffin and washed twice 3min in Xylenes (mixture of isomers). Subsequently, slides were washed in the following sequence of washes (3min each): Xylenes:Ethanol 1:1, twice in 100% Ethanol, 85% Ethanol, 70% Ethanol, 50% Ethanol. Finally, slides were rinsed in cold water. From now on, slides were always immersed in solution unless otherwise indicated to avoid drying out of the specimen. Antigen retrival was carried out by immersion of slides in 10mM Sodium Citrate, 0.05% Tween-20 pH 6. Submerged slides were heated in microwave at 700W for 10min and allowed to cool for 10min. This was repeated once. Subsequently, slides were again immersed in water and then washed twice for

3min each in 70%, 85%, 100% Ethanol in this order. Slides were allowed to dry out completely and hybridization mix was applied as described for IF-FISH. Denaturation was achieved by placing the slide at 84°C for 3min. Hybridization was allowed to proceed for 2h. This was followed by two washes in Wash #1 (10mM Tris-HCl pH 7.5, 1mg/mL BSA, 70% Formamide) for 15min and three washes in PBST for 5min each. Subsequently, primary and secondary antibodies were applied as described for IF-FISH. Washing and mounting was again performed as described for IF-FISH.

Image Analysis

Automated quantification of integrated mean intensity for each nuclear telomere FISH signal was carried out as a proxy for relative telomere length. To this end, multichannel greyscale images (telomere FISH, DAPI/Hoechst counterstain) were automatically imported and split into single channels using a custom FIJI[322] macro (Figure 8) and built-in batch processing mode. Resulting image pairs were imported into CellProfiler[323] and analysed using a custom pipeline. Overall, the performance of this pipeline was robust and required only minor adjustments between hybridizations related to automated detection of foci by thresholding. A representative pipeline is depicted in Figure 9. Briefly, a binary mask for nuclei was created by thresholding the DAPI/Hoechst counterstain image. Signal corresponding to telomere FISH was filtered to enhance edges of foci and a second binary mask was generated by thresholding using Otsu's method[324]. These masks were laid over the raw image of telomere FISH signal and quantification of signal intensity was achieved by determination of integrated mean intensity (signal area x mean intensity, [AU]) for each focus. For manual counting, analysis was computationally blinded using a Bash script which renames images randomly (Courtesy of Dr Mark Robinson, Feldhahn group).

Microscopy

Wide field images of Metaphase spreads were obtained manually on a Nikon Eclipse E400 upright microscope equipped with a 100x oil-immersion objective and Hamamatsu Orca camera. Image acquisition was controlled using Micromanager software[325] and performed by widefield microscopy as described for telomere FISH. For confocal images of BIR foci, an inverted laser scanning Olympus FLV1000 confocal setup was employed. 6-8 Z-stacks of 300nm were captured sequentially for each position which were then converted into a Maximum intensity projection for visualisation and analysis. Images used for co-localization analysis were acquired using a spinning disk confocal setup. Specifically, an inverted Nikon TiE microscope equipped with a spinning disk module (Yokogawa CSU-X1), an emission beam splitter unit and dual camera was used to capture two channels simultaneously with a large field of view (up to 20 cells per image). Using a 63x oil-immersion objective, xy co-ordinates and z-offset of fields of view were defined for each cover slip mounted into #1.5 glass-bottom 24-well Sensoplate (Greiner) using built-in Nikon NIS elements software. Subsequently, acquisition of 300nm interval, 9-step Z-stack was carried out automatically for every position at high speed and resolution.

Clonogenic Assay

500 cells per well were seeded into a 6-well plate and grown for 10-14 days until defined colonies were visible in untreated control conditions. Cells were washed with PBS and fixed using 4% Formaldehyde in PBS for 10min. Formaldehyde was washed out with fresh PBS and colonies stained in 0.5% Crystal Violet for 1-2h. Excess stain was removed under running water and plates dried completely for at least 24h. Colony counts were obtained by automated imaging and analysis using a GelCount system (Oxford Optronix).

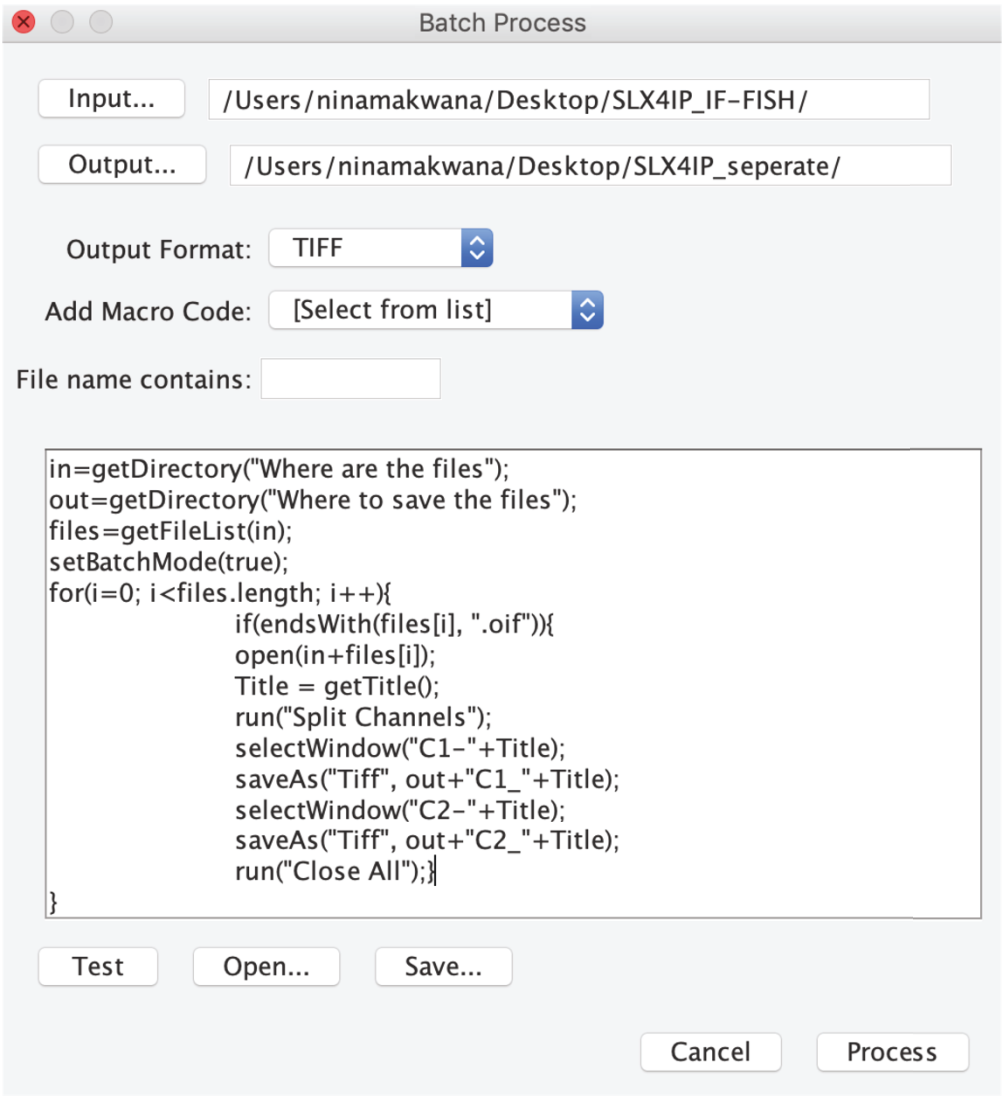

Figure 8: Channel separation batch macro in FIJI. Once triggered, this code prompts the user with a window which enables selection of input and output folder. Subsequent if loop will apply split channels function of FIJI to each image and save separated channels as a .tiff file named channel number + title of image.

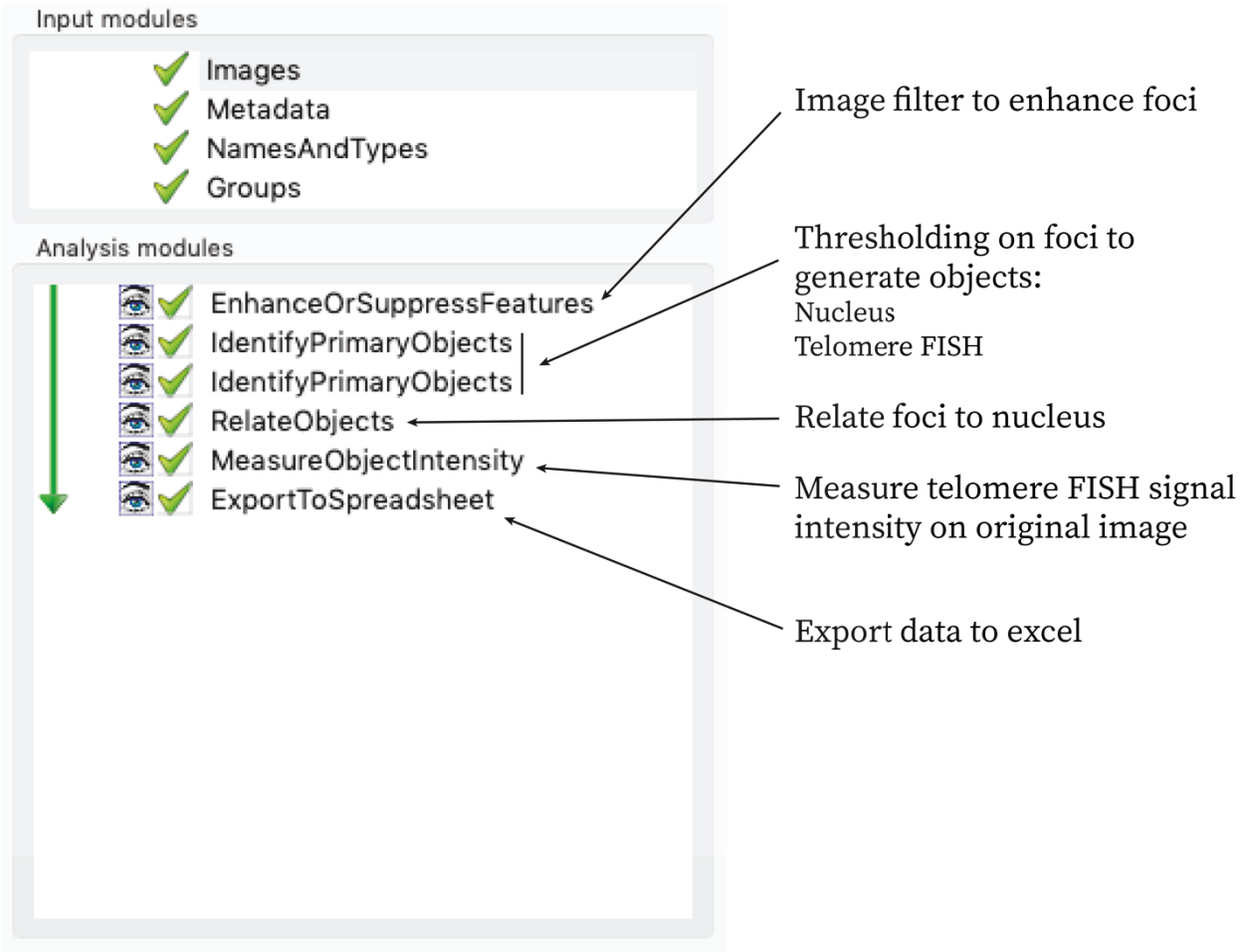

Figure 9: CellProfiler pipeline for automated telomere qFISH. Modules which were used for the analysis of MIPs are shown on the left. Briefly, images were filtered to enhance foci and thresholding was achieved using the three-class Otsu method. Each focus was related to the corresponding nucleus. Fluorescence intensity measurement was carried out in the area of each telomere object on the original image as defined in previous module (Mean intensity, integrated mean intensity, number of foci per nucleus). Finally, data was exported into an excel table.

De novo KSHV infection

iSLK rKSHV.219 producer cells[326] were cultured to 60% confluency and lytic replication was induced by treatment with 1μg/mL Doxycyclin and 1.2mM Sodium butyrate for 72h. This system allows the distinction of latent and lytic KSHV replication in infected cells by the presence of two fluorescent markers on the viral genome: i) Constitutive expression of GFP under human EF1-α promoter; ii) RFP under the control of the main lytic promoter of KSHV[327]. In addition to this, iSLK rKSHV.219 contains a puromycin resistance cassette on the KSHV genome as well as RTA, the main lytic activator as discussed in the introduction, under the control of a doxycycline-inducible promoter on an exogenous plasmid[282]. Cells were cultured to 60% confluency and lytic replication was induced by treatment with 1μg/mL Doxycyclin and 1.2mM Sodium butyrate for 72h The resulting supernatant was cleared of cells by centrifugation at 500 x g for 5min and drawn through a 0.45mm filter. Target SLK, U2OS, or EA.hy926 cells were seeded into 6-well plates at 60,000 cells per well on the day prior to infection. The virus preparation was applied to target cells in complete medium supplemented with 8μg/mL Polybrene. Infection was enhanced by spinoculation at 2,300rpm, 32°C for 1h 30mins and then incubated overnight at 37°C in the humidified incubator. Infectious medium was replaced with fresh medium the next day. Efficiency of infection was judged 48h post-spinoculation by observation of GFP^+ cells as a marker for rKSHV episomes under a fluorescent microscope. Using this approach, about 10-50% infection was routinely obtained as judged by GFP^+ cells three days post-infection. Stable 100% $KSHV^+$ cell lines were obtained by selection with Puromycin as described earlier for at least 1 week. All analysis was carried out at >20 days post-infection. At this time, there was a complete absence of RFP^+ cells which would be indicative of lytic replication.

RESULTS

Chapter 1: Protein markers of DNA damage and ALT activation are enriched at telomeres upon latent infection with KSHV

Introduction

The composition of telomeric chromatin may be altered in complex ways in response to diverse stimuli including DNA damage. This includes changes in proteins bound to the telomeric DNA. The present study aims to characterise the telomere-associated proteome in response to latent KSHV infection. In the following chapter, global analysis of the telomeric proteome by PICh coupled to mass spectrometry is performed in BJAB cells +/- latent KSHV. Key changes in telomere-associated proteins are subsequently validated by IF-FISH. The cell line models examined in this thesis are immortal cancer cell lines and as such, low level constitutive DNA damage at telomeres and globally is anticipated. Importantly, all cell lines are reported to be negative for EBV infection and have intact p53 signalling (ATCC). KSHV infection is carried out and all cell lines are analysed at >20 days post-infection and selection to ensure tight latency and near 100% KSHV infection as judged by GFP^+ cells in culture (Figure 11). Therefore, with these analyses an overview of key changes in the telomeric proteome upon latent KSHV infection is given. Some of the changes detected in this chapter are the basis for investigation carried out in subsequent parts of this work.

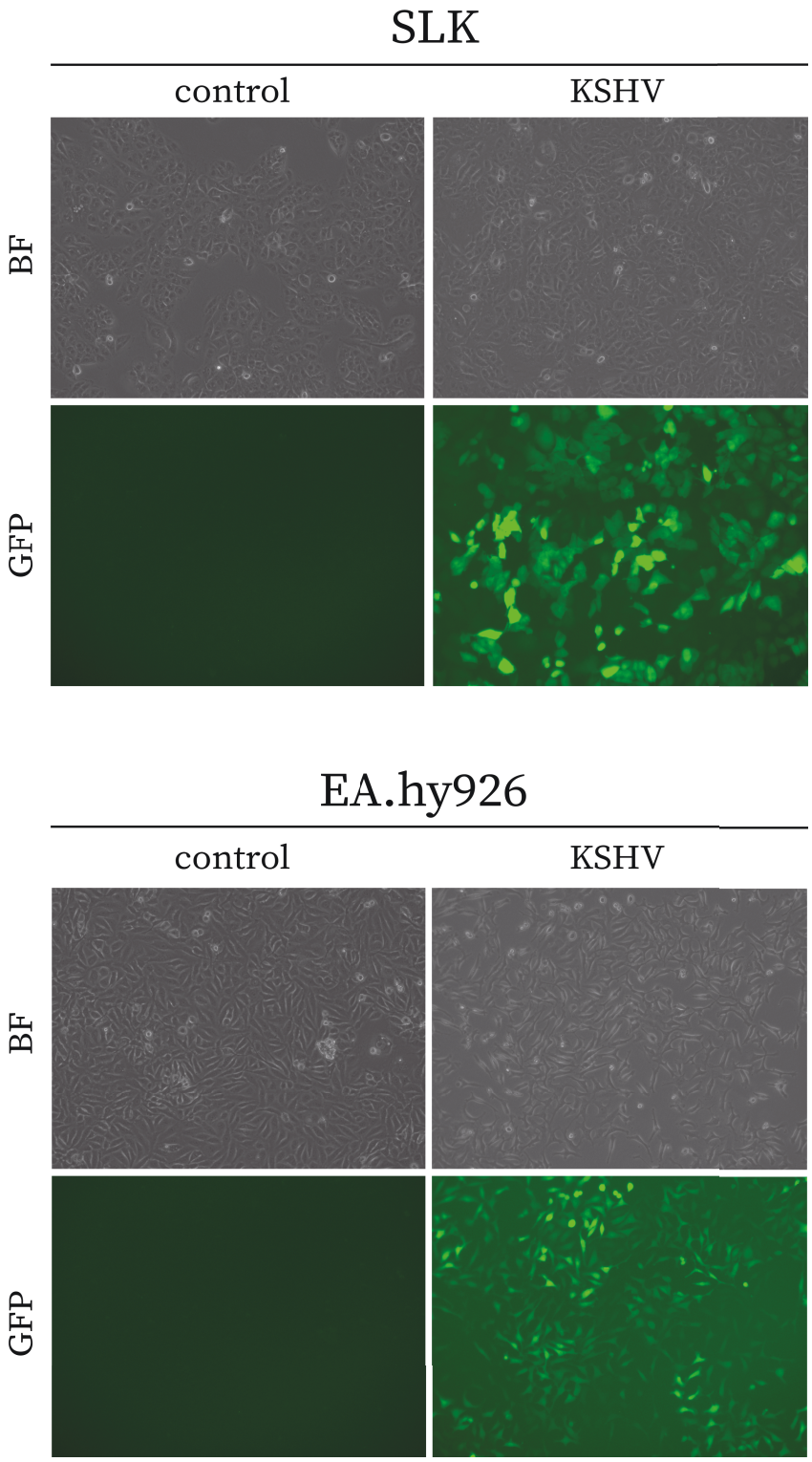

Figure 10: Example of rKSHV.219 infected cells. Representative images of cells at the time point of analysis are shown. GFP corresponds to the presence of the KSHV genome as discussed in text.

Detection of changes in telomeric proteome upon KSHV infection in BJAB cells by PICh

Proteomic analysis by PICh was performed in collaboration with Dr Paulina Marzec (Francis Crick Institute). Enrichment of telomere-associated proteins was carried out in parallel with a scramble control sequence and resulting material was analysed by mass spectrometry (Taplin group, Harvard Medical School). Figure 11 presents an overview of the PICh protocol. Enriched material from PICh was analysed by PAGE and silver staining. There was a clear enrichment for protein in the telomere pulldown with characteristic band pattern[188] presumably associated with shelterin and other bound telomeric proteins (Figure 12). Analysis of mass spectrometry data was carried out by calling spectral identity using SEQUEST algorithm[328]. This analysis was performed by Dr Ross Tomaino, Taplin group. In contrast to labelled mass spectrometry such as SILAC, this method is semi-quantitative and confirmation of any enrichment by additional experimentation is essential. The data from this experiment contained a measure for the number of unique peptides for each protein detected by reference to a database of the human proteome. Data was also referenced to the KSHV proteome. No peptides corresponding to KSHV proteins were detected int his experiment. Enrichment at telomeres was inferred by subtraction of number of unique peptides from scrambled control pulldown.

Shelterin proteins are selectively enriched in telomere probe pulldown fractions and increased in KSHV$^+$ cells

First, the robustness of the data was queried by analysis of enrichment for key telomeric protein complex shelterin in telomere-specific pulldown. Less than 1 unique peptide was detected for all shelterin proteins in a scrambled control pulldown, whereas a telomere-specific pulldown resulted in strong enrichment for such proteins (Table 4). The only shelterin protein, which we did not detect in this experiment is TPP1. This is in line with previously published analysis of the telomeric proteome in human cells by PICh[188,195,321] where TPP1 is also absent.

Comparison of shelterin enrichment in control and KSHV infected cells indicated that there is an approximately threefold increase in the enrichment of shelterin proteins upon infection with KSHV. In summary, analysis of these data indicated that telomeric pulldown resulted in strong enrichment for established telomere-associated proteins, and there may be an increase in the binding of shelterin proteins in response to infection. Such enrichment is difficult to interpret since no reports have examined the consequences of increased shelterin at telomeres. Possible explanations for this observation include a decrease in nucleosome density upon infection. Overall, these data indicate strong enrichment of shelterin proteins in telomere pulldowns, which confirms the robustness of loci-specific enrichment by PICh.

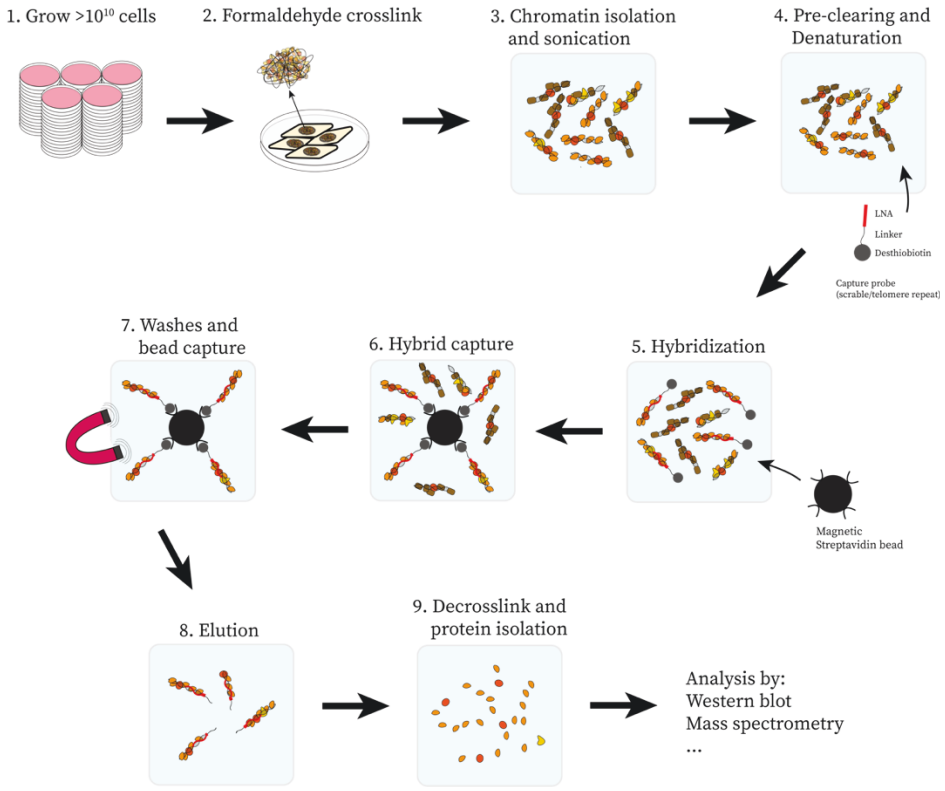

Figure 11: Overview of PICh protocol. Analysis of proteins associated with specific DNA sequences in cells of interest is performed by formaldehyde crosslinking, sonication, and hybridization capture using a LNA probe. Subsequent recovered material may be analysed by a variety of means including Western blot and mass spectrometry. Pulldowns are performed with probe specific for telomeric DNA in comparison to a scrambled control sequence during the course of this study.

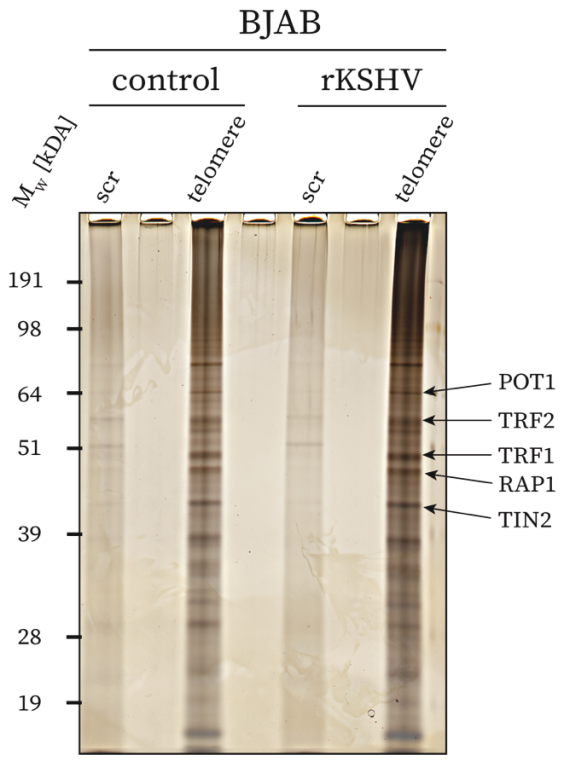

Figure 12: Proteins are enriched in telomere pulldown. Silver-stained polyacrylamide gel of material recovered from PICh. Equal amount of chromatin was used for each pulldown. In both uninfected co-culture and infected BJAB cells, there is significant and even recovery of protein in telomere-specific pulldown. Putative position of key shelterin proteins on the gel is indicated on the right, molecular weight ladder positions indicated on the left. Image obtained by analysis of fraction of material submitted for mass spectrometry.

	BJAB	
Protein	**ΔUP control**	**ΔUP KSHV⁺**
POT1	28	96
TRF1	29	92
TRF2	58	138
RAP1	35	109
TIN2	35	123
TPP1	nd	nd

Table 4: Selective increase in shelterin binding at telomeres in response to KSHV. Data is presented as the difference in the number of unique peptides upon subtraction of values obtained from scrambled control pulldown. TPP1 was not detected in any condition (nd). Delta UP denotes telomere-specific difference in number of unique peptides (telomere pulldown-scramble control pulldown).

Factors involved in classical NHEJ are decreased and MMEJ repair factors are increased at telomeres of KSHV infected cells

Next, we examined the presence of proteins involved in NHEJ at telomeres of infected cells. The data set contained DNAPk, Ku70, and Ku80, three of the main proteins involved in classical NHEJ. Other key factors such as Ligase 4, XRCC4, and Artemis were absent in the data. Overall, classical NHEJ factors showed a 1.5-2 fold decrease in their enrichment at telomeres in infected cells (Table 5A). A number of factors involved in the alternative NHEJ pathway (MMEJ) were detected including MRN complex, PARP1, Ligase 1, Ligase 3, and XRCC1 (Table 5B). MRN complex was significantly enriched at telomeres in response to infection, with a 4.5 fold increase in RAD50 and NBS1 enrichment as well as a 2.5 fold increase in MRE11. In addition to this, Ligase 3 was enriched threefold upon infection and XRCC1 was only detected in infected cells. However, Ligase 1 was not detectable in infected cells and was present with two unique peptides in control co-cultured cells. In addition to this, other important MMEJ proteins such as Polθ and CtIP were absent in all samples tested. Overall, these data provide an indication that NHEJ may be differentially enriched at telomeres in response to KSHV infection in BJAB cells. Specifically, the data suggest that classical NHEJ factors are found decreased at telomeres, whilst MMEJ proteins are relatively enriched.

However, it is important to note that the factors, which are shown to be differentially enriched in this analysis are not necessarily specific markers for the activity of these pathways at telomeres. As discussed, Ku70/80 is found at telomeres in conditions where there are no fusions and is in fact inhibited potently by TRF2, which was found differentially enriched as well (Table 5). MRN complex and CtIP-mediated resection is again not exclusive to cNHEJ but also occurs in the context of HR. There are additional drawbacks to this analysis. It does not take into account post-translational modification

A

	BJAB	
Protein	**ΔUP control**	**ΔUP KSHV⁺**
DNAPk	134	88
Ku70	32	26
Ku80	42	26
Lig4	nd	nd
XRCC4	nd	nd
Artemis	nd	nd

B

	BJAB	
Protein	**ΔUP control**	**ΔUP KSHV⁺**
MRE11	30	81
RAD50	36	160
NBS1	14	69
PARP1	11	24
Lig1	2	nd
Lig3	3	10
XRCC1	nd	6
Polθ	nd	nd
CtIP	nd	nd

Table 5: Differential enrichment of cNHEJ and MMEJ at telomeres upon infection. Main proteins involved in either pathway (table A: cNHEJ and table B: MMEJ respectively) are listed above and where detected (nd, not detected) number of unique peptides specifically at telomeres are given for each condition as indicated.

which is known to govern the activity of many DDR factors. For example, the detection of DNAPk by this method gives little insight into the level of DNAPk-mediated signalling since this is crucially dependent on phosphorylation. In summary, the data presented solely indicate the possibility of differential enrichment of these proteins at telomeres.

ALT HR factors are relatively enriched at telomeres in KSHV infected cells

Another class of DDR proteins, which were present in the data are factors involved in HR. One of the main factors that binds ssDNA prior to strand invasion in HR reactions is RPA. All three subunits of the RPA heterotrimer were found enriched at telomeres in response to latent KSHV infection (Table 6). Another protein involved in HR is RAD51 paralogue C and this was detected in the present data set. This protein may be present at telomeres of both uninfected and infected cells at telomeres (Table 6). No peptides referenced to RAD51 or RAD52 were detected. Further, factors involved in the resolution of HR intermediates specifically were detected at telomeres in our data set. Strikingly, the data show an almost 10 fold increase in SLX4 nuclease scaffold and key accessory protein SLX4IP and ERCC4 nuclease in KSHV infected cells (Table 6). On the other hand, SLX4-associated nuclease FEN1 showed a twofold decreased enrichment at telomeres in response to infection. Therefore, a consistent enrichment of key markers of active HR at telomeres was observed in infected cells with the exception of FEN1 nuclease. Interestingly, FEN1 and ERCC4 are interchangeable nucleases, which may form part of the SLX4-mediated cleavage scaffold involved in HR. This implies that there may be specific modulation of the binding of HR proteins, which may be addressed and confirmed by further experimentation.

ALT-specific nuclear orphan receptor binding to telomeres[195,329] was detected in the present data. NR2C2 enrichment at telomeres was increased sevenfold in response to infection and NR2C1 was only detected in infected cells exclusively (Table 6). Other ALT-specific factors were detected at telomeres at low levels. These include BLM helicase, which was found decreased in response to infection as well as changes in PML and associated proteins. There was a subtle decrease in PML enrichment at

	BJAB	
Protein	**ΔUP control**	**ΔUP KSHV⁺**
RPA1	12	41
RPA2	1	5
RPA3	nd	2
RAD51C	1	1
RAD52	nd	nd
SLX4	6	51
SLX4IP	1	17
ERCC4	1	12
FEN1	14	6
NR2C2	2	14
NR2C1	nd	1
BLM	6	1
PML	4	2
ATRX	nd	nd
DAXX	1	nd
Sp100	1	nd

Table 6: Increased enrichment of ALT HR factors at telomeres of infected cells. Analysis of proteins involved in HR and ALT was carried out in analogy to Table 1 and 2. Key factors involved in each step of HR reaction as well as selected ALT-specific telomeric proteins are listed.

telomeres in response to infection as well as a loss of DAXX and Sp100, which were undetectable in infected cells. ATRX was not detected in any conditions. Given that loss of DAXX and ATRX from PML bodies at telomeres is associated with ALT, confirmation of this phenomenon by alternative means may yield data in support of ALT activation.

To summarise, semi-quantitative analysis of the telomere-associated proteome in BJAB cells in response to latent infection with KSHV showed broad modulation of protein binding to telomeres in response to the virus. Specifically, this suggests that KSHV infection may modulate telomeres in a manner where, i) shelterin enrichment is increased, ii) NHEJ pathways were shifted towards MMEJ, and iii) ALT telomere maintenance by HR is active. It is important to note that the analysis performed has several important limitations. The complexity of the experiment meant that it was performed in isolation without biological replicates. Label-free spectral peak calling mass spectrometry is semi-quantitative and results where fewer than three unique peptides are detected are susceptible to considerable errors in this analysis. In awareness of these limitations, I next aimed to examine whether these changes in the telomeric proteome upon infection are reproducible and detectable using different cell line models and experimental methods. Specifically, I took the data set as a starting point for investigation into enrichment of proteins involved in ALT at telomeres in response to KSHV infection.

Preliminary analysis suggests the presence of APBs upon KSHV infection

To investigate whether the association of telomeres with ALT factors observed by PICh in KSHV-infected cells could relate to the activation of ALT, I analysed KSHV-infected and mock-treated control cells for presence of ALT-associated PML bodies (APBs) using IF-FISH. This was performed in an independently generated KSHV+ cell line, SLK. Indeed, significant telomere clustering was observed in KSHV-infected interphase cells (examined in detail in Chapter 2) and such signals co-localized with PML and BLM, indicative of the presence of APBs (Figure 13). Such structures were observed in infected cells specifically and in 5% of the overall population which is reminiscent of their incidence in established models of ALT[200]. The occurrence of APBs in a subset of infected cells further supports the notion of ALT telomere maintenance upon latent infection.

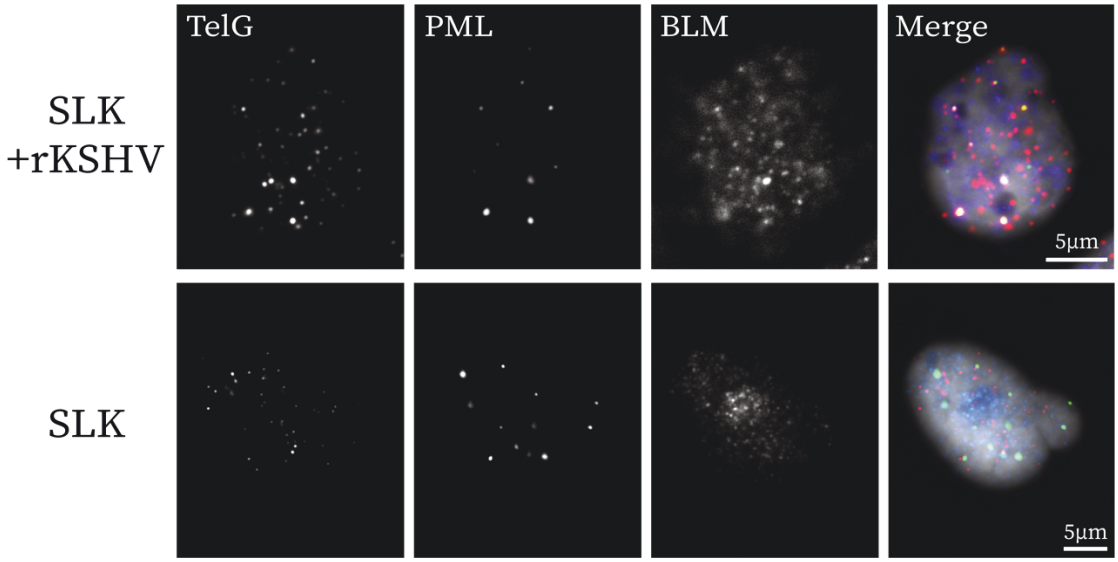

Figure 13: Occurrence of APBs in KSHV infected cells. Representative micrograph is shown from SLK cell line infected with latent KSHV. Similar phenomena occur in other cell lines infected with KSHV, which show telomere clustering, analysed in later chapters. Telomere FISH (TelG) and double IF (PML/BLM respectively) are shown individually and as a merged image on the right. White signals correspond to triple positive telomeres, which represent APBs.

Summary

This chapter examined the telomere-associated proteome in multiple cell lines upon latent infection with KSHV. Systematic analysis of the proteome at telomeres by PICh in BJAB cells +/- KSHV revealed broad modulation of the factors bound to telomeric DNA. This included differential enrichment of proteins involved in all major pathways of DNA repair including cNHEJ, MMEJ, and HR. In addition to this, binding of shelterin proteins to telomeric DNA was reproducibly increased upon infection. In line with this, pilot analysis of infected cells by IF-FISH indicates that they may show classical APBs. Taken together, the findings presented thus far provide the basis for a number of hypotheses related to the modulation of telomeric DDR in response to latent KSHV infection. From these, I focussed on the possibility that KSHV infection may induce ALT telomere maintenance.

Chapter 2: ALT is activated in SLK and EA.hy926 cells infected with KSHV

Introduction

To evaluate whether KSHV infection is a trigger for ALT activation, experiments concerned with the characterisation of the active telomere maintenance mechanism in cell lines +/- KSHV are presented in this chapter. Cell lines used are initially telomerase^{+}, thus also allowing to investigate the potential interference of these two telomere maintenance mechanisms. Biological replicates of strictly latent cell lines were generated by *de novo* infection and analysis was carried out at >20 days post-infection as described in Chapter 1. For both SLK and EA.hy926 cell lines presented in this chapter, analysis was carried out in biological triplicate or duplicate unless indicated otherwise to control for any stochastic effects of clonal selection. In many cases ALT induction is accompanied by a decrease or complete loss of telomerase activity[131] and therefore it is necessary to address the status of telomerase to rigorously conclude induction of ALT. Regarding telomerase, activity as well as expression of the enzyme in the presence of KSHV are measured relative to uninfected co-cultured cell lines. This is achieved by TRAP assay, a protocol in which protein lysate is added to template containing telomeric repeats, which is extended if telomerase is present. Expression of *hTERT* is measured via a standard RT-qPCR approach. The same cell lines are analysed for hallmarks of ALT. These include the presence of homologous recombination at telomeres, telomere length heterogeneity, telomere clustering and presence of C-circles. Taken together, these assays aim to investigate the possibility of ALT activation upon KSHV infection *in vitro*, which arose from the results in the previous chapter.

Activity of telomerase is downregulated upon KSHV infection

Transcription of *hTERT* is downregulated in response to KSHV infection

Analysis of *hTERT* by RT-qPCR has been used in numerous studies[200,319,330,331] to infer indirectly the activity of telomerase as a telomere maintenance mechanism. To this end, qPCR was performed on cDNA obtained from cell lines of interest in this study using primers, which amplify *hTERT* or *GAPDH* as a housekeeping gene respectively (primer sequences in Table 2). Both primer pairs resulted in a single, specific amplicon as determined by melt curve analysis (Figure 14), there was no amplification in water only controls, and standard deviation of the mean C_t of *GAPDH* was low (data not shown) which confirms the robustness of the PCR carried out for this experiment. Relative mean expression data was obtained by subtraction of mean *GAPDH* signal and normalization to uninfected control co-culture ($\Delta\Delta C_t$ method[332]). Analysis of the mean relative expression of *hTERT* across biological replicates showed statistically significant reduction of mRNA levels to 70% (SLK) and 52% (EA.hy926) of uninfected control respectively (Figure 14). However, there was considerable variation between biological replicates of this experiments, which is shown in Figure 14, right panel. Importantly, these data suggest that while some cell lines show significant downregulation of *hTERT* expression, at least one replicate of the infected SLK cell line retained expression relative to uninfected levels. Overall, these data indicate that telomerase downregulation at the transcriptional level may occur in response to infection with KSHV in our models.

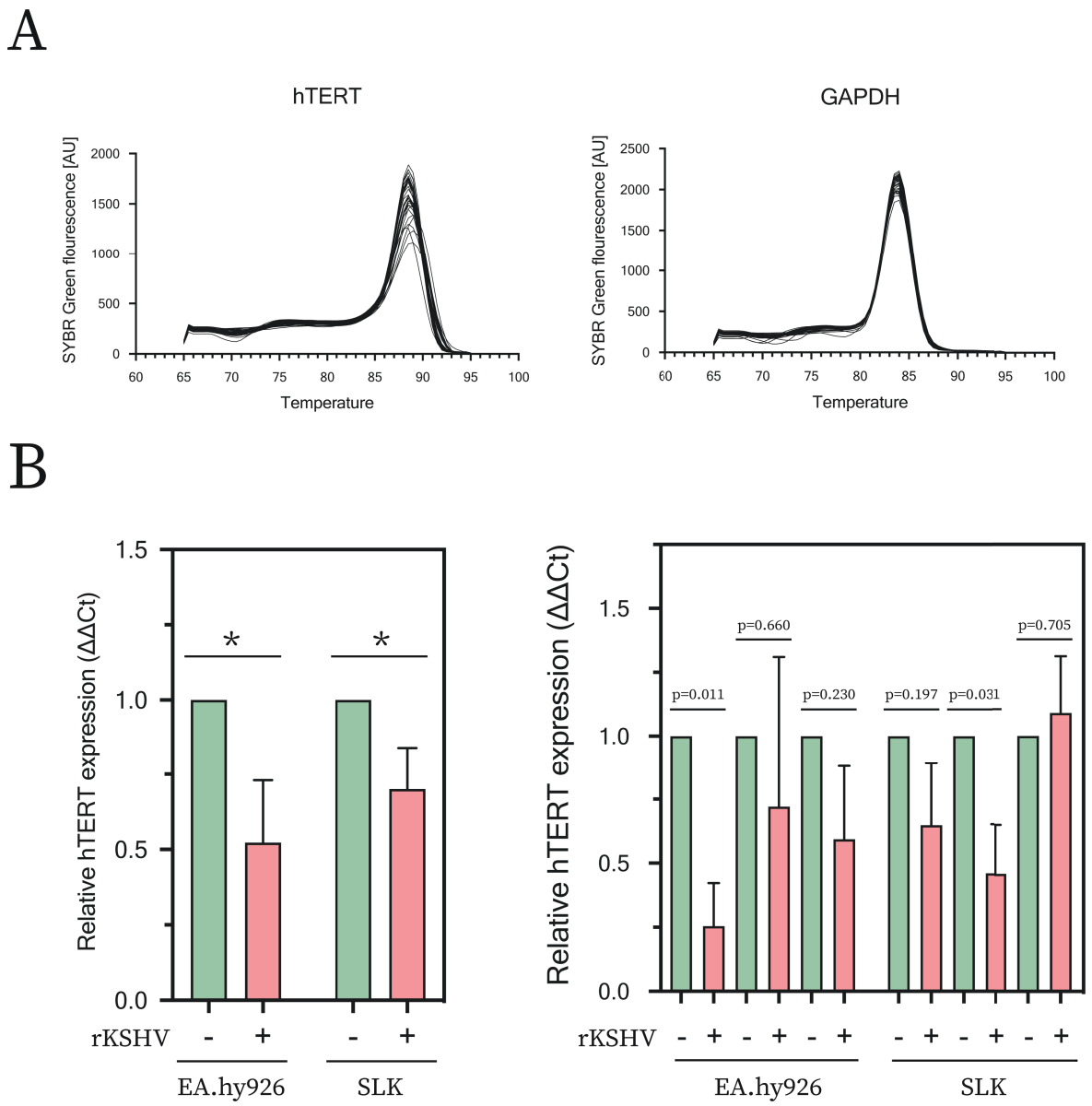

Figure 14: Expression of *hTERT* is downregulated upon latent KSHV infection. Equivalent amounts of cDNA are amplified for each cell line and *hTERT* expression is inferred by subtraction of signal of GAPDH control and normalization to the uninfected co-cultured cell line. (A) Shows melt curve of product generated by PCR for each of the primer pairs used in this analysis; (B) Quantification of relative expression as described. Left panel shows average of biological triplicate for each cell line. Right panel shows each biological triplicate in isolation. All experiments were carried out in technical triplicate. Significance was tested by student's t-test (*p<0.1).

Activity of telomerase is downregulated in response to KSHV infection in TRAP assay

Direct measurement of the activity of telomerase in cells may be achieved by TRAP assay. In this analysis, step-wise elongation of a oligonucleotide template with telomeric repeats ($[TTAGGG]_n$) is catalysed by co-incubation with cell lysate. PCR amplification is carried out in the presence of an Internal Control (IC) template, which competes with substrate elongated by telomerase. Analysis of resulting amplicons by non-denaturing polyacrylamide gel electrophoresis showed complete absence of elongated template in heat-denatured HeLa lysate (Figure 15, lane 1) where the enzyme is inactivated as a negative control. On the other hand, chilled HeLa lysate (positive control) resulted in strong laddering corresponding with the addition of varying number of telomeric repeats to the template (Figure 15, lane 2). Therefore, the experiment detects telomerase activity in a manner free from PCR contamination or non-specific amplification, which may interfere with interpretation of the data. Analysis of biological triplicate SLK and EA.hy926 cells +/- KSHV indicated a decreased activity of telomerase in response to the virus (Figure 15) in all but one pair of SLK cell lines (Figure 15, lane 7&8) where the activity remained approximately equal. These results are in line with previously presented analysis by RT-qPCR in so far that they indicate a downregulation of telomerase activity in response to the virus overall with the exception of one biological replicate in the SLK cell line.

Further analysis by TRAP would be necessary to generate a precise quantification of the product produced by this reaction. Specifically, a repeat of this experiment which includes a heat-treated control in analogy to the one performed for HeLa lysate in the present data would be necessary to quantify the signal using standard methods as described [333]. Nevertheless, it is reasonable to conclude that the trend, which is observed, e.g. a slight downregulation in the activity and expression of telomerase, is valid and reproducible.

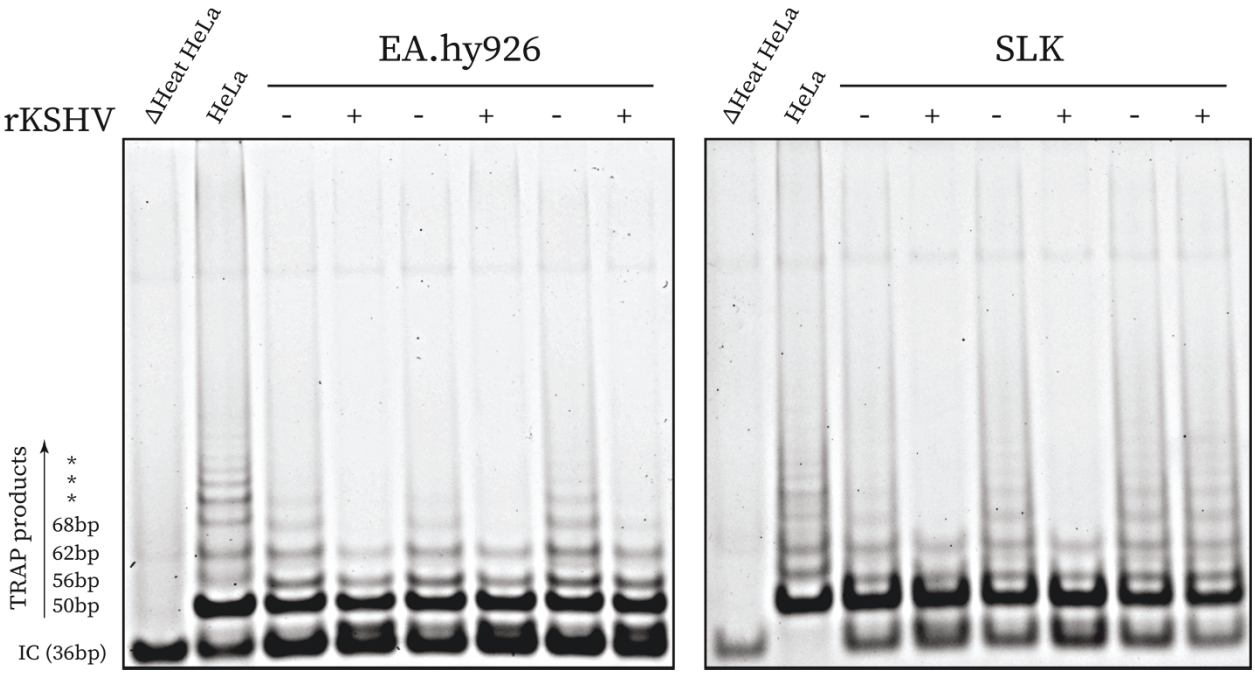

Figure 15: Telomerase activity is downregulated upon infection with KSHV. Protein lysate corresponding to equal cell numbers for each condition was subjected to TRAP protocol and PCR amplification. As a control an amount of lysate from HeLa (telomerase^{+}) cells was denatured and subjected to the same reaction (lane 1 of each gel). Each lane contained 1/10 of total PCR product generated using standard TRAP assay. Analysis was performed in technical duplicate with reproducible results. IC band corresponds to un-extended template and negatively correlates with telomerase activity.

Latent KSHV infection induces a telomeric phenotype associated with ALT activation

Infected cells have increased HR at telomeres resulting in T-SCE

In cells that maintain telomere length via ALT, inter-telomeric recombination by HR occurs to initiate DNA synthesis at telomeric repeats[156,160]. The incidence of telomeric HR may be quantified directly through analysis of metaphases by CO-FISH. To this end, metaphase spreads are generated in which one strand was digested specifically by BrdU/C incorporation, Hoechst/UV treatment, and exonuclease digestion as reported[170]. Subsequently, directional FISH probes for leading C-rich and lagging G-rich telomere repeats are applied and double positive signals are considered direct evidence of T-SCE (Figure 16A). In the absence of HR globally or an even number of HR events, signals corresponding to either of the two strands will be found diagonally opposite as depicted in Figure 16A. In the event of extensive global HR, an increase in chromosomes which show a pattern in which the signals corresponding to either strand are found within the same chromatid may be anticipated. No such trend was observed. However, quantification of % chromosomes with T-SCE per metaphase by blinded manual counting was performed on biological triplicate of SLK and EA.hy926 cells +/- KSHV (Figure 15B). Uninfected, co-cultured cell lines showed a low level of mean 0.5-1% (<1 chromosome) T-SCE across all replicates. Infection with KSHV led to a consistent and significant increase to mean 4-8% corresponding to 2-5 chromosomes with T-SCE (Figure 16B). There was variation between metaphases from infected cells, which showed this overall increase and some had a striking number of T-SCE events with more than 12 chromosomes displaying T-SCE. These data provide evidence for telomeric HR in KSHV$^+$ SLK and EA.hy926 cell lines as determined by the incidence of T-SCE by CO-FISH, which is consistent with the notion of ALT activation upon KSHV infection.

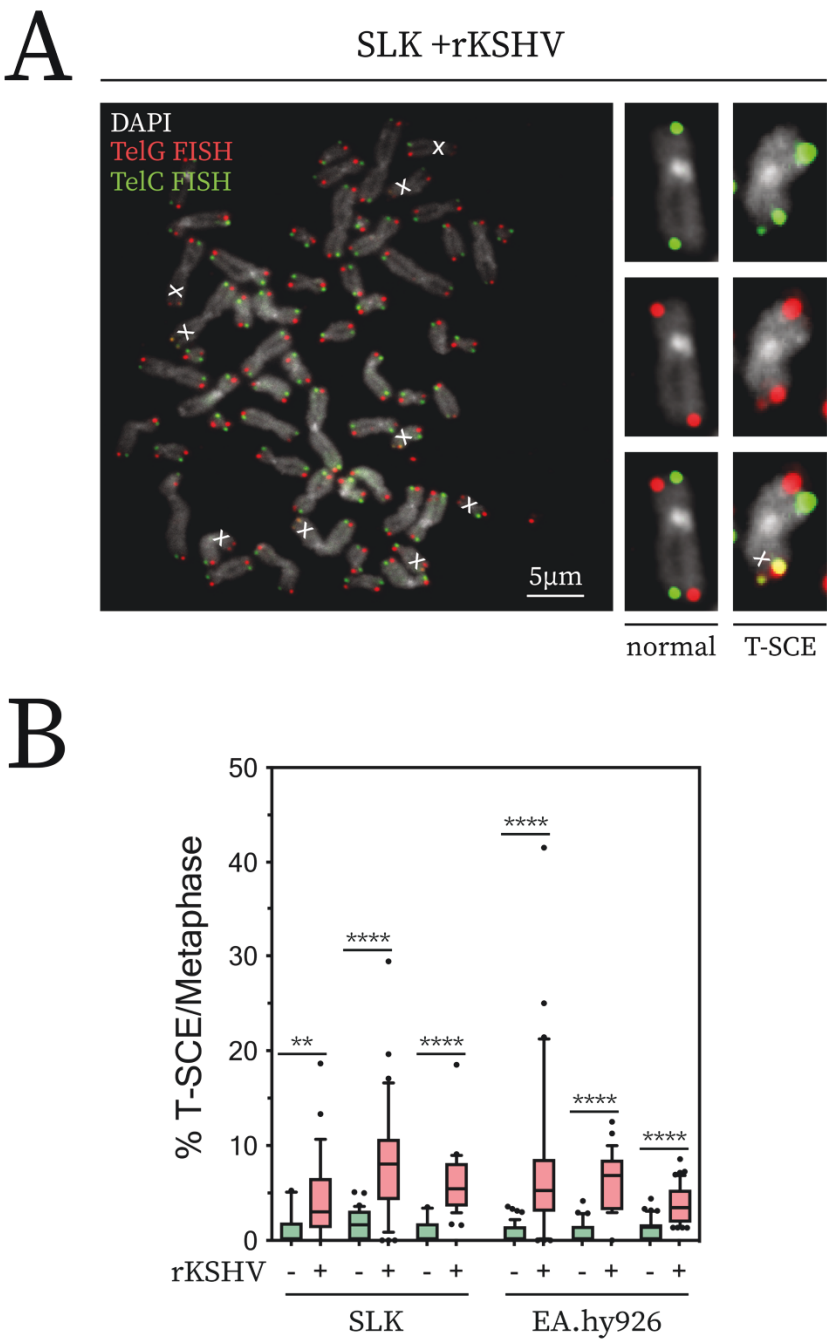

Figure 16: Incidence of T-SCE is increased upon latent KSHV infection. (A) Representative widefield micrograph is shown for illustrative purposes. Large image shows an overview of full metaphase as obtained in this experimental setup. Smaller images show leading/lagging strand in isolation and merged respectively to highlight their relative position on individual chromosomes. Normal, no recombination situation is shown with diagonally opposing signals respectively as well as T-SCE characterised by the occurrence of double positive ends (yellow, marked with an X in image). (B) Quantification of the occurrence of T-SCE. Blinded count of the incidence of chromosomes with double positive ends indicative of T-SCE. Biological triplicate, at least 50 metaphases per condition. Significance inferred by student's t-test (**p>0.01; ****p>0.0001).

KSHV infection results in increased telomere fragility

Replicative stress at telomeres occurs in ALT cells[161,201]. Telomere fragility is a phenotype associated with replicative stress at telomeres and may occur under a number of conditions including TRF1 knockout[119] and depletion of DDR proteins[76,320]. Telomere fragility may be quantified by telomere FISH on metaphase spreads where fragility manifests itself as a smeared or doublet signal in contrast to normal punctate signals. Such fragile telomeres were readily detectable by CO-FISH on metaphases from the cell lines of this study (Figure 17A). Quantification was carried out in analogy to T-SCE analysis described in the previous section. Again, the incidence of this phenotype was very low in all uninfected control cell lines at mean <1%, eg. <1 chromosome with fragile telomeres per metaphase. Infection with KSHV resulted in a significant increase in the mean % chromosomes that exhibit telomere fragility across all biological and technical replicates of the experiment (Figure 16B). Similar to T-SCE analysis, there was considerable variability in the magnitude of this increase, however most infected cell lines showed approximately a mean of 4% fragile telomeres (>2 chromosomes per metaphase). One cell line showed an increase to a mean of 10% fragility, which corresponds to 6 chromosomes with telomere fragility on an average metaphase. Overall, these data provide evidence for replicative stress at telomeres upon KSHV infection in both SLK and EA.hy926 cell lines, as indicated by the occurrence of telomere fragility. Given that such a phenomenon occurs in response to replicative stress at telomeres during ALT, these data are in agreement with ALT induction upon KSHV infection.

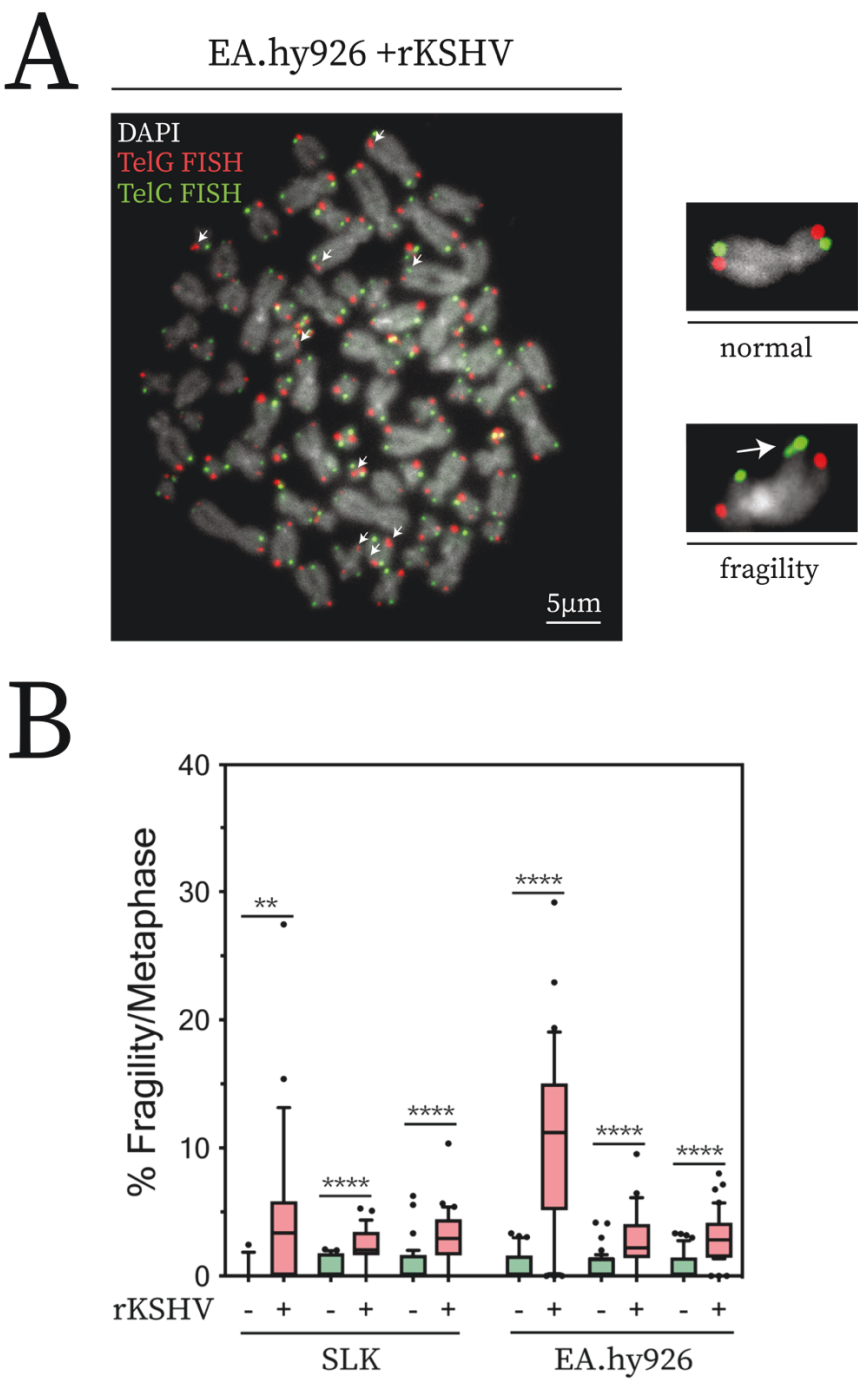

Figure 17: Incidence of telomere fragility is increased upon latent KSHV infection. (A) Representative wide field micrograph is shown. Large image presents an overview of full metaphase as obtained in this experimental setup with incidences of telomere fragility marked by an arrow symbol. Illustrative example of normal chromosome and telomere fragility shown on the right. (B) Quantification of the occurrence of telomere fragility. Blinded count of the incidence of chromosomes with at least one fragile telomere was carried out. Biological triplicate, at least 50 metaphases per condition. Significance inferred by student's t-test (**p>0.01; ****p>0.0001).

Telomeres are clustered and elongated heterogeneously in response to KSHV infection

Telomere length is increased in cells that exhibit active telomere maintenance mechanisms. Based on the data presented in this chapter thus far, any increase in telomere length upon infection is unlikely to be due to telomerase hyperactivation but rather relate to the induction of ALT. To further examine this possibility, relative telomere length was analysed in infected cells by telomere qFISH and TRF Southern blotting. Due to the HR-based mechanism of ALT, telomere length is more heterogeneous between chromosomes in comparison to telomeres elongated by telomerase activity. In addition to this, telomeres are often found in clusters during interphase, an observation, which is reminiscent of inter-telomeric strand invasions during ALT.

Automated analysis of telomere FISH signal intensity in interphase cells was carried out to determine relative telomere length in cell lines infected with KSHV. Strong telomere clustering was observed in a subset of KSHV$^+$ cells upon initial inspection under the microscope (Figure 18A). Quantification of mean integrated signal intensity (qFISH) of telomeres in nuclei of SLK and EA.hy926 cells +/- KSHV confirmed this observation. Both mean and variability were increased significantly upon infection with KSHV in most cases (Figure 18B). One KSHV $^+$ EA.hy926 cell line showed a subtle increase in telomere length and no statistically significant increase in variability as determined by F-test. In order to consolidate these observations, absolute telomere length was determined for a candidate pair of SLK cell lines by TRF Southern blot. Mean telomere length was increased upon infection with KSHV relative to uninfected co-culture from approximately 5.5kb to 6.5kb (Figure 18C). In addition to this, the pattern of telomere length in infected SLK cells analysed was more heterogeneous and resembled the size distribution observed in U2OS cells, a prototypic ALT$^+$ cell line (lane 1, Figure 18C).

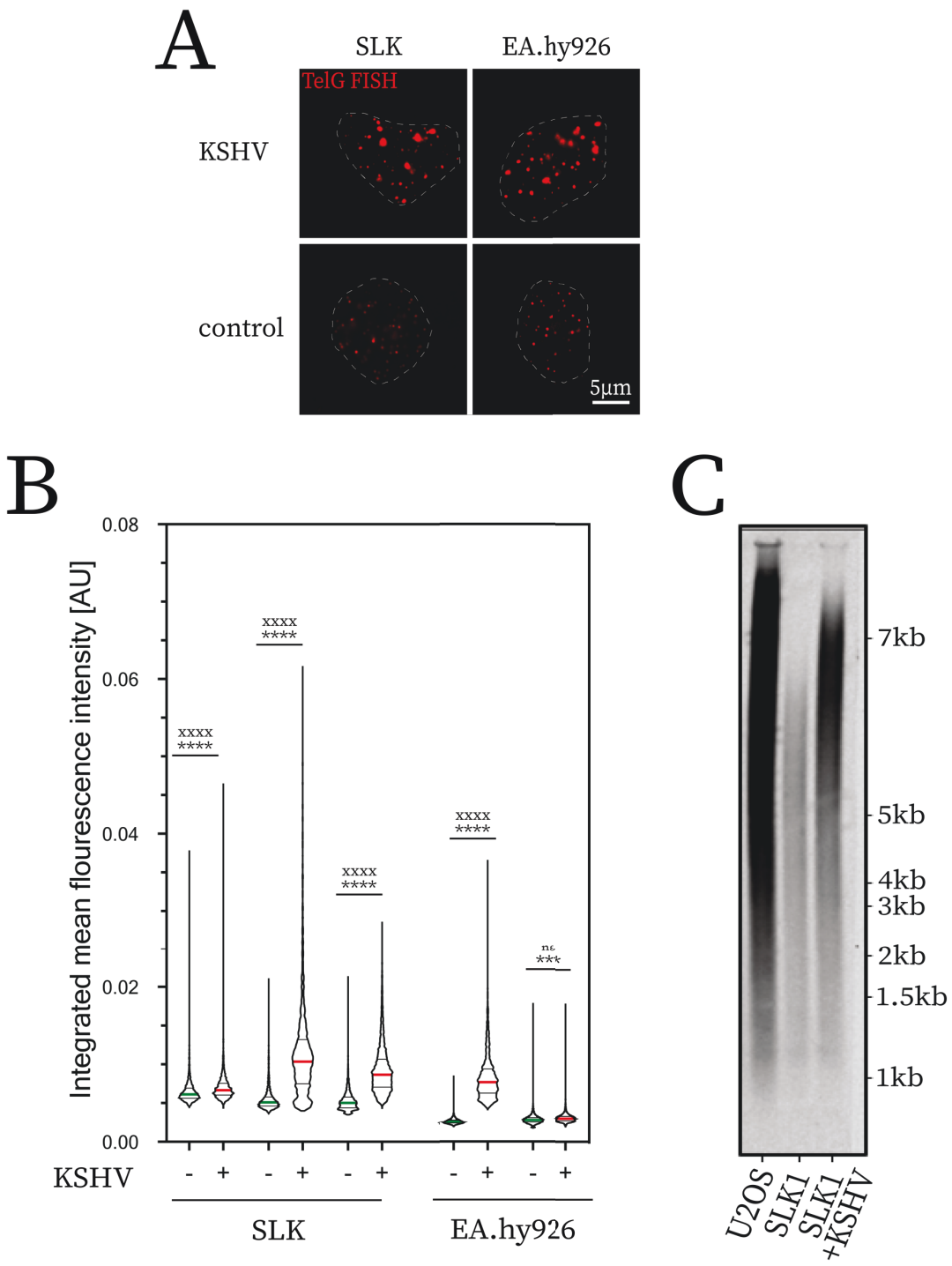

Figure 18: Telomere length/heterogeneity increases upon KSHV infection. (A) Image of telomere FISH signals quantified in automated analysis. In both cell lines, telomere clustering may be observed as indicated, top row. Dashes outline presents DAPI nuclear counterstain in each image. (B) Automated quantification of telomere FISH integrated mean signal intensity (mean pixel intensity x area of signal). Mean differences tested with student's t-test (**p<0.01, ****p<0.0001), heterogeneity tested with F-test of variance (^{xxxx}p<0.0001). (C) Preliminary TRF Southern blot of SLK cell line pair, equal amounts of gDNA used per lane.

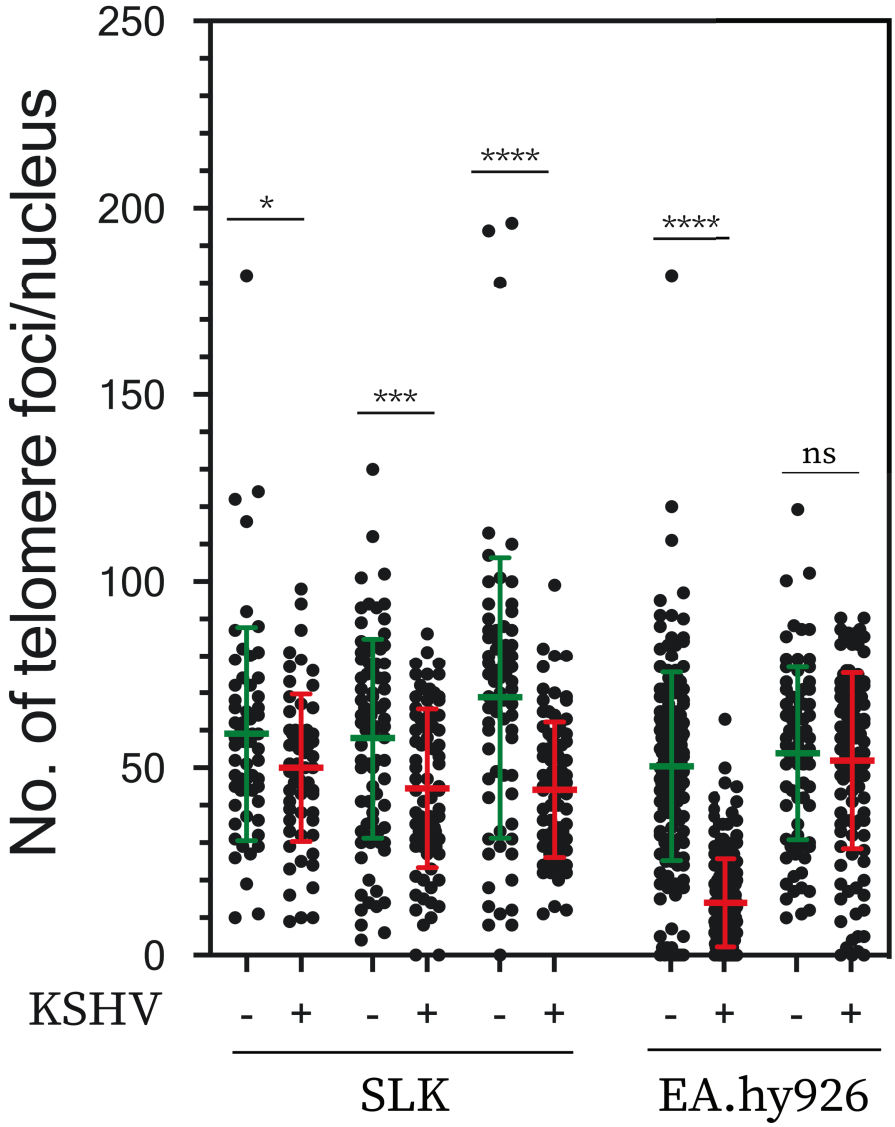

Figure 19: Mean number of telomere foci decreases upon infection. Quantification of the count of telomere FISH foci per nucleus is presented for all cells included in qFISH analysis as determined by CellProfiler. Biologcial triplicate, technical duplicate as previously. Significance inferred by student's t-test (*p<0.1, ***p<0.001, ****p<0.0001).

Taken together, these experiments suggest that telomere length is increased reproducibly upon infection with KSHV in both cell lines by qFISH. Such increases may be confirmed by TRF Southern blotting to determine absolute telomere length as demonstrated in a pilot experiment for the SLK cell line +/- KSHV and U2OS (Figure 18C).

Next, I evaluated the number of individual telomere FISH foci detected by the automated analysis pipeline upon infection. If several telomeres cluster together in a given nucleus, the expected outcome of this analysis would be a decrease in the number of distinct foci. From the data set generated for qFISH, automated counting was carried out (Figure 19). Most cell lines infected with KSHV showed a significant decrease in the number of individual foci detected in comparison to uninfected co-culture (Figure 19). The same KSHV$^+$ EA.hy926 cell line, which showed a subtle but not significant increase in variability and small significant increase in mean intensity upon quantitation of FISH signal, also failed to reach significance in this measurement. However, the decrease in number of foci per nucleus was still observed and no opposite trend was present. In summary, the analysis presented indicates that KSHV infection induces clustering of telomeres reproducibly but to varying degrees, as indicated by mean increase in intensity and heterogeneity of telomere FISH signals as well as a decrease in the number of individual foci per nucleus.

Preliminary data indicate that C-circles may be induced upon infection with KSHV

Complementary to the experiments presented so far, we next measured the occurrence of C-circles as a proxy for ALT activation upon KSHV infection. To this end, defined quantities of DNA were treated with or without Φ29 polymerase, which selectively extends circular DNA molecules by rolling circle amplification. The

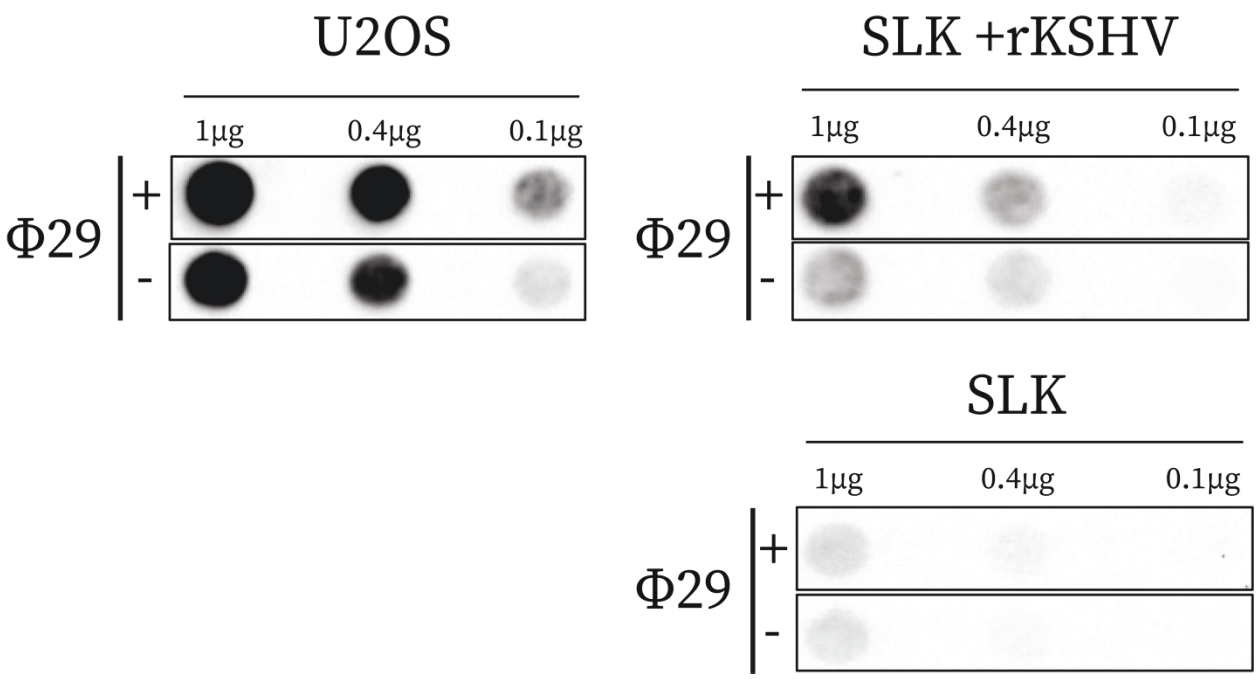

Figure 20: C-circles are present in an infected SLK cell line. Analysis of the presence of circular, partially double-stranded C-circles by Φ29 polymerase amplification. Equal amounts of DNA of cell lines indicated was subjected to rolling circle amplification reaction (+/- Φ29) and incidence of telomeric DNA from resulting reaction was quantified by dot blotting onto Nylon membrane coupled to Southern blot as described. U2OS cell line was included as positive control.

experiment was carried out on the same pair of SLK cell lines described for the preliminary TRF Southern blot analysis. As a positive control for Φ29 amplification, DNA from U2OS cells was treated with the enzyme (Figure 20, left panel). Amplification of telomeric DNA was then visualized by telomere dot blot, indicating the presence of C-circle as reported in a number of studies[163,178]. In uninfected SLK cells no such amplification was observed, which suggests an absence of C-circles (Figure 20, lower right panel). However, the infected SLK cell line showed an increase in telomeric DNA upon Φ29-induced amplification (Figure 20, upper right panel). This experiment provides preliminary data suggesting that KSHV infection induces C-circles. Although these observations require confirmation in full biological triplicate and EA.hy926 cell line, they do strengthen the notion of ALT activation upon KSHV infection.

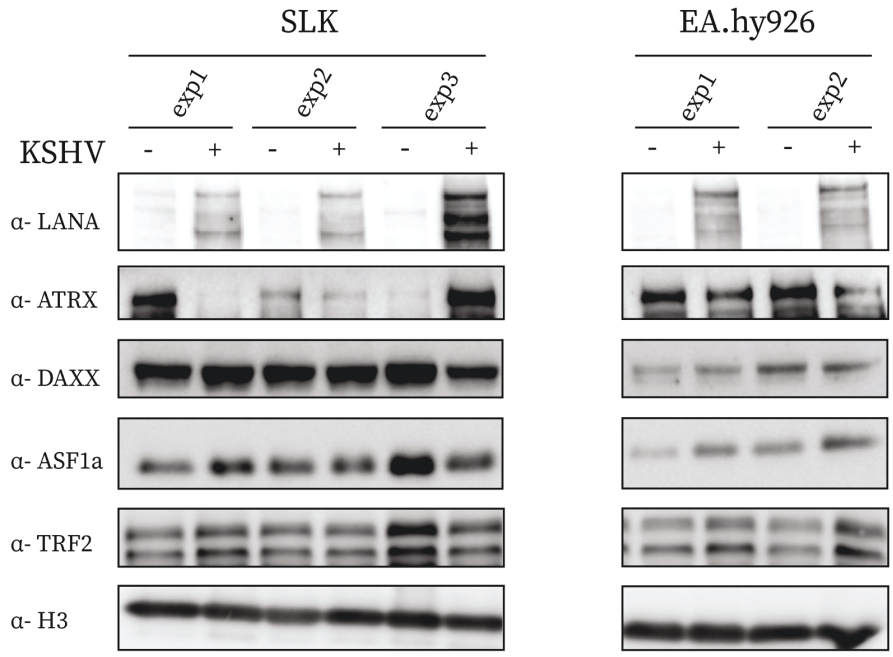

Figure 21: Analysis of the expression of ALT markers by Western blot. Representative blot was generated by staining with antibodies as indicated. 5µg of protein was analysed for each condition. Proteins were detected at expected molecular weight based on the information available form respective manufacturers and the literature.

No consistent loss of ATRX, DAXX or ASF1a is detected in KSHV-induced ALT cell lines

Next, I evaluated the expression of proteins which have a published role in suppressing the activity of ALT in cells by Western blot. Namely, the expression of ASF1a was examined based on the only other previous demonstration of ALT induction which was achieved by downregulation of ASF1a[200]. Loss of ATRX and DAXX at the protein level has been associated with ALT activity in cells as discussed extensively previously. Analysis of both SLK and EA.hy926 cell lines showed that ASF1a and DAXX expression was unaffected by KSHV infection and protein levels remained near identical across conditions (Figure 21). In comparison, levels of ATRX were more variable. However, no clear trend was observed and protein was detected in all conditions indicating that loss of ATRX is not a reproducible feature of KSHV infected SLK and EA.hy926 cells. In summary, analysis of ASF1a, DAXX, and ATRX protein levels indicates that changes in these factors are unlikely to play a role in the ALT phenotype which is observed upon KSHV infection.

Summary

In this chapter, various assays were employed to evaluate the activity of telomere maintenance mechanisms in initially telomerase$^+$ cell line models SLK an EA.hy926 upon KSHV infection. The experiments described show that there is no relative upregulation of telomerase activity as detected by RT-qPCR or TRAP assay in response to KSHV infection in either cell line. Instead, a subtle but visible downregulation of telomerase activity was detected reproducibly in the majority of infected cell lines. Next, we examine whether ALT is active as the telomere maintenance mechanism in KSHV-infected SLK or EA.hy926 cells. Data presented shows an increase in key hallmarks of ALT in response to the virus including T-SCE, telomere fragility, telomere clustering, and potentially C-circles. Importantly, there is a clear indication for an absence of telomerase hyperactivation in the presence of telomere elongation as well as features of ALT. . In contrast to some previous reports in the literature, this seems to be independent of ASF1a, DAXX, or ATRX protein levels, as demonstrated by Western blot. In summary, the assays described show that a phenotype resembling ALT activation is induced upon infection with KSHV in SLK and EA.hy926 cell lines by an uncharacterised mechanism.

Chapter 3: KSHV reprograms cells upon infection to facilitate viral genome replication by BIR

Introduction

KSHV interacts with host cells in a complex manner to enable maintenance and propagation of its episomes. Given that our data indicate activation of ALT telomere maintenance *de novo* in response to KSHV infection, we aimed to examine the importance of this pathway for infected cells and the viral life cycle. We measured whether siRNA knockdown of key ALT factors BLM, PolD3, RAD52, SLX4 had an impact on the survival of infected SLK cells. Conversely, the impact of ALT factor knockdown on KSHV episome maintenance and their importance for viral genome replication was evaluated. The dependency of latent viral replication on features of ALT and factors involved in ALT BIR (PolD3, RAD52, BLM) was further analysed in the context of an ALT positive cell line, U2OS. Finally, the presence of ALT-specific heterochromatin marks on the latent viral genome was examined by ChIP/qPCR as a further proxy for the notion that KSHV episomes reside in a chromatin niche resembling ALT telomeres, which would be permissive of BIR. Taken together, the experiments presented begin to address the relevance of ALT activation in the context of the KSHV life cycle upon latent infection in infected cell lines.

Key ALT factors are decreased specifically upon siRNA knockdown

In order to establish a system in which interrogation of the role of key proteins involved in the ALT mechanism may be studied, RNA interference was carried out. Transfection of both infected and uninfected cells was carried out using a pool of siRNA for each protein of interest. Efficiency of this knockdown was evaluated at

three days post-transfection by Western blot (Figure 22A). Analysis was carried out relative to a scrambled control sequence to exclude any toxicity of the RNAi overall. Clear bands were detected in all cases of scrambled control transfection for BLM, RAD52, and PolD3 (Figure 22A). Consistently, transfection with corresponding siRNA pools against BLM, RAD52, and PolD3 decreased the abundance of these proteins to levels below detection by Western blot. However, it was challenging to detect SLX4 by this technique and only a faint band was achieved after trial of multiple antibodies. This is despite high amounts of protein loading per lane, i.e. 30µg. Overall, an efficient method to deplete BLM, RAD52, and PolD3 is given by this RNAi as indicated by Western blot analysis. This knockdown was significant and resulted in a depletion of >90% of protein respectively. The level of SLX4 upon treatment remains ambiguous from these data alone.

Proliferation of infected SLK cells is impaired upon knockdown of ALT factors

Next, we investigated whether cells harbouring latent KSHV are dependent on ALT factors for their effective proliferation and survival. Colony formation assay (Clonogenic assay) was carried out using a low number of SLK cells +/- KSHV, +/- ALT factor RNAi at three days post-interference as established previously. Both cell lines grew into distinct colonies when seeded at low density and counting was performed automatically (see Materials & Methods, Figure 22B). The number of colony forming, i.e. proliferating cells was quantified relative to scrambled control siRNA transfection for each experiment. Un-transfected cells were also analysed in each experiment and examined manually relative to scrambled siRNA transfection to exclude any toxicity due to the transfection procedure overall. Only experiments where no non-specific toxicity was observed were included in subsequent analysis.

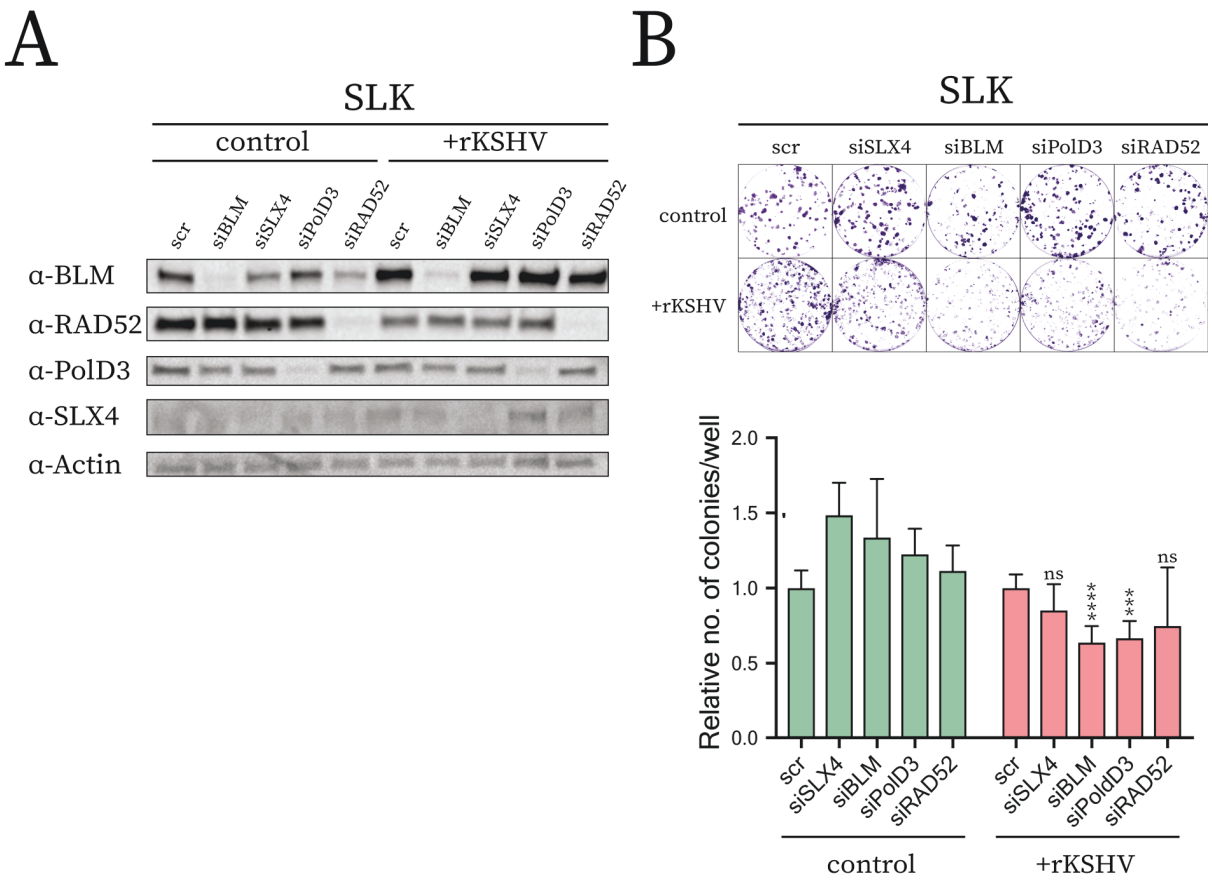

Figure 22: Survival of infected cells is impaired upon knockdown of ALT factors. (A) Representative confirmation of knockdown efficiency by Western blot in SLK cells. Upper panel in (B) show representative wells from Clonogenic assay plates stained with Crystal Violet. Automated quantification of colonies shown in (B) relative to scrambled control knockdown. Data presented from three independent experiments performed in technical triplicate each. Significance tested by student's t-test (**p<0.01, ****p<0.0001).

Knockdown of ALT factors in uninfected SLK cells resulted in a relative 1.2-1.5 fold increase in the number of colonies (Figure 22B). This indicates a subtle increase in their proliferative capacity upon depletion of these proteins. The opposite trend was observed in infected SLK cells. Such cells were reproducibly and significantly impaired in their capacity to proliferate upon depletion of BLM and PolD3, which was evident by a reduction of colonies to approximately 60% (Figure 22). Mean reduction to similar levels was also recorded upon knockdown of SLX4 and RAD52, albeit this failed to reach statistical significance in biological triplicate (Figure 22).

In addition to the data described above, it is interesting to note that infected SLK cells show an overall increase in their proliferative potential in this assay relative to uninfected co-culture. This is evident by a relative 2-fold increase of colonies in KSHV^{+} cells in both cell lines un-transfected as well as scramble knockdown (quantification not shown, see upper panels Figure 22). In summary, KSHV infection has an effect on the proliferative capacity of both SLK cell lines. Knockdown of ALT factors SLX4, BLM, PolD3, and RAD52 impairs proliferation of such cells specifically in the presence of latent KSHV infection. Taken together, these data indicate that cells that harbour KSHV episomes may be dependent on such factors for efficient proliferation and survival.

Episomes were not lost in SLK cells upon knockdown of ALT factors but there was signs of viral BIR

Based on the data presented in this chapter thus far, infected cells become dependent on ALT factors involved in BIR for their effective proliferation. Next, I evaluated whether the latent viral genome was replicated by a BIR-like mechanism in the context of KSHV latency. To examine this possibility, we measured the absolute number of KSHV episomes per live cell by qPCR. This was achieved by generation of a standard curve by SYBR qPCR on precise amounts of product obtained from primers specific to the KSHV TR (details in Materials & Methods). Extracted DNA from cells of interest was subjected to the same qPCR and this reaction resulted in a single, specific amplicon in infected cells as indicated by melt curve analysis. To better monitor potential KSHV episome loss upon ALT interference, we did not perform the experiments described in the following under Puromycin selection. Notably, as it is published that KSHV episomes are progressively lost within one month if selection is removed from infected cells[282], I quantified ALT interference on episome loss in direct relation to the natural occurring episome loss observed upon withdrawal of selection. In a pilot

experiment, weekly RNAi was performed in analogy to transfection for Clonogenic assays for constant and significant decrease in ALT protein levels.

Analysis of KSHV episome copy number was performed at three time points post-withdrawal (day 0, 10, 32) in SLK cells as described above. As controls, uninfected cells (negative control) as well as cells kept under Puromycin selection (positive control) were included in the analysis. Copy number is expressed relative to Puromycin selected cells, which stably maintain episomes. There was no amplification from DNA obtained from uninfected cells throughout. No significant loss of KSHV episomes was detected in SLK cells under all conditions tested after 32 days (Figure 23A). Therefore, for this cell line, the experiment is inconclusive and no information about the role of ALT factors in KSHV episome maintenance may be drawn from these data.

As discussed, the ALT factors presented in this chapter are important mediators of BIR and this is thought to be the main mechanism of telomere replication in ALT$^+$ cells[160]. Therefore, we next examined whether latent KSHV episomes may replicate in an analogous manner in infected cell lines. Recent studies have established that DNA synthesized by BIR may be tagged by incorporation of EdU in G2/M phase [156,160,163]. This is due to the fact that BIR occurs specifically in G2/M and is therefore separated from bulk S-phase DNA replication. The method employed for the visualization is therefore crucially dependent on an exclusion of cells in S-phase by sequential cell cycle arrest, which can be achieved by Cdk1 inhibitor (Cdk1i) and Thymidine treatment, which arrest cells in at G2/M and G1, respectively (see Materials & Methods). To test whether cells obtained by our experimental setup qualify for analysis by microscopy, Click-iT chemistry coupled to Flow Cytometry was employed to analyse the cell cycle upon sequential arrest (Representative data

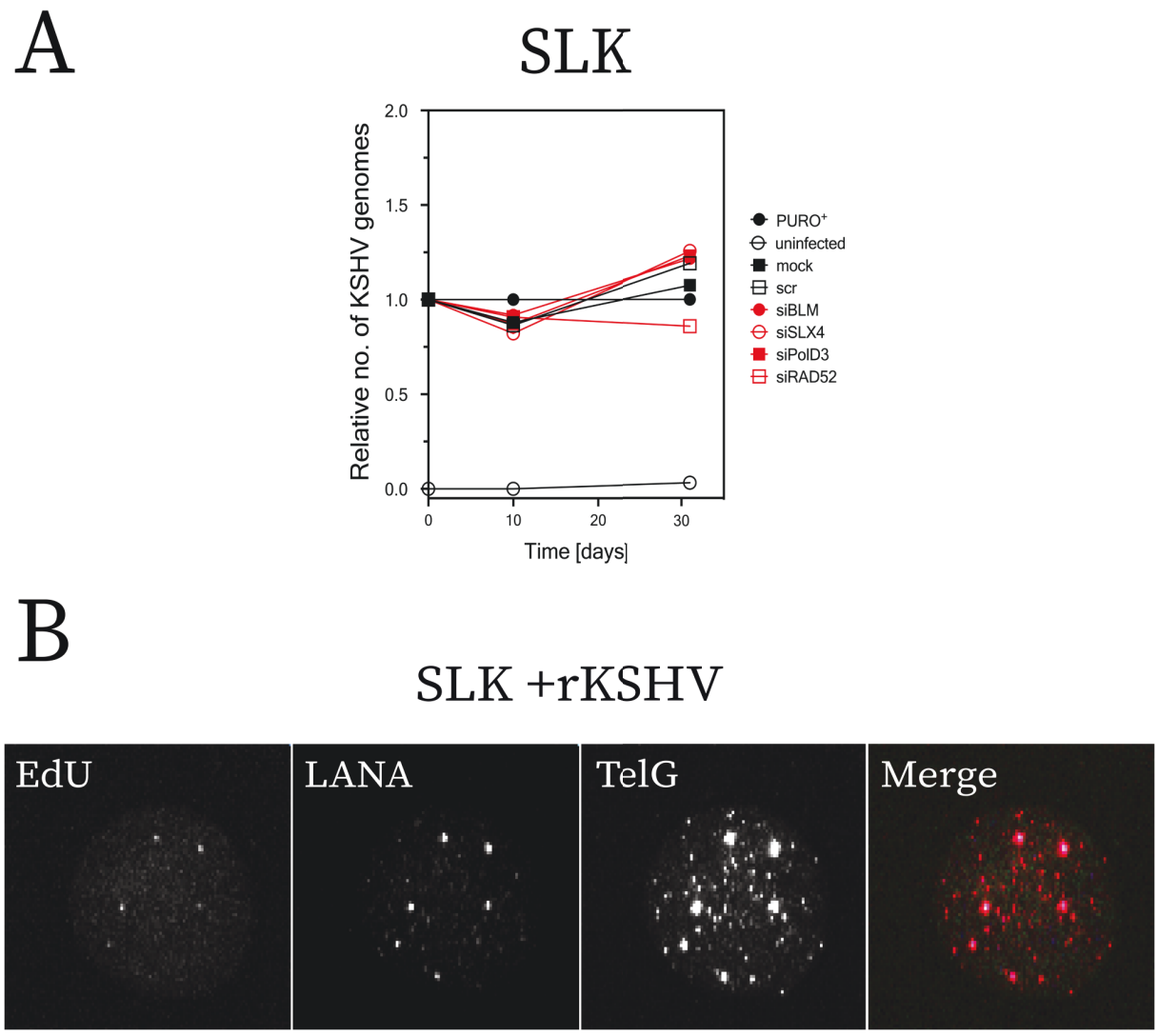

Figure 23: Analysis of the incidence of viral BIR in infected SLK cells. (A) Data is presented for SLK cell line. Each time point normalized to the absolute number of KSHV episomes in control cells, which were kept under selection. Knockouts are shown in red, control conditions shown in black. Data represents one experiment. (B) Representative MIPs of confocal Z-stacks obtained after Click-iT chemistry/IF-FISH. Separated channels are shown for each stain and merged image on the left (green: EdU-Alexa488, red: telomere FISH, light blue: LANA IF). Triple positive signals appear white in merged image (right).

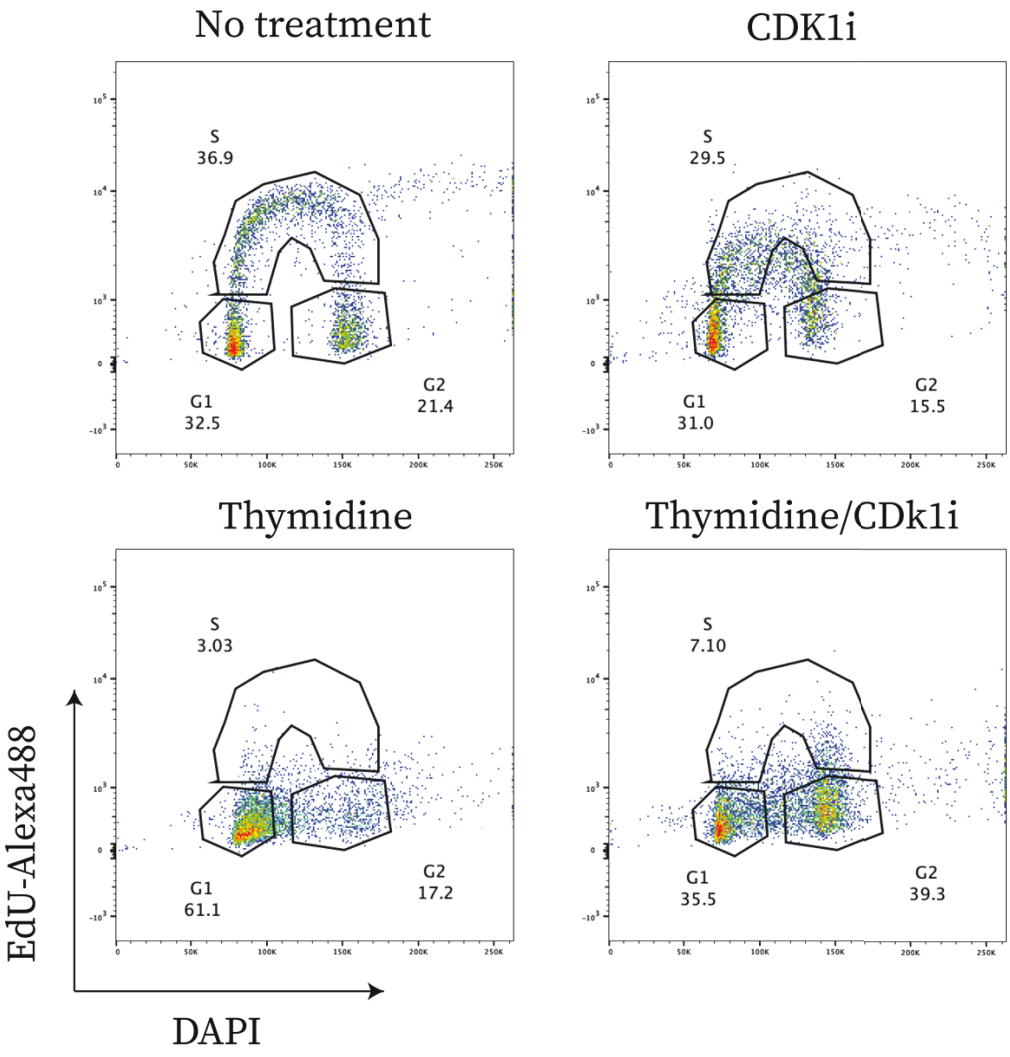

Figure 24: Cell cycle arrest for BIR foci assay. Representative data from one cell line (EA.hy926) is shown. Cells were treated with inhibitors as indicated above plots. Gating was identical for all conditions and based on populations observed in untreated cells. 500,000 cells are plotted for each condition for illustrative purposes.

Shown in Figure 24). Click-iT chemistry allows coupling of a fluorochrome, in this case Alexa 488, to incorporated EdU in a reaction dependent on $CuSO_4$. Such analysis by flow cytometry indicated that treatment with both inhibitors (Cdk1i/Thymidine) resulted in a near complete abrogation of S-phase cells and 40% enrichment of cells in G2/M phase (Figure 24, lower right panel). 7% of cells may be considered to be in late S-phase under the conditions employed for this experiment. However, late S-phase cells are easily excluded in Click-iT microscopy since they show strong pan-nuclear EdU staining which is clearly distinct from BIR EdU foci (see Ref.[163] for examples of this). Overall, the data presented indicate that the combined cell cycle block used results in an increase in G2/M cells and a complete exclusion of potentially BIR false-positive cells in early S-phase.

Next, Click-iT chemistry was performed in combination with IF-FISH and confocal microscopy to evaluate whether KSHV genomes coincide with sites of telomeric BIR in infected cells. Intra-nuclear location of viral genomes was inferred by co-staining for the KSHV episome tether protein LANA. The experiment was performed on SLK cell lines +/- latent KSHV infection. Uninfected cells had no LANA or BIR foci and narrow range, dim telomere FISH signals in confocal MIPs as analysed in chapter 2. Latent KSHV infection altered the appearance of these signals models drastically (Figure 23B). As expected, clear LANA foci were detected in infected cells. In addition to this, distinct EdU foci in G2/M cells indicative of BIR were present in such cells. Striking co-localization of BIR and LANA was observed, indicative of active BIR at the site of viral genomes. Such foci localized to telomeres in some, but not all cases. Detailed quantification to elucidate to which degree this phenomenon occurs at telomeres specifically is outstanding at this point. Overall, this experiment suggests that BIR foci occur in infected cells at the site of viral genomes.

Episomes are lost rapidly in infected U2OS cells upon knockdown of ALT factors and show signs of viral BIR

Next, I examined whether the knockdown of key ALT-specific BIR factors had an effect on viral BIR in the setting of a cell line where the ALT phenotype was already persistent. To evaluate this, an identical experimental setup was employed as described for SLK cells in the previous section. Again, KSHV episome copy number was determined by qPCR at day 0, 10, and 32 respectively. Infected U2OS cells lost the episome to some degree over this period in mock-treated and scrambled control cells beginning at day 10 post-withdrawal (Figure 25A). This was more rapid than SLK cells treated in the same manner, which had not lost any viral episomes o0ver the time course examined in this experiment. Strikingly, in infected U2OS cells, knockdown of BLM, PolD3, and RAD52 resulted in a complete loss of viral genome by day 32, a time point at which mock-treated and scrambled control cells still showed levels comparable to Puromycin treated cells (Figure 25A). In similarity to infected SLK cells, BIR foci co-localized with LANA and therefore the latent KSHV genome in this experiment (Figure 25B).

In summary, I suggest that the notion of a role for ALT factors in maintenance of the viral episome during latency is strengthened based on these pilot experiments. Certainly, the experimental system presented (serial RNAi over several weeks, qPCR on fixed number of live cells by Trypan Blue exclusion) is not ideal and a comprehensive analysis must include improved methodology. However, from these data I was drawn to hypothesize a role for ALT factors in viral genome maintenance.

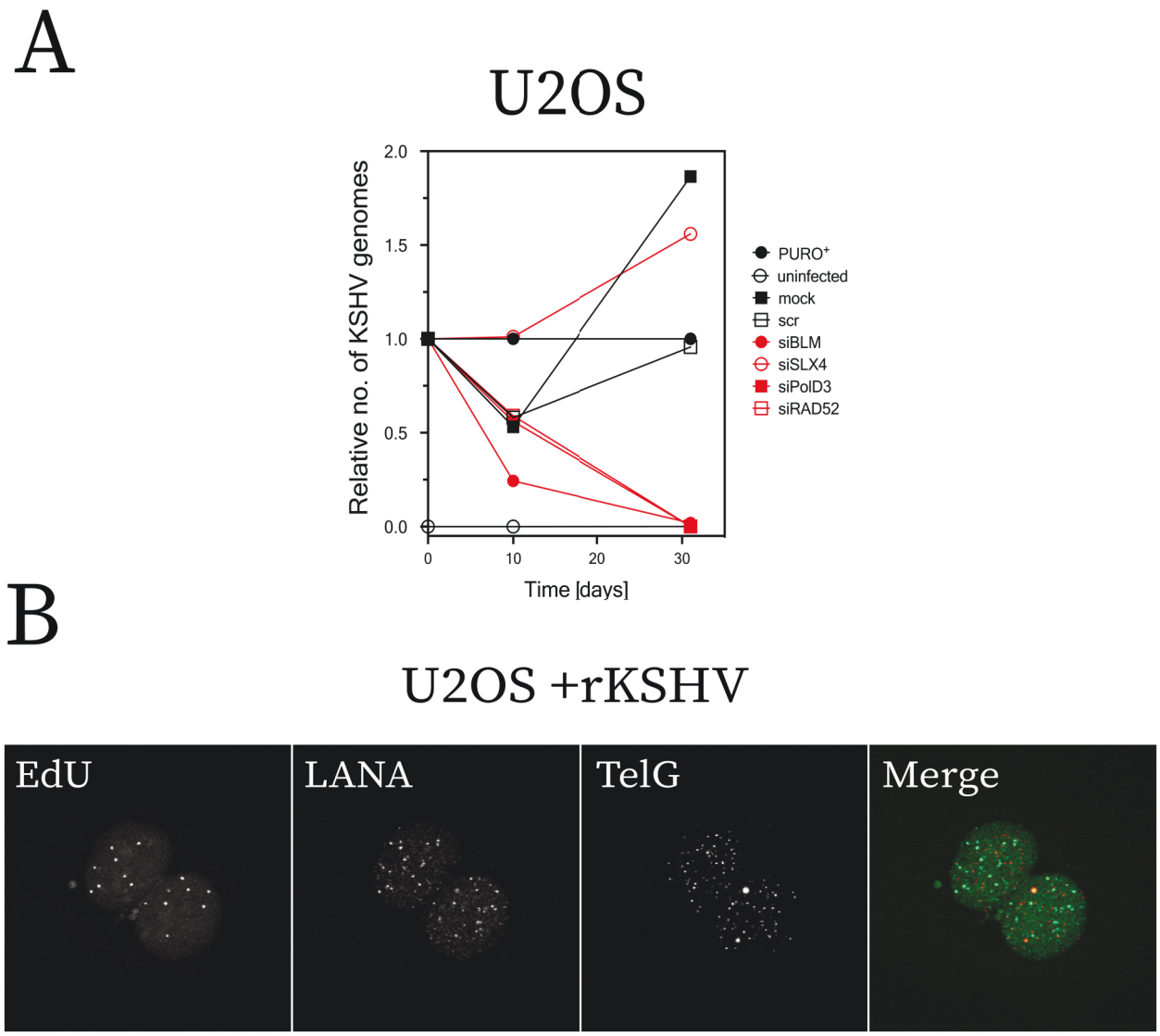

Figure 25: Analysis of the incidence of viral BIR in infected U2OS cells. (A) Quantification of KSHV episome number in cells under the conditions indicated. Knockdown conditions are depicted in red, controls in black. (B) Representative MIPs of confocal Z-stacks obtained after Click-iT chemistry/IF-FISH. Separated channels are shown for each stain and merged image on the left (green: EdU-Alexa488, red: telomere FISH, light blue: LANA IF). Triple positive signals appear white in merged image (right).

KSHV episomes exhibit heterochromatin marks permissive of viral replication by BIR

As described, changes in chromatin marks mediated by the activity of HP1α are detected at ALT telomeres including H3K9me3 and H4K20me3. Crucially, the presence of such marks promotes HR in the context of ALT. Therefore, I examined whether such marks were present on the viral episome. To thoroughly evaluate this possibility, primers were used for all three annotated origins of replication on KSHV episomes, the terminal repeat (TR), OriA, and OriLyt. All primer pairs resulted in a clear and specific amplicon as indicated by melt curve analysis (Figure 26, right panels) DNA in complex with histones, which harbour the heterochromatin marks described was obtained by ChIP. As a control for the presence of any host sequences, with sufficient similarity to the amplicons of the KSHV replication origins measured by this analysis I included unprecipitated input chromatin from uninfected cells (Figure 26, left panels). No amplification was observed from such DNA and this confirms that the qPCR employed here is specific to viral sequences. In addition to this, pulldown with an unspecific isotype control antibody corresponding to the remaining conditions was performed. Again, no amplification was observed in this control which rules out enrichment of DNA of interest due to non-specific binding to antibodies. Finally, H3 pulldown was utilised as a positive control since this histone protein is present ubiquitously in nucleosomes. In line with this, strong amplification was observed for all primer pairs under these conditions. Taken together, the data presented indicates that the experiment resulted in specific and efficient pulldown of chromatin-associated proteins of interest.

Heterochromatin marks associated with ALT telomeres were found at viral episomes in both SLK and U2OS cells. This was evident by strong amplification of viral sequence corresponding to all published origins of episome replication (Figure 26, left panels) when chromatin was precipitated using antibody specific to H3K9me3, H4K20me3, and finally HP1α. Pulldown with shelterin protein TRF2 resulted in a weaker, but detectable enrichment for such sequences. In summary, these data suggest that heterochromatin marks associated with ALT are present on viral chromatin, which may facilitate BIR at KSHV episomes.

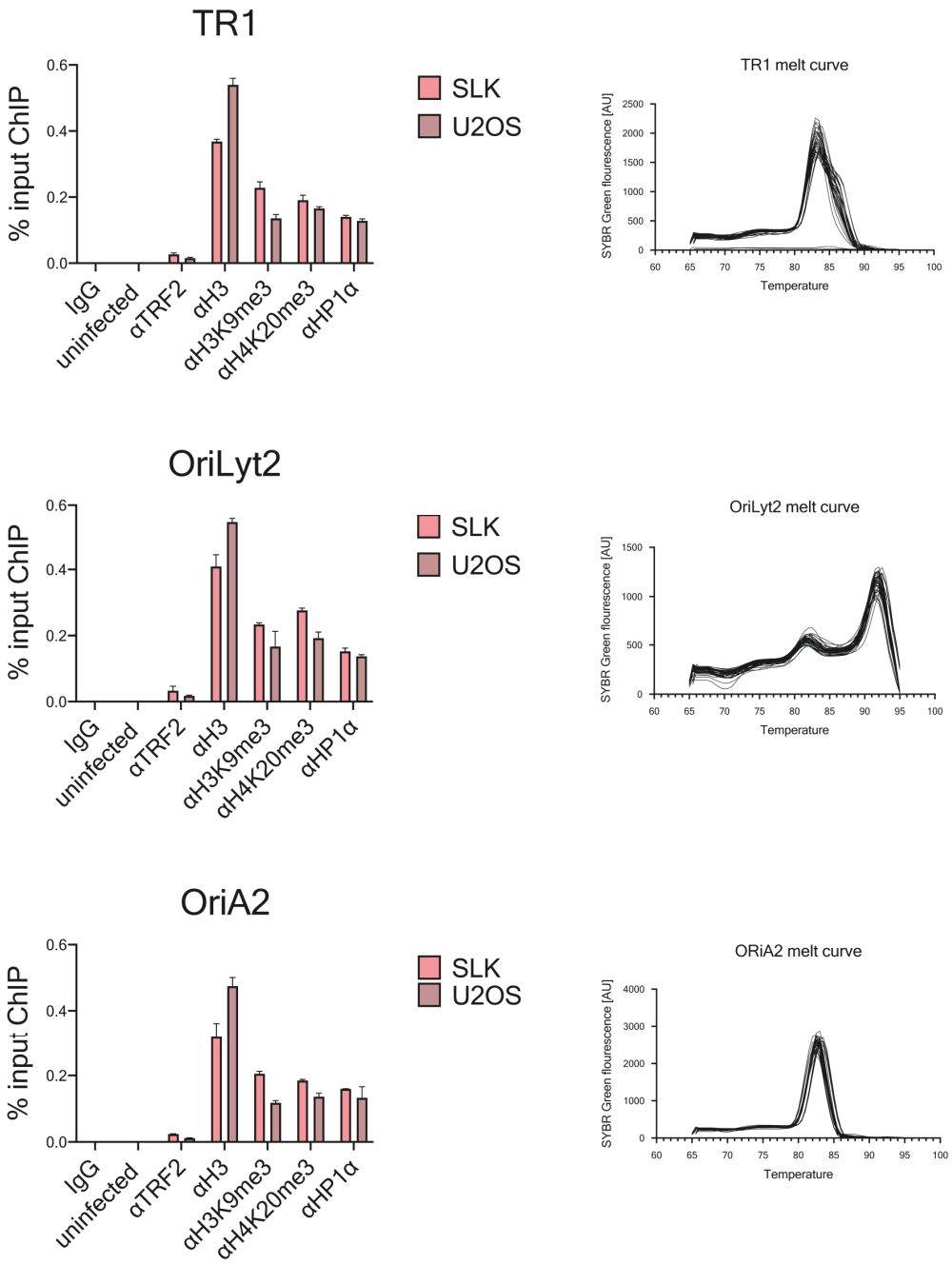

Figure 26: Analysis of heterochromatin marks at viral episomes. Equal amounts of material recovered from pulldowns indicated was subjected to qPCR with primer pairs as indicated. Uninfected control condition corresponds to 10% input of such cells. All data is quantified relative to input material from infected cell line, which was used for all pulldowns. Data representative of one experiment.

Summary

The data presented in this chapter aims to address the relevance of ALT activation for the life cycle of KSHV. Clonogenic data was generated which suggests that latently infected SLK cells are dependent on ALT factors for their efficient proliferation. In addition to this, preliminary measurements of KSHV episome copy number were performed which indicate that maintenance of the viral genome is dependent on ALT factors BLM, PolD3, and RAD52 in infected U2OS cells. Direct visualization of ALT BIR sites within the nuclei of infected SLK and U2OS cells showed that these coincide with LANA. Finally, a preliminary ChIP/qPCR experiment indicated that marks associated with ALT heterochromatin are enriched at viral episomes, which creates conditions permissive for viral BIR. Taken together, the experiments described indicate that ALT may be a novel mechanism for replication of KSHV episomes. Therefore, it is tempting to propose that episome replication is the step of the KSHV life cycle which benefits from ALT activity in infected cells which may explain the induction of this pathway upon latent infection.

Chapter 4: Signs of ALT activity are detected in KSHV-associated PEL and KS tumour cells

Introduction

Given that latent infection with KSHV appears to be a novel trigger for telomere elongation by ALT in multiple cell line models, I next explore whether this is also the case in tumours associated with KSHV infection. To this end, paraffin-embedded sections of tumours from 8 KS patients and 7 PEL patients were analysed by IHC-FISH. Histological features such as the distribution of LANA in infected tumour cells and morphology of each tumour type was analysed. Subsequently, telomere length was analysed by qFISH in a manner analogous to *in vitro* experiments presented in previous chapters. These experiments form the basis for an evaluation of the ability of KSHV to induce ALT telomere elongation *in vivo*, specifically in the context of KS and PEL.

Overview of KS sections: Identification of spindle cells and other features by IHC

KS is characterised by a 3D meshwork of immortalised endothelial-like spindle cells, neovascularisation, and infiltration of numerous lymphocytes. KS may occur at several sites in the body and our current collection of paraffin-embedded tumour sections includes gastric, lymphatic, and dermal KS. For simplicity, this preliminary analysis only focussed on patients with dermal KS. Results from 8 patients are shown in this chapter and these had varying HIV status (2/8 negative, 6/8 positive). In all lesions, some features were immediately prominent upon examination of the tumour. Firstly, the epidermis was clearly distinguishable as a layer of cells close to the edge of each section (Figure 27A, a). Infiltrating lymphocytes were apparent by a rounded nuclear morphology and RBCs were also present in the lesion with distinct

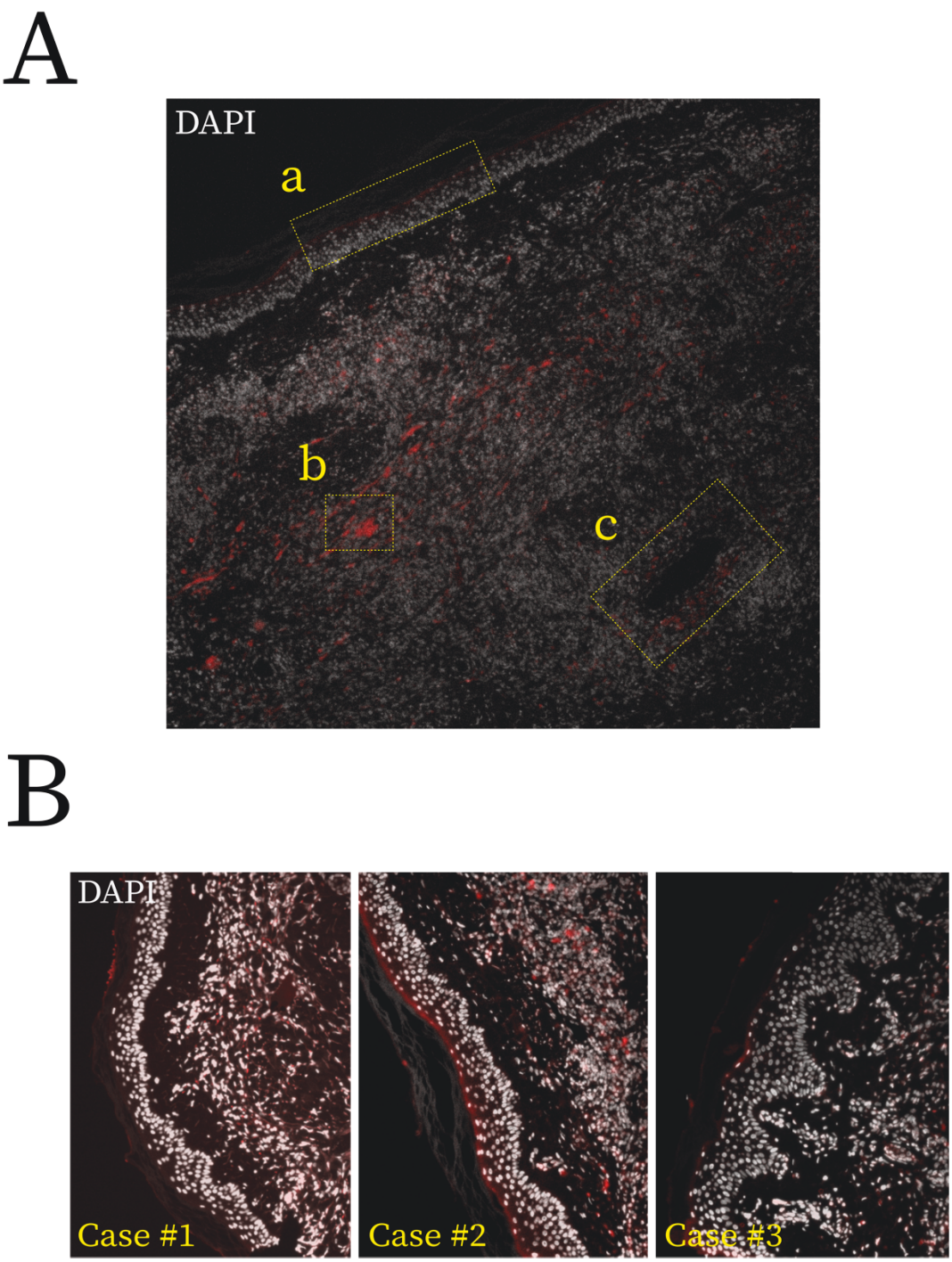

Figure 27: Overview of dermal KS sections. (A) Low magnification overview of representative KS section. Prominent features which were observed in all patients are highlighted: (a) Prominent epidermal layer with distinct stratum corneum at edge; (b) Invading RBCs, depicted and visible due to strong autofluorescence in Cy3 channel; (c) Neovascularisation within lesion. (B) Representative example of distinct epidermal layer at edge of biopsies. Examples from three distinct cases of dermal KS are shown.

and strong autofluorescence as reported[334] (Figure 27A, b). Neovascular spaces, which also included some RBCs, were apparent in all tumours (Figure 27A, c). In order to evaluate any differences in telomere length upon infection with KSHV from such tumour material, I set out to define a population of cells, which could serve as a baseline control of average telomere length within a patient. This is important due to the fact that telomere length varies significantly between individuals and with progressive age[335]. The epidermis within dermal KS lesions presented an ideal opportunity in this regard as it is: i) Clearly and reproducibly distinguishable from underlying tumour tissue (Figure 27B); ii) Free from KSHV infection (Figure 28B); iii) Present in all cases of dermal KS at the same location, namely the edge of the dermal biopsy section.

IHC/FISH was performed to identify KSHV infected cells within the tumour lesion and to obtain relative telomere length measurement for each case. LANA is routinely used in diagnostics to determine KSHV infection status of cells. Spindle cells were detected within all dermal KS cases and LANA was characteristically detectable as nuclear foci. Such spindle cells showed significantly elongated nuclear morphology and prominent LANA staining (Figure 28A). This was in stark contrast to the round morphology of bystander lymphocytes, which also occasionally showed LANA foci (<5% cells). These were excluded from automated analysis by size exclusion. In stark contrast to these cells, epidermal cells did not show any LANA foci and there was merely weak background localised to the epidermal ECM (Figure 28B). All cells showed clear telomere FISH foci with negligible background staining which enabled analysis of relative telomere length by qFISH in analogy to data presented on cell lines in chapter 2.

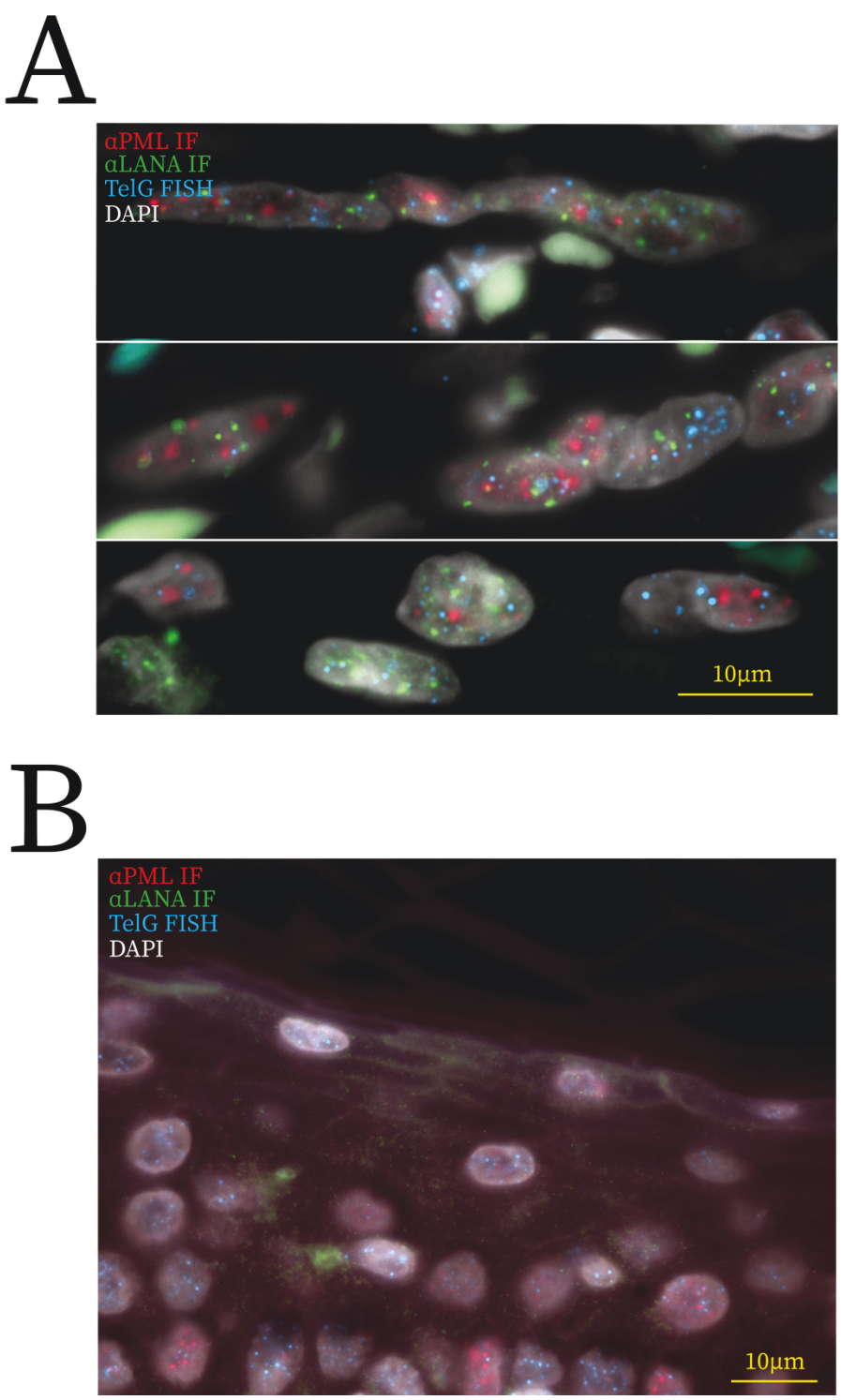

Figure 28: KS spindle cells and epidermis. (A) Representative images of spindle cells from three different patients. Strong LANA dots are prominent (green) within elongated nuclei as expected based on previous reports. (B) Example of uninfected epidermal cells from the same patient as top image of spindle cells. Weak background staining for LANA in the ECM, no LANA foci in confirmation of the uninfected state of patient epidermis.

Overview of PEL TMA

Examination of PEL patient material was carried using a tissue microarray (TMA) generated by Mr Mohamed Elsheikh and Prof. Naresh Kikkeri (Hammersmith hospital). This included selection of paraffin-embedded tumour material from 7 representative cases of PEL, generation of tissue cores, and re-sectioning. As expected, the predominant cell type detected upon IHC/FISH staining of array slides was plasmablast-like lymphocyte tumour cells with occasional uninfected bystander cells (Figure 29). As reported in previous analyses of this disease, there was an abundance of mitotic figures within cores from all patients[336]. LANA staining was very prominent in tumour cells. Telomere length changes were again evaluated by IHC/FISH in analogy to the approach described for KS. To this end, uninfected bystander cells within each core were compared directly with the LANA positive tumour cells.

Tumour cells have a heterogeneous number of LANA foci

LANA foci were detected in both KS and PEL as a proxy for determination of infected tumour cells for automated, comparative image analysis. During the course of this, the number of LANA foci per cell was determined and plotted for each patient. Overall, infected cells within each tumour varied considerably in the number of LANA foci per cell (Figure 30). The majority of KS spindle cells showed less than 10 individual LANA foci per nucleus and a maximum of 36 foci across all patients. In contrast to this, PEL tumour cells showed a relative increase in the number of LANA foci, and more than 10 foci were observed frequently in most patients (with the exception of PEL3 and PEL7). This is in agreement with published literature which strongly suggests increased KSHV copy number and LANA foci in PEL relative to KS. In summary, there is considerable heterogeneity in regards to the number of LANA foci in infected tumour cells both between patients and disease, which may indicate differences in viral copy number.

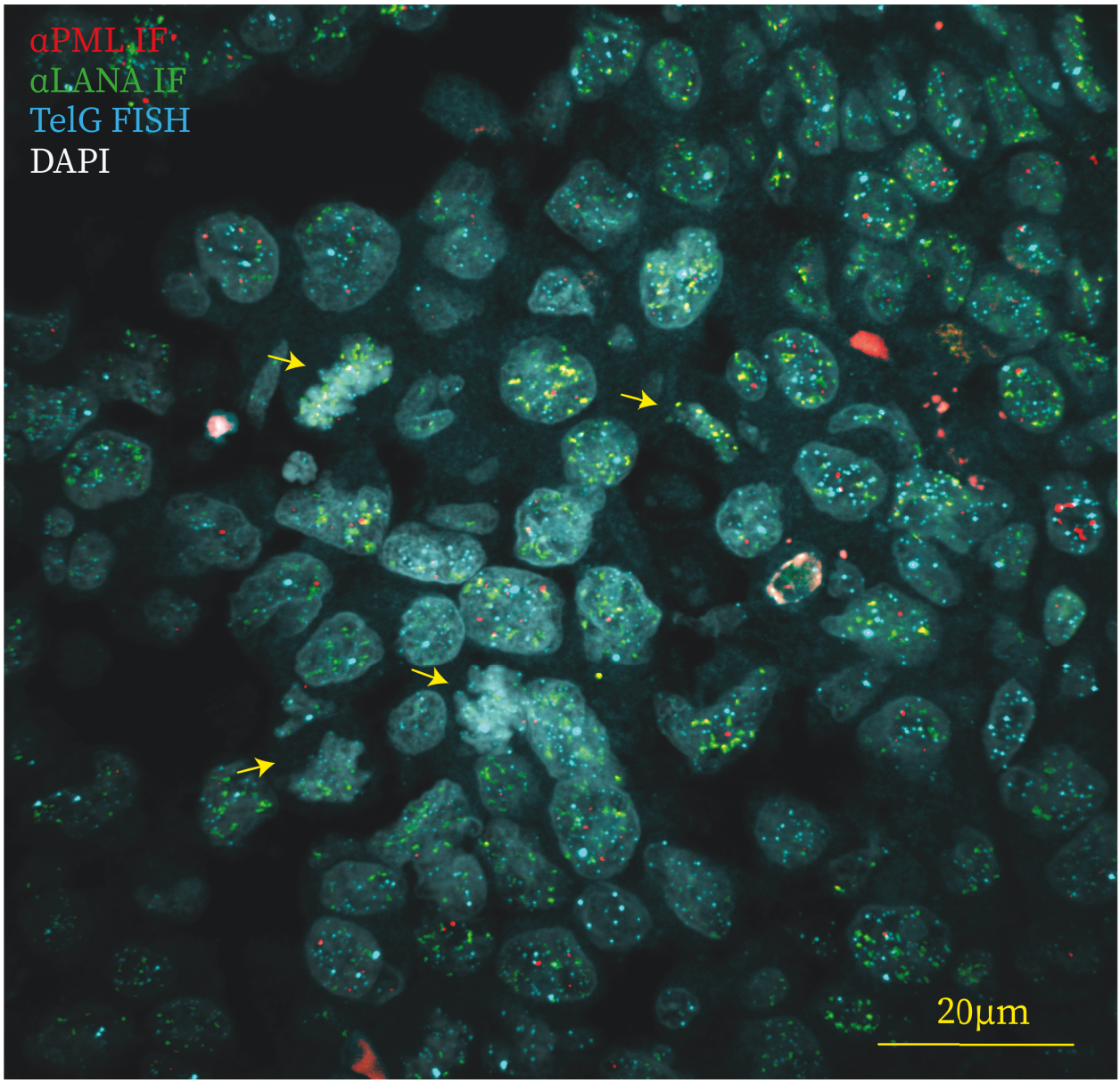

Figure 29: Example of PEL TMA section. Maximum intensity projection of confocal micrograph from a representative patient (PEL5) is shown from the PEL TMA included in this analysis. Plasmablast-like tumour cells with strong and numerous LANA foci (green) are visible as well as mitotic figures (indicated with arrows).

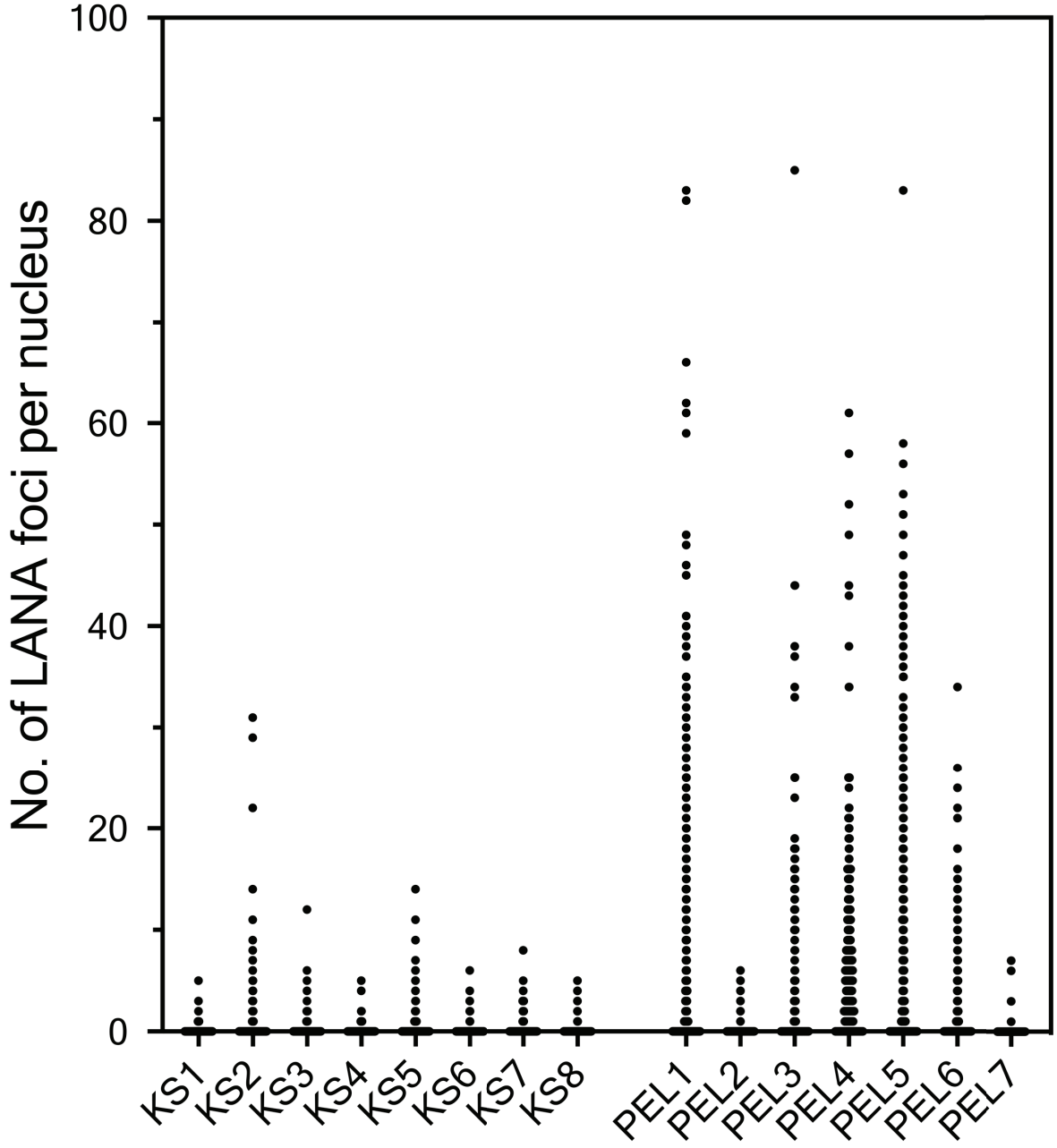

Figure 30: Quantification of LANA foci in tumour cells. Dot plot presenting the number of LANA foci per nucleus detected by CellProfiler in each patient included in subsequent analysis. All nuclei in every image obtained were considered in this analysis. Nuclear localization of foci was determined by thresholding on DAPI counterstain for each cell and relation to LANA signals.

Relative telomere length is increased and more heterogeneous in infected KS and PEL tumour cells

As described, spindle cell telomere length was determined by qFISH and compared to uninfected epidermal bystander cells. Only cells with LANA foci and elongated morphology were included in the analysis. The mean signal intensity was significantly higher in all KS patients (8/8) examined by this method (Figure 31). In addition to this, telomere length was found to be more heterogeneous in spindle cells. In material from PEL tumours, the effect of KSHV infection was analysed by comparison of LANA positive tumour cells with uninfected bystanders, regardless of cell morphology. Again, mean signal intensity was increased significantly in 3/7 patients whereas heterogeneity was significantly different in 6/7 cases. The increase in mean telomere signal intensity was consistently observed in infected cells relative to uninfected bystanders in 6/7 PEL cases, although this failed to reach significance in cases where the number of infected cells within the tumour was low (PEL2,3,7). Overall, the trend of mean increase and increased signal heterogeneity in telomere qFISH using biopsy material was highly consistent in KS patients (8/8) whereas cases of PEL showed greater variability.

There are a number of crucial follow-up and control experiments, which are necessary to consolidate these data. In the case of KS, biopsy across a tumour lesion to include neighbouring healthy tissue should be performed to control for cell-type specific variations in telomere length and application for ethical approval for such a biopsy is underway In addition to this, examination of PML co-localisation with telomeres as well as other markers of ALT activation will be carried out in analogy to the analysis performed in Chapter 1.

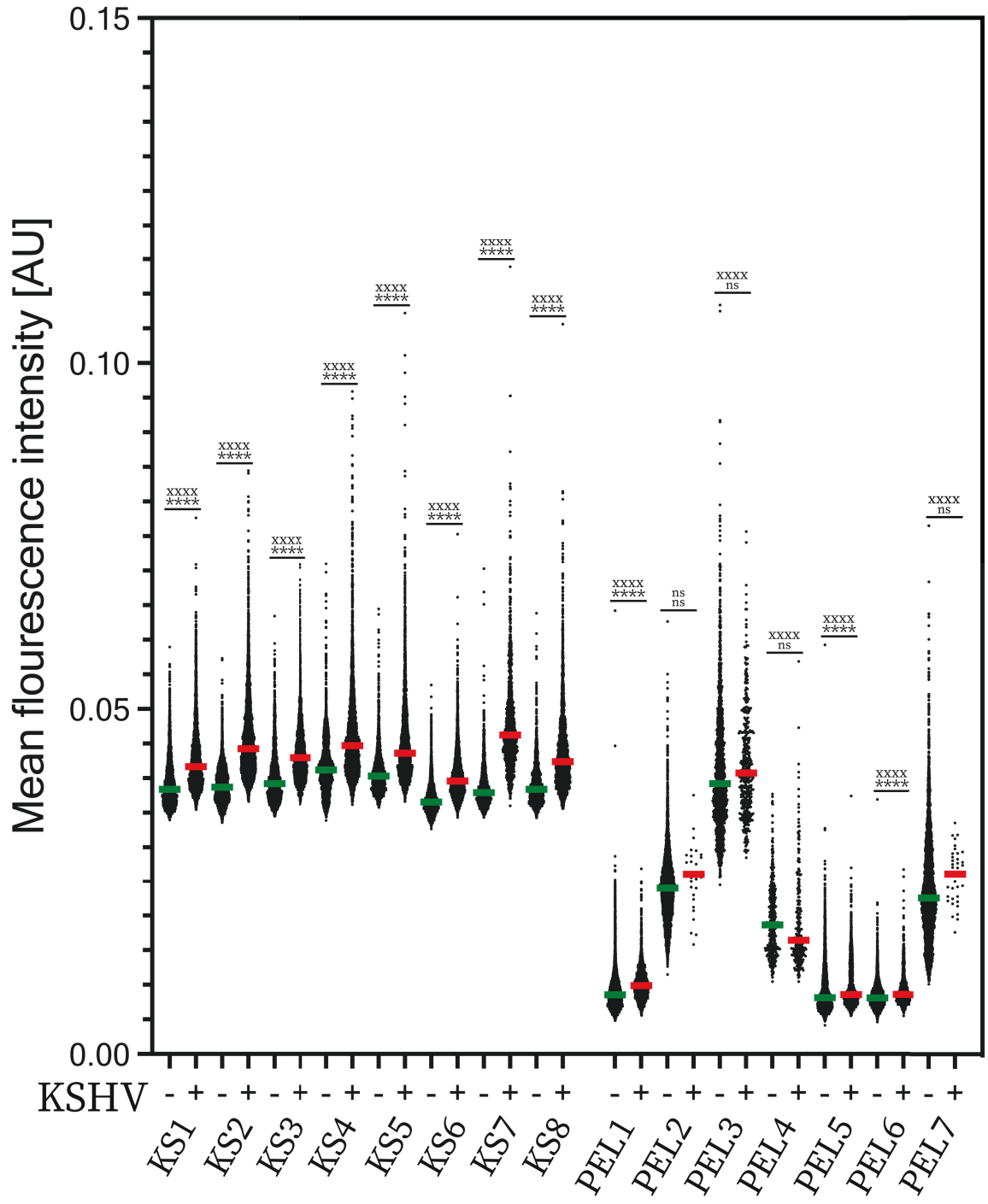

Figure 31: Relative telomere length is increased and heterogeneous in tumour cells. Automated quantification of telomere FISH mean signal intensity. Maximum of 3,000 individual telomere FISH foci were quantified for each condition. Differences are tested for significance with student's t-test ($^{ns}p>0.1$; $^{****}p<0.0001$) and heterogeneity is inferred by F-test of variance ($^{ns}p>0.1$; $^{xxxx}p<0.0001$).

Summary

Preliminary study of primary KS and PEL tumour sections was carried out with the aim of determining relative telomere length in KSHV infected cells within the tumour. The present work indicates that there is an increase in mean telomere length and heterogeneity in spindle cells within KS lesions and this is consistent in all 8 patients examined to date. In the PEL cases analysed, 3/7 showed significantly increased telomere length. Further analysis is necessary to consolidate these difference in telomere length and to conclude the existence of telomere maintenance via ALT *in vivo*. However, these data provide further incentive to pursue such analysis and present a system by which co-localisation of ALT factors with telomeric DNA as well as relative telomere length may be quantified by automated image analysis IHC/qFISH.

DISCUSSION

The present study uncovered broad modulation of the proteins bound to telomeric DNA in latently KSHV infected cells. This includes proteins involved in all major pathways that contribute to the repair of ds breaks and the relevance of these findings will be discussed. Intriguingly, proteins involved in HR were selectively enriched at telomeres, which led to the hypothesis that KSHV infection may trigger telomere maintenance by ALT. In line with this notion, telomeres in infected cells showed multiple features associated with ALT. Specifically, the data indicate that KSHV infection results in an increase in T-SCE, telomere fragility, telomere length heterogeneity, overall telomere length, and a dependency on ALT factors in terms of cellular proliferation. Further, ALT-associated DNA synthesis co-localized with LANA, the molecular tether of KSHV to host chromatin, and preliminary data suggests that maintenance of the latent episome may be dependent on ALT factors. Finally, telomere length and heterogeneity is increased in virus-infected cells within KS tumours, which indicates that the activation of ALT may also occur in the context of KSHV-associated cancer.

ALT is induced in initially telomerase^{+} cell lines upon KSHV infection

The data generated during the course of this project thus far indicate that telomere maintenance via ALT may be triggered in at least two cell lines in a reproducible fashion. These were initially solely reliant on telomerase for telomere elongation. The induction of the ALT phenotype was persistent and hallmarks of ALT were still detectable as long as 4 months after infection without any proliferative defect or induction of apoptosis. On the contrary, I consistently detected an increase in the rate of proliferation in infected cells relative to uninfected co-culture. This is in stark contrast to the reported ALT induction upon Asf1 knockdown where this was accompanied by progressive cell death[200] Interestingly, analysis of telomerase

activity by TRAP and RT-qPCR revealed that KSHV-ALT cell lines still expressed active telomerase. This is similar to what was observed upon ASF1 knockdown where the activity of telomerase was reduced relatively but not ablated completely upon ALT induction. The data generated so far are not sufficient to deduce the mechanism of telomerase downregulation and exclusion of remaining active telomerase from telomeres. Possible mechanisms which may underlie the observed downregulation in telomerase activity include the induction of telomeric transcription, TERRA as observed upon infection with HSV1[337]. TERRA expression has been reported to inhibit telomerase activity in multiple mouse and human cell types by direct competition with TERC and inhibition of TERT[338–340]. In addition to this, ectopic expression of TERRA alone in telomerase$^+$ cell lines was shown to inhibit telomerase activity and trigger progressive cellular senescence[341]. Another potential explanation is that activity may be reduced due to decreased expression of *hTERT*. During latency, KSHV LANA is a potent transcriptional regulator, which represses many host genes, and *hTERT* expression may be decreased in an analogous manner[267]. The decrease in telomerase activity observed in the models examined in this study may therefore be due to virus-induced transcription of telomeres resulting in TERRA accumulation as observed upon HSV1 infection[337] which blocks access of telomeres for the enzyme in combination with the subtle transcriptional downregulation of *hTERT* as described.

Induction of ALT is thought to be a multistep process, which involves remodelling of telomeric chromatin and DNA damage at telomeres. Multiple experiments support the induction of telomeric DNA damage in response to infection including PICh/mass spectrometry and IF-FISH experiments of various cell lines. Telomeric chromatin may be enriched for HP1α and associated heterochromatin marks such as H3K9me3 and K3K27me3. Perhaps somewhat counter intuitively, some studies have shown that HP1α-associated heterochromatin promotes HR[342]. LANA has been reported to interact directly with HP1α and other chromatin remodelling factors which promote heterochromatin such as PRC1/2[343], KAP1[344], and SET1[267]. These interactions are likely

not the only effect that LANA binding to chromatin has on host histone modification and deposition. LANA binds tightly to host histone H2A/B as well H3 and H4 with lower affinity via a conserved acidic patch on the overall nucleosome structure. This interaction induces compaction of chromatin fibres, a process which aids heterochromatin formation[345]. The same acidic patch on nucleosomes is the docking site for host chromatin remodelling enzymes including RCC3, Sir3, HMGN2 and LANA has been proposed to compete with these based on their shared chromatin binding site[346]. In addition to this, extensive heterochromatin formation and nucleosome compaction is a source and consequence of DNA damage[347,348]. Given that LANA binds host chromatin at telomeres in at least a subset of chromosomes in a metaphase of an infected cell, the onset of heterochromatin and nucleosome condensation via LANA in combination with DNA damage occurring in KSHV infected cells may induce ALT. On the other hand, other latency-associated factors may be responsible for the induction of ALT in the cell lines examined via different mechanisms. It is essential to evaluate these possibilities by future experiments, which will include ablation of KSHV protein binding to candidate host factors and a measure of subsequent ability of such virus to induce the ALT phenotype. However, based on existing literature as described above, we hypothesize that LANA, a potent chromatin remodeller which interacts and competes with the host histone modification/deposition machinery, promotes an ALT-like heterochromatin state at telomeres. Breakage of DNA to initiate ALT may be achieved by chromatin deregulation or other means such as recruitment of viral replication factors or replication-associated DNA damage in this setting. In summary, the underlying mechanism behind induction of the ALT phenotype reported in this study is unknown but may involve LANA-mediated modification of host chromatin.

ALT may be important for KSHV genome latency and replication

Co-evolution of KSHV with the human host provides precedent for a role of documented virus-host interactions in either viral propagation or host immune response. In the case of this study, preliminary data suggests that factors, which mediate ALT are important for the maintenance of KSHV episomes and survival of

infected cells. Whether this impeded survival is linked to the addiction of infected cells to viral factors encoded during latency remains to be determined. Nevertheless, these data suggest that the induction of ALT creates a state, which promotes viral latency and maintenance of latent episomes. In addition to this, the fact that ALT-associated DNA synthesis co-localizes with LANA, eg. KSHV episomes, could indicate that the site of active ALT telomere maintenance is in turn the site of episome persistence and/or replication.

KSHV latency establishment is crucially dependent on silencing of transcription on large parts of the viral episome. Repressive marks such as H3K27me3 and H2AK119ub are found on latent episomes and this is reported to occur in a PRC-dependent manner[349]. Highlighting the essential role of chromatin silencing for KSHV latency, inhibition of EZH2, the essential mediator of histone modification within the PRC complex, induces lytic reactivation of the virus[266]. Analogous chromatin repression by PRC complex has been reported to occur at telomeres in the setting of ALT[187] and, likewise, are found on KSHV episomes. It is therefore reasonable to propose that silencing of KSHV episomes in tandem with host telomeres may be beneficial for the virus. In other words, infection may trigger ALT to promote the activity of repressive chromatin remodelling enzymes such as PRC or HP1α at sites of viral episome tethering such as telomeres to facilitate the establishment of latency. However, it is also possible that such repressive factors are recruited to the viral episome in a manner independent of ALT induction and that the induction of ALT is an indirect consequence of occasional proximity of this repressive environment to host telomeres. Although we are not able to categorically rule out the latter possibility, the preliminary finding that knockdown of ALT factors leads to episome loss implicates that the ALT phenotype overall is essential for the persistence of viral genomes. Further experimentation is needed to clarify this such as the confirmation of HP1α and associated repressive marks on viral episomes or mutagenesis of the HP1α or PRC interaction site on KSHV LANA coupled to episome qPCR. In conclusion, the present data are in support of a model by which KSHV

infection induces ALT to create a cellular environment in which episomes are silenced effectively for the establishment of viral latency.

As described in the introduction to this thesis, existing literature suggests that KSHV episomes replicate in an atypical manner, which may be uncoupled from bulk S-phase DNA synthesis. The present study now indicates for the first time that this may occur through a BIR-like mechanism. Specifically, this hypothesis is supported by the incidence of ALT BIR foci at the site of LANA (and likely KSHV episomes) as well as by the aforementioned loss of viral episomes upon knockdown of key factors involved in ALT BIR. There are some interesting consequences of replication by BIR. It is inherently recombinogenic and produces mutations at a higher frequency than conventional DNA synthesis[350]. If the hypothesis that KSHV episomes may replicate via BIR proves to be correct, this provides a novel explanation for the observed recombinogenic nature of the KSHV genome. Further confirmation of KSHV episome replication by BIR is necessary and such experiments may be undertaken by extension of the methods performed during the course of this study. Taken together, the current work has provided first evidence for replication of KSHV episomes by a BIR-like mechanism during latency, which provides an intriguing explanation for the observed induction of ALT in infected cells.

However, a number of open questions remain conceptually in regards to the putative mechanism by which episome replication via BIR may proceed in infected cells. Firstly, the present data does by no means resolve the question as to how the initial break, which is necessary to generate a DNA end capable of BIR is generated on episomes. A number of scenarios are plausible in this respect. Firstly, the KSHV episome is highly GC-rich overall[211] and is known to form difficult to replicate DNA secondary structures such as G4 quadruplexes which limit replication during latency[351]. Thus, it is possible that even if normal S-phase replication is initiated on the episome, this process is prone to fork stalling due to the GC-rich nature of the KSHV genome overall and specifically at terminal repeats which are 85% GC[352].

Subsequent replication fork collapse and breakage may be sufficient to initiate BIR, especially considering the clustered nature of KSHV genomes which has been shown to be essential for replication during latency[271,353]. Another putative mode of break generation is the recruitment of endonucleases to the viral episome such as MUS81, ERCC4, or FEN1, which are capable of generating the substrate necessary for initiation of BIR. In summary, BIR at KSHV episome clusters within latently infected cells may be initiated by breaks occurring due to replication fork stalling and collapse or the recruitment of endonucleases.

Another unresolved aspect of this putative mechanism is revealed when considering the fact that replication of KSHV episomes during latency proceeds in a manner which does not result in a large-scale amplification of copy number. Therefore, the question arises as to how a BIR-like replication mechanism may exist that only results in a mean duplication of viral episomes during each cycle of cell division. One possible explanation is that KSHV episomes are tightly bound by many copies of LANA at the terminal repeats. In fact, each KSHV genome harbours 5-15 of such repeats, and binding of LANA oligomer binding results in strong curvature and compaction of this region on the episome[354]. In addition to this, replication is preferentially initiated immediately upstream of the terminal repeat region[355]. Thus, a model in which BIR-like DNA replication is initiated by invasion into a region adjacent to the terminal repeat region and proceed for one round prior to encountering the LANA oligomer may be suggested based on these reports. The action of factors which resolve and terminate BIR in the context of ALT are an additional factors which may be important for such termination. Both SLX4-mediated nuclease cleavage or BLM-mediated d-loop resolution are in theory sufficient to end DNA synthesis by BIR. Therefore, multiple rounds of BIR in the context of KSHV episome replication may be restricted by tethering of LANA to the terminal repeats and/or the activity of BLM and SLX4.

KSHV is capable of ALT induction and this may be used for efficient establishment of latency or viral episome replication by BIR. Additional open questions remain concerning the initiation and termination of such a reaction at KSHV episomes. In summary, the induction of ALT by latent KSHV infection may have evolved as a mechanism by which a chromatin niche within the host genome is created which facilitates the establishment of latency or to enable episome replication by BIR.

KSHV infection may induce ALT *in vivo*

The activation of ALT by latent KSHV infection, which has been documented in this study, may not be limited to cell culture and this is supported by preliminary analysis of KSHV-associated tumours. Thus far, an increase in telomere length and heterogeneity has been detected in KSHV infected cells relative to uninfected bystander cells within the same tissue. Further work is needed to ratify the presence of ALT telomere maintenance in patients. This includes thorough analysis of the existing collection of KS tumour sections (43 patient total) and PEL tissue microarray (7 patients) for the presence of DDR and ALT markers at telomeres. In addition to this, access to fresh tissue from KS biopsy has been obtained and analysis of these by TRAP and C-circle assay will provide a means to evaluate the activation of ALT in the context of KSHV-associated cancer. Given the presence of lytic reactivation within KSHV-associated cancer[224,261,295], additional factors which have not been considered in terms of induction of ALT in our strictly latent *in vitro* systems may be important in this context. Taken together, the current work has uncovered the induction of telomere maintenance in strictly latent cell line models and this may be taken as a starting point for confirmation in patients based on preliminary data.

Clinical relevance

As discussed, there is an outstanding clinical need for new, targeted therapy in the context of KSHV-associated blood cancers. Compounds that target ALT specifically are under development by several parties. Further validation of the activity of this pathway in KSHV-associated PEL and MCD primary tumour samples may provide the basis for trial of such drugs in the context of these diseases.

Another interesting application of these findings results from the dependency of KSHV episome replication on factors involve in ALT as indicate by preliminary data generated during the course of this work (Figure 21). This implicates that induction of ALT may be necessary for episome persistence and establishment of latency. As discussed, evaluation of the viral factor which is underlying the activation of ALT telomere maintenance is underway. If the precise virus-host interaction can be determined and mutated in the viral genome, this may provide a mutant strain which is only able to infect cells which already have active ALT telomere maintenance. The implications of the generation of such a strain are significant since to date, no tool exists to label and determine the identity of cells which are ALT^{+} in a mixed population. This may be achieved by generation of such a strain which carries a selectable marker. Theoretically, the establishment of such a system may also serve as a means to deliver a gene product to ALT cells specifically which would provide the basis for mutant KSHV-based gene therapy. Such a tool would be then applicable to identify ALT cells and potentially deliver a death signal of therapeutic modality to such cells specifically.

Another important consideration is the transfer of such findings into other related infections with oncogenic EBV. There are many significant similarities between KSHV and EBV including its persistence as an episome during viral latency. Again, the precise mechanism of viral genome replication during latency is not established for this virus either. Intriguingly, there are some reports of aspects of an ALT-like

phenotype in LCLs generated by transformation of primary B-cells with EBV including the presence of γH2AX, 53bp1, and PML at telomeres[356]. In a follow-up report by the same group, comparison with mitogen-transformed LCLs indicated relative telomere length heterogeneity and a transient increase in T-SCEs[357]. Further work *in vitro* is needed to clearly indicate the induction of ALT in analogy to the work carried out in this study on KSHV. In addition to this, an evaluation of the status of ALT in EBV-associated cancers should be carried out including nasopharyngeal carcinomas, gastric cancers, and Burkitt's lymphoma. Overall, the present study together with the previous reports in the literature described above provide merit for an investigation into the induction of ALT in the context of EBV-associated cancers.

Future work

The first aim of the future work carried out on this project is the extension of my evidence on ALT induction upon infection with KSHV. Current work *in vitro* will be complemented by C-circle analysis in biological triplicate in EA.hy926 and SLK cells. In addition to this, existing data indicating enrichment of key ALT factors at telomeres will be extended by IF-FISH. Concerning the confirmation of the phenotype *in vivo*, two principle approaches will be taken. Firstly, existing analysis by IHC/FISH will be extended on the existing collection of paraffin-embedded KS/PEL tumour sections compiled for this project. Second, fresh tumour tissue from biopsy of KS will be subjected to analysis by TRAP and C-circle assay. Together, these experiments will unequivocally confirm the induction of ALT *in vitro* and indicate whether this is also the case in patient tumours, namely KS and PEL.

The next aim of the work going forward on this project is the confirmation of the role of ALT factors in the maintenance of latent KSHV episomes as indicated by pilot experiments. Specifically, direct evidence for this model could be generated by EdU pulse-labelling during G2/M in analogy to the visualization of active BIR by

click-iT chemistry and microscopy. If the episome is replicated via a BIR-like mechanism, biotinylation by Click-iT chemistry coupled to Streptavidin pulldown and qPCR against episome sequences will result in a specific amplicon and provide direct evidence for the model proposed. In addition to this, the dependency of episome replication on the expression of ALT factors as indicated by preliminary data will be confirmed by further experimentation. To this end, constitutive RNAi or CRISPRi cell lines +/- rKSHV may be established to improve the existing experimental setup. Concerning the hypothesis that episome latency utilises chromatin modifications which are synthesised in tandem with ALT telomere chromatin modification, confirmation of such modifications on the viral episome will be carried out by ChIP/qPCR. This assay should also be carried out in systems where interaction with chromatin remodelling enzymes such as HP1α is mutated, as described for the final aim.

This encompasses the examination of the mechanism which underlies the induction of ALT. As discussed, LANA is considered a likely candidate based on careful examination of the literature as well as preliminary data generated during the course of the project. There are a number of candidate interactions which may be examined with the aim of delineating the underlying molecular mechanism of ALT induction. This includes interaction with TRF1 and RPA heterotrimer as indicated by proteomic screens[303,304] as well as histone remodelling factor HP1α. This will be carried out by endogenous IP/Western blot as well as the expression of recombinant protein in insect cells for biochemical interaction studies. Peptide arrays corresponding to the full length of LANA have been synthesised and will be probed with recombinant protein with the aim of determining the precise interaction site on LANA. These experiments will be taken as a basis for mutagenesis of LANA at the site of interaction with potential factors underlying the induction of ALT. There are significant challenges in terms of editing the KSHV episome and therefore an approach using the KSHV TR mini-plasmid and ectopic expression of LANA will be used for this aim. Such cell lines have been generated and will be tested for their

ALT status prior to LANA mutagenesis experiments. Overall, the future work on delineating the precise mechanism by which KSHV induces ALT will focus on LANA based on the data generated thus far with the focus of generating a mutation in LANA which will render KSHV incapable of ALT induction and therefore prove a direct causal relationship.

Conclusion

Analysis of the telomere-associated proteome in response to KSHV infection indicates broad modulation of all major DDR pathways at telomeres including cNHEJ, MMEJ, and HR. Of these candidate differences in protein enrichment, the modulation of HR at telomeres in response to infection was examined in greater detail. This study provides evidence that KSHV is capable of inducing ALT in several cell lines, which initially used telomerase to maintain their telomeres. This is only the second time that such a phenomenon has been recorded to date. Further investigation suggests a model in which the virus induces this phenotype for the maintenance of its episome genome. Specifically, the present data suggest that an ALT BIR-like mechanism contributes to the replication of KSHV episomes. KSHV induced ALT activation may not be limited to cell lines as the present study shows some indication of ALT in sections of primary KS and PEL tumours. Further investigation to validate these findings is underway with the aim of establishing ALT as a potential future therapeutic target for KSHV-associated cancers. These findings give an unprecedented indication that KSHV has evolved a mechanism by which it is capable of modulating the DDR at telomeres to its advantage, perhaps as a means of replicating its episomes during latency.

REFERENCES

1. Hoeijmakers JHJ. DNA Damage, Aging, and Cancer. 2009:1475-1485.
2. Lindahl T. Instability and decay of the primary structure of DNA. *Nature*. 1993;362(6422):709-715. doi:10.1038/362709a0
3. Haber JE. DNA recombination: The replication connection. *Trends Biochem Sci*. 1999;24(7):271-275. doi:10.1016/S0968-0004(99)01413-9
4. Vilenchik MM, Knudson AG. Endogenous DNA double-strand breaks: Production, fidelity of repair, and induction of cancer. *Proc Natl Acad Sci U S A*. 2003;100(22):12871-12876. doi:10.1073/pnas.2135498100
5. Khanna KK, Jackson SP. DNA double-strand breaks: Signaling, repair and the cancer connection. *Nat Genet*. 2001;27(3):247-254. doi:10.1038/85798
6. Grawunder U, Zimmer D, Fugmann S, Schwarz K, Lieber MR. for V (D) J Recombination and DNA Double-Strand Break Repair in Human Precursor Lymphocytes. *Cell*. 1998;2(D):477-484.
7. Susumu T. Somatic generation of antibody diversity. *Nature*. 1983;302:575-581. https://www.nature.com/articles/302575a0.pdf%0Ahttps://proxy.library.upenn.edu:2611/articles/302575a0.pdf.
8. Kenter A, Wuerffel R. Immunoglobulin switch recombination may occur by a DNA end-joining mechanism. *Ann N Y Acad Sci*. 1999;870:206-217. doi:10.1111/j.1749-6632.1999.tb08880.x
9. Mahaney BL, Meek K, Lees-Miller SP. Repair of ionizing radiation-induced DNA double-strand breaks by non-homologous end-joining. *Biochem J*. 2009;417(3):639-650. doi:10.1042/BJ20080413
10. Muslimović A, Nyström S, Gao Y, Hammarsten O. Numerical analysis of etoposide induced DNA breaks. *PLoS One*. 2009;4(6):e5859-e5859. doi:10.1371/journal.pone.0005859
11. Sears CR, Turchi JJ. Complex cisplatin-double strand break (DSB) lesions directly impair cellular non-homologous end-joining (NHEJ) independent of downstream damage response (DDR) pathways. *J Biol Chem*. 2012;287(29):24263-24272. doi:10.1074/jbc.M112.344911
12. Greinert R, Volkmer B, Henning S, et al. UVA-induced DNA double-strand breaks result from the repair of clustered oxidative DNA damages. *Nucleic Acids Res*. 2012;40(20):10263-10273. doi:10.1093/nar/gks824
13. Blackford AN, Jackson SP. ATM, ATR, and DNA-PK: The Trinity at the Heart of the DNA Damage Response. *Mol Cell*. 2017;66(6):801-817. doi:10.1016/j.molcel.2017.05.015
14. Scully R, Panday A, Elango R, Willis NA. DNA double-strand break repair-pathway choice in somatic mammalian cells. *Nat Rev Mol Cell Biol*. 2019. doi:10.1038/s41580-019-0152-0
15. Bednarski JJ, Pandey R, Schulte E, et al. RAG-mediated DNA double-strand breaks activate a

cell type-specific checkpoint to inhibit pre{\textendash}B cell receptor signals. *J Exp Med*. 2016;213(2):209-223. doi:10.1084/jem.20151048

16. Sonoda E, Sasaki MS, Buerstedde JM, et al. Rad51-deficient vertebrate cells accumulate chromosomal breaks prior to cell death. *EMBO J*. 1998;17(2):598-608. doi:10.1093/emboj/17.2.598
17. Saha J, Wang SY, Davis AJ. *Examining DNA Double-Strand Break Repair in a Cell Cycle-Dependent Manner*. Vol 591. 1st ed. Elsevier Inc.; 2017. doi:10.1016/bs.mie.2017.03.012
18. Gurley KE, Vo K, Kemp CJ. DNA double-strand breaks, p53, and apoptosis during lymphomagenesis in scid/scid mice. *Cancer Res*. 1998;58(14):3111-3115.
19. Li J, Stern DF. Regulation of CHK2 by DNA-dependent Protein Kinase *. 2005;280(12):12041-12050. doi:10.1074/jbc.M412445200
20. Matsuoka S, Huang M, Elledge SJ. Linkage of ATM to cell cycle regulation by the Chk2 protein kinase. *Science (80-)*. 1998;282(5395):1893-1897. doi:10.1126/science.282.5395.1893
21. Xu X, Tsvetkov LM, Stern DF. Chk2 Activation and Phosphorylation-Dependent Oligomerization. *Mol Cell Biol*. 2002;22(12):4419-4432. doi:10.1128/mcb.22.12.4419-4432.2002
22. Falck J, Mailand N, Syljua RG. The ATM-Chk2 - Cdc25A checkpoint pathway guards against radioresistant DNA synthesis. *Nature*. 2001;410(April):842-847.
23. Ahn J, Prives C. Checkpoint kinase 2 (Chk2) monomers or dimers phosphorylate Cdc25C after DNA damage regardless of threonine 68 phosphorylation. *J Biol Chem*. 2002;277(50):48418-48426. doi:10.1074/jbc.M208321200
24. Buisson R, Boisvert JL, Benes CH, Zou L. Distinct but Concerted Roles of ATR, DNA-PK, and Chk1 in Countering Replication Stress during S-Phase. *Mol Cell*. 2015;59(6):1011-1024. doi:10.1016/j.molcel.2015.07.029
25. Gatei M, Sloper K, Sörensen C, et al. ATM and NBS1 dependent phosphorylation of CHK1 on S317 in response to IR Kum Kum Khanna. 2003.
26. Chehab NH, Malikzay A, Appel M, Halazonetis TD. Chk2/hCds1 functions as a DNA damage checkpoint in G1 by stabilizing p53. *Genes Dev*. 2000;14(3):278-288.
27. Lukas J, Bartek J. Mammalian G1- and S-phase checkpoints in response to DNA damage. *Curr Opin Cell Biol*. 2001;13:738-747.
28. Bree RT, Neary C, Samali A, Lowndes NF. The switch from survival responses to apoptosis after chromosomal breaks. *DNA Repair (Amst)*. 2004;3(8-9):989-995. doi:10.1016/j.dnarep.2004.03.016
29. Boehme KA, Kulikov R, Blattner C. p53 stabilization in response to DNA damage requires Akt/PKB and DNA-PK. *Proc Natl Acad Sci*. 2008;105(22):7785-7790. doi:10.1073/pnas.0703423105

30. Mayo LD, Turchi JJ, Berberich SJ. Mdm-2 Phosphorylation by DNA-dependent Protein Kinase Prevents Interaction with p53. *Cancer Res*. 1997;57(22):5013-5016. https://cancerres.aacrjournals.org/content/57/22/5013.

31. Khosravi R, Maya R, Gottlieb T, Oren M, Shiloh Y, Shkedy D. Rapid ATM-dependent phosphorylation of MDM2 precedes p53 accumulation in response to DNA damage. *Proc Natl Acad Sci*. 1999;96(26):14973-14977. doi:10.1073/pnas.96.26.14973

32. Maya R, Balass M, Kim ST, et al. ATM-dependent phosphorylation of Mdm2 on serine 395: role in p53 activation by DNA damage. *Genes Dev*. 2001;15(9):1067-1077. doi:10.1101/gad.886901

33. Nakano K, Vousden KH. PUMA , a Novel Proapoptotic Gene , Is Induced by p53 National Cancer Institute at Frederick. *Mol Cell*. 2001;7:683-694. doi:10.1177/1080569904265421

34. Yu J, Zhang L, Hwang PM, Kinzler KW, Vogelstein B. Molecular Cell 674. 2001;7:673-682. doi:10.1016/s1097-2765(00)80265-8

35. Oda E, Ohki R, Murasawa H, et al. Noxa, a BH3-Only Member of the Bcl-2 Family and Candidate Mediator of p53-Induced Apoptosis. *Science* 288(5468), 2000:1053-1058. doi:10.1126/science.288.5468.1053

36. Shibue T, Takeda K, Oda E, et al. Integral role of Noxa in p53-mediated apoptotic response. *Genes Dev*. 2003;17(18):2233-2238. doi:10.1101/gad.1103603

37. Frit P, Ropars V, Modesti M, Charbonnier JB, Calsou P. Plugged into the Ku-DNA hub: The NHEJ network. *Prog Biophys Mol Biol*. 2019. doi:https://doi.org/10.1016/j.pbiomolbio.2019.03.001

38. Mao Z, Bozzella M, Seluanov A, Gorbunova V. DNA repair by nonhomologous end joining and homologous recombination during cell cycle in human cells. *Cell Cycle*. 2008;7(18):2902-2906. doi:10.4161/cc.7.18.6679

39. Orthwein A, Fradet-Turcotte A, Noordermeer SM, et al. Mitosis inhibits DNA double-strand break repair to guard against telomere fusions. *Science* 2014;344(6180):189-193. doi:10.1126/science.1248024

40. Britton S, Coates J, Jackson SP. A new method for high-resolution imaging of Ku foci to decipher mechanisms of DNA double-strand break repair. *J Cell Biol*. 2013;202(3):579-595. doi:10.1083/jcb.201303073

41. Walker JR, Corpina RA, Goldberg J. Structure of the Ku heterodimer bound to dna and its implications for double-strand break repair. *Nature*. 2001;412(6847):607-614. doi:10.1038/35088000

42. Gottlieb TM, Jackson SP. The DNA-dependent protein kinase: Requirement for DNA ends and association with Ku antigen. *Cell*. 1993;72(1):131-142. doi:https://doi.org/10.1016/0092-8674(93)90057-W

43. Singleton BK, Torres-Arzayus MI, Rottinghaus ST, Taccioli GE, Jeggo PA. The C Terminus of Ku80 Activates the DNA-Dependent Protein Kinase Catalytic Subunit. *Mol Cell Biol*. 1999;19(5):3267-3277. doi:10.1128/MCB.19.5.3267

44. Stiff T, O'Driscoll M, Rief N, Iwabuchi K, Löbrich M, Jeggo PA. ATM and DNA-PK Function Redundantly to Phosphorylate H2AX after Exposure to Ionizing Radiation. *Cancer Res*. 2004;64(7):2390-2396. doi:10.1158/0008-5472.CAN-03-3207

45. Nick McElhinny SA, Snowden CM, McCarville J, Ramsden DA. Ku Recruits the XRCC4-Ligase IV Complex to DNA Ends. *Mol Cell Biol*. 2000;20(9):2996 LP - 3003. doi:10.1128/MCB.20.9.2996-3003.2000

46. Ochi T, Blackford AN, Coates J, et al. PAXX, a paralog of XRCC4 and XLF, interacts with Ku to promote DNA double-strand break repair. *Science* 2015;347(6218):185-188. doi:10.1126/science.1261971

47. Ahnesorg P, Smith P, Jackson SP. XLF interacts with the XRCC4-DNA Ligase IV complex to promote DNA nonhomologous end-joining. *Cell*. 2006;124(2):301-313. doi:10.1016/j.cell.2005.12.031

48. Hammel M, Yu Y, Radhakrishnan SK, et al. An intrinsically disordered APLF links Ku, DNA-PKcs, and XRCC4-DNA ligase IV in an extended flexible non-homologous end joining complex. *J Biol Chem*. 2016;291(53):26987-27006. doi:10.1074/jbc.M116.751867

49. Graham TGW, Walter JC, Loparo JJ. Two-Stage Synapsis of DNA Ends during Non-homologous End Joining. *Mol Cell*. 2016;61(6):850-858. doi:10.1016/j.molcel.2016.02.010

50. Corbeski I, Dolinar K, Wienk H, Boelens R, Van Ingen H. DNA repair factor APLF acts as a H2A-H2B histone chaperone through binding its DNA interaction surface. *Nucleic Acids Res*. 2018;46(14):7138-7152. doi:10.1093/nar/gky507

51. Kurosawa A, Saito S, So S, et al. DNA Ligase IV and Artemis Act Cooperatively to Suppress Homologous Recombination in Human Cells: Implications for DNA Double-Strand Break Repair. *PLoS One*. 2013;8(8). doi:10.1371/journal.pone.0072253

52. Gerodimos CA, Chang HHY, Watanabe G, Lieber MR. Effects of DNA end configuration on XRCC4-DNA ligase IV and its stimulation of Artemis activity. *J Biol Chem*. 2017;292(34):13914-13924. doi:10.1074/jbc.M117.798850

53. Daniel Aceytuno R, Piett CG, Havali-Shahriari Z, et al. Structural and functional characterization of the PNKP-XRCC4-LigIV DNA repair complex. *Nucleic Acids Res*. 2017;45(10):6238-6251. doi:10.1093/nar/gkx275

54. Li J, Summerlin M, Nitiss KC, Nitiss JL, Hanakahi LA. TDP1 is required for efficient non-homologous end joining in human cells. *DNA Repair (Amst)*. 2017;60(March):40-49. doi:10.1016/j.dnarep.2017.10.003

55. Guirouilh-Barbat J, Huck S, Bertrand P, et al. Impact of the KU80 Pathway on NHEJ-Induced

Genome Rearrangements in Mammalian Cells. *Mol Cell*. 2004;14(5):611-623. doi:https://doi.org/10.1016/j.molcel.2004.05.008

56. Sun J, Lee KJ, Davis AJ, Chen DJ. Human Ku70/80 protein blocks exonuclease 1-mediated DNA resection in the presence of human Mre11 or Mre11/Rad50 protein complex. *J Biol Chem*. 2012;287(7):4936-4945. doi:10.1074/jbc.M111.306167
57. Escribano-Diaz C, Orthwein A, Fradet-Turcotte A, et al. A cell cycle-dependent regulatory circuit composed of 53BP1-RIF1 and BRCA1-CtIP controls DNA repair pathway choice. *Mol Cell*. 2013;49(5):872-883. doi:10.1016/j.molcel.2013.01.001
58. Takata M, Sasaki MS, Sonoda E, et al. Homologous recombination and non-homologous end-joining pathways of DNA double-strand break repair have overlapping roles in the maintenance of chromosomal integrity in vertebrate cells. *EMBO J*. 1998;17(18):5497-5508. doi:10.1093/emboj/17.18.5497
59. Myler LR, Gallardo IF, Soniat MM, et al. Single-Molecule Imaging Reveals How Mre11-Rad50-Nbs1 Initiates DNA Break Repair. *Mol Cell*. 2017;67(5):891-898.e4. doi:10.1016/j.molcel.2017.08.002
60. Desai-Mehta A, Cerosaletti KM, Concannon P. Distinct Functional Domains of Nibrin Mediate Mre11 Binding, Focus Formation, and Nuclear Localization. *Mol Cell Biol*. 2001;21(6):2184-2191. doi:10.1128/mcb.21.6.2184-2191.2001
61. Falck J, Coates J, Jackson SP. Conserved modes of recruitment of ATM, ATR and DNA-PKcs to sites of DNA damage. *Nature*. 2005;434(7033):605-611. doi:10.1038/nature03442
62. Lee J-H, Paull TT. Direct Activation of the ATM Protein Kinase by the Mre11/Rad50/Nbs1 Complex. *Science (80-)*. 2004;304(5667):93-96. doi:10.1126/science.1091496
63. Rogakou EP, Pilch DR, Ann H, et al. DNA Double-stranded Breaks Induce DNA Double-stranded Breaks Induce Histone H2AX Phosphorylation on Serine 139 *. *J Biol Chem*. 1998;273(10):1-12. doi:10.1074/jbc.273.10.5858
64. Sacho EJ, Maizels N. DNA repair factor MRE11/RAD50 cleaves 3′-phosphotyrosyl bonds and resects DNA to repair damage caused by topoisomerase 1 poisons. *J Biol Chem*. 2011;286(52):44945-44951. doi:10.1074/jbc.M111.299347
65. Sartori AA, Lukas C, Coates J, et al. Human CtIP promotes DNA end resection. *Nature*. 2007;450(7169):509-514. doi:10.1038/nature06337
66. Anand R, Ranjha L, Cannavo E, Cejka P. Phosphorylated CtIP Functions as a Co-factor of the MRE11-RAD50-NBS1 Endonuclease in DNA End Resection. *Mol Cell*. 2016;64(5):940-950. doi:10.1016/j.molcel.2016.10.017
67. Nimonkar A V., Genschel J, Kinoshita E, et al. BLM-DNA2-RPA-MRN and EXO1-BLM-RPA-MRN constitute two DNA end resection machineries for human DNA break repair. *Genes Dev*. 2011;25(4):350-362. doi:10.1101/gad.2003811

68. San Filippo J, Sung P, Klein H. Mechanism of eukaryotic homologous recombination. *Annu Rev Biochem*. 2008;77:229-257. doi:10.1146/annurev.biochem.77.061306.125255
69. Wong JMS, Ionescu D, Ingles CJ. Interaction between BRCA2 and replication protein A is compromised by a cancer-predisposing mutation in BRCA2. *Oncogene*. 2003;22(1):28-33. doi:10.1038/sj.onc.1206071
70. Prakash R, Zhang Y, Feng W, Jasin M. Homologous recombination and human health: the roles of BRCA1, BRCA2, and associated proteins. *Cold Spring Harb Perspect Biol*. 2015;7(4):a016600. doi:10.1101/cshperspect.a016600
71. Marmorstein LY, Ouchi T, Aaronson SA. The BRCA2 gene product functionally interacts with p53 and RAD51. *Proc Natl Acad Sci*. 1998;95(23):13869-13874. doi:10.1073/pnas.95.23.13869
72. Zhao W, Steinfeld JB, Liang F, et al. BRCA1–BARD1 promotes RAD51-mediated homologous DNA pairing. *Nature*. 2017;550:360. https://doi.org/10.1038/nature24060.
73. Maloisel L, Fabre F, Gangloff S. DNA polymerase delta is preferentially recruited during homologous recombination to promote heteroduplex DNA extension. *Mol Cell Biol*. 2008;28(4):1373-1382. doi:10.1128/MCB.01651-07
74. Bachrati CZ, Borts RH, Hickson ID. Mobile D-loops are a preferred substrate for the Bloom's syndrome helicase. *Nucleic Acids Res*. 2006;34(8):2269-2279. doi:10.1093/nar/gkl258
75. Opresko PL, Sowd G, Wang H. The Werner syndrome helicase/exonuclease processes mobile D-loops through branch migration and degradation. *PLoS One*. 2009;4(3). doi:10.1371/journal.pone.0004825
76. Vannier J-B, Petalcorin MIR, Boulton SJ, et al. RTEL1 is a replisome-associated helicase that promotes telomere and genome-wide replication. *Science (80-)*. 2013;342(6155):239-242. doi:10.1126/science.1241779
77. Barber LJ, Youds JL, Ward JD, et al. RTEL1 Maintains Genomic Stability by Suppressing Homologous Recombination. *Cell*. 2008;135(2):261-271. doi:10.1016/j.cell.2008.08.016
78. Fasching CL, Cejka P, Kowalczykowski SC, Heyer W-D. Top3-Rmi1 dissolve Rad51-mediated D loops by a topoisomerase-based mechanism. *Mol Cell*. 2015;57(4):595-606. doi:10.1016/j.molcel.2015.01.022
79. Sun W, Nandi S, Osman F, et al. The FANCM Ortholog Fml1 Promotes Recombination at Stalled Replication Forks and Limits Crossing Over during DNA Double-Strand Break Repair. *Mol Cell*. 2008;32(1):118-128. doi:10.1016/j.molcel.2008.08.024
80. Svendsen JM, Smogorzewska A, Sowa ME, et al. Mammalian BTBD12/SLX4 Assembles A Holliday Junction Resolvase and Is Required for DNA Repair. *Cell*. 2009;138(1):63-77. doi:10.1016/j.cell.2009.06.030
81. Amangyeld T, Shin YK, Lee M, Kwon B, Seo YS. Human MUS81-EME2 can cleave a variety of DNA structures including intact Holliday junction and nicked duplex. *Nucleic Acids Res*.

2014;42(9):5846-5862. doi:10.1093/nar/gku237

82. Wyatt HDM, Sarbajna S, Matos J, West SC. Coordinated actions of SLX1-SLX4 and MUS81-EME1 for holliday junction resolution in human cells. *Mol Cell*. 2013;52(2):234-247. doi:10.1016/j.molcel.2013.08.035
83. Rothenberg E, Grimme JM, Spies M, Ha T. Human Rad52-mediated homology search and annealing occurs by continuous interactions between overlapping nucleoprotein complexes. *Proc Natl Acad Sci U S A*. 2008;105(51):20274-20279. doi:10.1073/pnas.0810317106
84. Grimme JM, Honda M, Wright R, et al. Human Rad52 binds and wraps single-stranded DNA and mediates annealing via two hRad52-ssDNA complexes. *Nucleic Acids Res*. 2010;38(9):2917-2930. doi:10.1093/nar/gkp1249
85. Motycka TA, Bessho T, Post SM, Sung P, Tomkinson AE. Physical and Functional Interaction between the XPF/ERCC1 Endonuclease and hRad52. *J Biol Chem*. 2004;279(14):13634-13639. doi:10.1074/jbc.M313779200
86. Wright WD, Shah SS, Heyer WD. Homologous recombination and the repair of DNA double-strand breaks. *J Biol Chem*. 2018;293(27):10524-10535. doi:10.1074/jbc.TM118.000372
87. Sotiriou SK, Kamileri I, Lugli N, et al. Mammalian RAD52 Functions in Break-Induced Replication Repair of Collapsed DNA Replication Forks. *Mol Cell*. 2016;64(6):1127-1134. doi:10.1016/j.molcel.2016.10.038
88. Robert I, Dantzer F, Reina-San-Martin B. Parp1 facilitates alternative NHEJ, whereas Parp2 suppresses IgH/c-myc translocations during immunoglobulin class switch recombination. *J Exp Med*. 2009;206(5):1047-1056. doi:10.1084/jem.20082468
89. Audebert M, Salles B, Calsou P. Involvement of poly(ADP-ribose) polymerase-1 and XRCC1/DNA ligase III in an alternative route for DNA double-strand breaks rejoining. *J Biol Chem*. 2004;279(53):55117-55126. doi:10.1074/jbc.M404524200
90. Mateos-Gomez PA, Gong F, Nair N, Miller KM, Lazzerini-Denchi E, Sfeir A. Mammalian polymerase θ promotes alternative NHEJ and suppresses recombination. *Nature*. 2015;518(7538):254-257. doi:10.1038/nature14157
91. Wyatt DW, Feng W, Conlin MP, et al. Essential Roles for Polymerase θ-Mediated End Joining in the Repair of Chromosome Breaks. *Mol Cell*. 2016;63(4):662-673. doi:10.1016/j.molcel.2016.06.020
92. Ahmad A, Robinson AR, Duensing A, et al. ERCC1-XPF Endonuclease Facilitates DNA Double-Strand Break Repair. *Mol Cell Biol*. 2008;28(16):5082-5092. doi:10.1128/mcb.00293-08
93. Masani S, Han L, Meek K, Yu K. Redundant function of DNA ligase 1 and 3 in alternative end-joining during immunoglobulin class switch recombination. *Proc Natl Acad Sci*. 2016;113(5):1261-1266. doi:10.1073/pnas.1521630113
94. Lu G, Duan J, Shu S, et al. Ligase I and ligase III mediate the DNA double-strand break ligation

in alternative end-joining. *Proc Natl Acad Sci U S A*. 2016;113(5):1256-1260. doi:10.1073/pnas.1521597113

95. de Lange T. Shelterin : the protein complex that shapes and safeguards human telomeres. *Genes Dev*. 2005;19:2100-2110. doi:10.1101/gad.1346005.quence
96. Erdel F, Kratz K, Willcox S, Griffith JD, Greene EC, de Lange T. Telomere Recognition and Assembly Mechanism of Mammalian Shelterin. *Cell Rep*. 2017;18(1):41-53. doi:https://doi.org/10.1016/j.celrep.2016.12.005
97. Baumann P, Cech TR. Pot1, the putative telomere end-binding protein in fission yeast and humans. *Science (80-)*. 2001;292(5519):1171-1175. doi:10.1126/science.1060036
98. Lei M, Podell ER, Cech TR. Structure of human POT1 bound to telomeric single-stranded DNA provides a model for chromosome end-protection. *Nat Struct Mol Biol*. 2004;11(12):1223-1229. doi:10.1038/nsmb867
99. Loayza D, De Lange T. POT1 as a terminal transducer of TRF1 telomere length control. *Nature*. 2003;423(6943):1013-1018. doi:10.1038/nature01688
100. Liu D, Safari A, O'Connor MS, et al. PTOP interacts with POT1 and regulates its localization to telomeres. *Nat Cell Biol*. 2004;6(7):673-680. doi:10.1038/ncb1142
101. de Lange T, Griffith JD, Comeau L, et al. Mammalian telomeres end in a large duplex loop. *Cell*. 1999;97(4):503-514. http://www.ncbi.nlm.nih.gov/pubmed/10338214.
102. Doksani Y, Wu JY, De Lange T, Zhuang X. XSuper-resolution fluorescence imaging of telomeres reveals TRF2-dependent T-loop formation. *Cell*. 2013;155(2):345. doi:10.1016/j.cell.2013.09.048
103. Van Steensel B, Smogorzewska A, De Lange T. TRF2 protects human telomeres from end-to-end fusions. *Cell*. 1998;92(3):401-413. doi:10.1016/S0092-8674(00)80932-0
104. Smogorzewska A, Karlseder J, Holtgreve-Grez H, Jauch A, De Lange T. DNA ligase IV-dependent NHEJ of deprotected mammalian telomeres in G1 and G2. *Curr Biol*. 2002;12(19):1635-1644. doi:10.1016/S0960-9822(02)01179-X
105. Chow TT, Zhao Y, Mak SS, Shay JW, Wright WE. Early and late steps in telomere overhang processing in normal human cells: the position of the final RNA primer drives telomere shortening. *Genes Dev*. 2012;26(11):1167-1178. doi:10.1101/gad.187211.112
106. Wu P, van Overbeek M, Rooney S, de Lange T. Apollo contributes to G overhang maintenance and protects leading-end telomeres. *Mol Cell*. 2010;39(4):606-617. doi:10.1016/j.molcel.2010.06.031
107. Lam YC, Akhter S, Gu P, et al. SNMIB/Apollo protects leading-strand telomeres against NHEJ-mediated repair. *EMBO J*. 2010;29(13):2230-2241. doi:10.1038/emboj.2010.58
108. Touzot F, Callebaut I, Soulier J, et al. Function of Apollo (SNM1B) at telomere highlighted by a splice variant identified in a patient with Hoyeraal-Hreidarsson syndrome. *Proc Natl Acad Sci*

U S A. 2010;107(22):10097-10102. doi:10.1073/pnas.0914918107

109. Stroik S, Kurtz K, Hendrickson EA. CtIP is essential for telomere replication. *Nucleic Acids Res*. August 2019. doi:10.1093/nar/gkz652
110. Mirman Z, Lottersberger F, Takai H, et al. 53BP1–RIF1–shieldin counteracts DSB resection through CST- and Polα-dependent fill-in. *Nature*. 2018;560(7716):112-116. doi:10.1038/s41586-018-0324-7
111. Gupta R, Somyajit K, Narita T, et al. DNA Repair Network Analysis Reveals Shieldin as a Key Regulator of NHEJ and PARP Inhibitor Sensitivity. *Cell*. 2018;173(4):972-988.e23. doi:10.1016/j.cell.2018.03.050
112. Noordermeer SM, Adam S, Setiaputra D, et al. The shieldin complex mediates 53BP1-dependent DNA repair. *Nature*. 2018;560(7716):117-121. doi:10.1038/s41586-018-0340-7
113. Dai X, Huang C, Bhusari A, Sampathi S, Schubert K, Chai W. Molecular steps of G-overhang generation at human telomeres and its function in chromosome end protection. *EMBO J*. 2010;29(16):2788-2801. doi:10.1038/emboj.2010.156
114. Miyake Y, Nakamura M, Nabetani A, et al. RPA-like Mammalian Ctc1-Stn1-Ten1 Complex Binds to Single-Stranded DNA and Protects Telomeres Independently of the Pot1 Pathway. *Mol Cell*. 2009;36(2):193-206. doi:10.1016/j.molcel.2009.08.009
115. Okamoto K, Bartocci C, Ouzounov I, Diedrich JK, Yates III JR, Denchi EL. A two-step mechanism for TRF2-mediated chromosome-end protection. *Nature*. 2013;494:502. https://doi.org/10.1038/nature11873.
116. Ribes-Zamora A, Indiviglio SM, Mihalek I, Williams CL, Bertuch AA. TRF2 interaction with Ku heterotetramerization interface gives insight into c-NHEJ prevention at human telomeres. *Cell Rep*. 2013;5(1):194-206. doi:10.1016/j.celrep.2013.08.040
117. Sarthy J, Bae NS, Scrafford J, Baumann P. Human RAP1 inhibits non-homologous end joining at telomeres. *EMBO J*. 2009;28(21):3390-3399. doi:10.1038/emboj.2009.275
118. Denchi EL, De Lange T. Protection of telomeres through independent control of ATM and ATR by TRF2 and POT1. *Nature*. 2007;448(7157):1068-1071. doi:10.1038/nature06065
119. M. Z, T. K, S. K, T. de L. TRF1 negotiates TTAGGG repeatassociated replication problems by recruiting the BLM helicase and the TPP1/POT1 repressor of ATR signaling. *Genes Dev*. 2014;28(22):2477-2491. doi:10.1101/gad.251611.114 LK - http://linksource.ebsco.com/linking.aspx?sid=EMBASE&issn=15495477&id=doi:10.1101%2Fgad.251611.114&atitle=TRF1+negotiates+TTAGGG+repeatassociated+replication+problems+by+recruiting+the+BLM+helicase+and+the+TPP1%2FPOT1+repressor+of+ATR+signaling&stitle=Genes+Dev.&title=Genes+and+Development&volume=28&issue=22&spage=2477&epage=2491&aulast=Zimmermann&aufirst=Michal&auinit=M.&aufull=Zimmermann+M.&coden=GEDEE&isbn=&pages=2477-2491&date=2014&auinit1=M&auinitm=

120. Rai R, Li JM, Zheng H, et al. The E3 ubiquitin ligase Rnf8 stabilizes Tpp1 to promote telomere end protection. *Nat Struct Mol Biol*. 2011;18(12):1400-1407. doi:10.1038/nsmb.2172

121. Celli GB, Denchi EL, de Lange T. Ku70 stimulates fusion of dysfunctional telomeres yet protects chromosome ends from homologous recombination. *Nat Cell Biol*. 2006;8(8):885-890. doi:10.1038/ncb1444

122. Palm W, Hockemeyer D, Kibe T, de Lange T. Functional Dissection of Human and Mouse POT1 Proteins. *Mol Cell Biol*. 2009;29(2):471-482. doi:10.1128/mcb.01352-08

123. Wang RC, Smogorzewska A, De Lange T. Homologous Recombination Generates T-Loop-Sized Deletions at Human Telomeres (Marciniak et al we document that HR can delete large segments of telomeric DNA in human and mouse cells meric segments resulting in rapid shortening of telo-2 Present address: D. *Cell*. 2004;119:355-368. http://www.

124. Vannier JB, Pavicic-Kaltenbrunner V, Petalcorin MIR, Ding H, Boulton SJ. RTEL1 dismantles T loops and counteracts telomeric G4-DNA to maintain telomere integrity. *Cell*. 2012;149(4):795-806. doi:10.1016/j.cell.2012.03.030

125. Sarek G, Vannier JB, Panier S, Petrini HJ, Boulton SJ. TRF2 recruits RTEL1 to telomeres in s phase to promote t-loop unwinding. *Mol Cell*. 2015;57(4):622-635. doi:10.1016/j.molcel.2014.12.024

126. Wan B, Yin J, Horvath K, et al. SLX4 assembles a telomere maintenance toolkit by bridging multiple endonucleases with telomeres. *Cell Rep*. 2013;4(5):861-869. doi:10.1016/j.celrep.2013.08.017

127. Sarkar J, Wan B, Yin J, et al. SLX4 contributes to telomere preservation and regulated processing of telomeric joint molecule intermediates. *Nucleic Acids Res*. 2015;43(12):5912-5923. doi:10.1093/nar/gkv522

128. WATSON JD. Origin of Concatemeric T7DNA. *Nat New Biol*. 1972;239(94):197-201. doi:10.1038/newbio239197a0

129. Greider CW, Blackburn EH. The telomere terminal transferase of tetrahymena is a ribonucleoprotein enzyme with two kinds of primer specificity. *Cell*. 1987;51(6):887-898. doi:10.1016/0092-8674(87)90576-9

130. Bryan M, Reddel R. Telomere Dynamics and Telomerase Immortalised Cells In In V & -o. *Eur J Cancer*. 1997;8049(97):767-773.

131. Gaspar TB, Sá A, Lopes JM, Sobrinho-Simões M, Soares P, Vinagre J. Telomere maintenance mechanisms in cancer. *Genes (Basel)*. 2018;9(5). doi:10.3390/genes9050241

132. Shay JW, Wright WE. Telomeres and telomerase: three decades of progress. *Nat Rev Genet*. 2019;20(5):299-309. doi:10.1038/s41576-019-0099-1

133. Shippen-Lentz D, Blackburn EH. Functional evidence for an RNA template in telomerase. *Science (80-)*. 1990;247(4942):546-552. doi:10.1126/science.1689074

134. Bodnar AG, Ouellette M, Frolkis M, et al. Extension of life-span by introduction of telomerase into normal human cells. *Science (80-)*. 1998;279(5349):349-352. doi:10.1126/science.279.5349.349

135. Yuan X, Larsson C, Xu D. Mechanisms underlying the activation of TERT transcription and telomerase activity in human cancer: old actors and new players. *Oncogene*. 2019:6172-6183. doi:10.1038/s41388-019-0872-9

136. Liu L. Linking Telomere Regulation to Stem Cell Pluripotency. *Trends Genet*. 2017;33(1):16-33. doi:10.1016/j.tig.2016.10.007

137. Tefferi A, Lasho TL, Begna KH, et al. A Pilot Study of the Telomerase Inhibitor Imetelstat for Myelofibrosis. *N Engl J Med*. 2015;373(10):908-919. doi:10.1056/NEJMoa1310523

138. Tefferi A, Al-Kali A, Begna KH, et al. Imetelstat therapy in refractory anemia with ring sideroblasts with or without thrombocytosis. *Blood Cancer J*. 2016;6:e405. https://doi.org/10.1038/bcj.2016.13.

139. Huff CA, Wang Q, Badros AZ, et al. The Telomerase Inhibitor, Imetelstat, Rapidly Reduces Myeloma Cancer Stem Cells (CSCs) in a Phase II Trial. *Blood*. 2012;120(21):4898. http://www.bloodjournal.org/content/120/21/4898.

140. Baerlocher GM, Oppliger Leibundgut E, Ottmann OG, et al. Telomerase Inhibitor Imetelstat in Patients with Essential Thrombocythemia. *N Engl J Med*. 2015;373(10):920-928. doi:10.1056/NEJMoa1503479

141. Fenaux P, Steensma DP, Eygen K Van, et al. Treatment with Imetelstat Provides Durable Transfusion Independence in Heavily Transfused Non-Del (5q) Lower Risk MDS Relapsed / Refractory to Erythropoiesis-Stimulating Agents Background : Myelodysplastic Syndromes (MDS) and Imetelstat. *Conf Abstr Eur Hematol Assoc Annu Congr*. 2019:S837.

142. Bryan TM, Englezou A, Gupta J, Bacchetti S, Reddel RR. Telomere elongation in immortal human cells without detectable telomerase activity. *EMBO J*. 1995;14(17):4240-4248. https://www.ncbi.nlm.nih.gov/pubmed/7556065.

143. Bryan TM, Reddel RR. Telomere dynamics and telomerase activity in in vitro immortalised human cells. *Eur J Cancer*. 1997;33(5):767-773. doi:10.1016/S0959-8049(97)00065-8

144. Bryan TM, Englezou A, Dalla-Pozza L, Dunham MA, Reddel RR. Evidence for an alternative mechanism for maintaining telomere length in human tumors and tumor-derived cell lines. *Nat Med*. 1997;3(11):1271-1274.

145. Bryan TM, Marusic L, Bacchetti S, Namba M, Reddel RR. The Telomere Lengthening Mechanism in Telomerase-Negative Immortal Human Cells Does Not Involve the Telomerase RNA Subunit. *Hum Mol Genet*. 1997;6(6):921-926. doi:10.1093/hmg/6.6.921

146. Cesare AJ, Reddel RR. Alternative lengthening of telomeres: models, mechanisms and implications. *Nat Rev Genet*. 2010;11(5):319-330. doi:10.1038/nrg2763

147. De Vitis M, Berardinelli F, Sgura A. Telomere Length Maintenance in Cancer: At the Crossroad between Telomerase and Alternative Lengthening of Telomeres (ALT). *Int J Mol Sci*. 2018;19(2). doi:10.3390/ijms19020606

148. Dunham MA, Neumann AA, Fasching CL, Reddel RR. Telomere maintenance by recombination in human cells. 2000;26(december):447-450.

149. Bechter OE, Zou Y, Shay JW, Wright WE. Homologous recombination in human telomerase-positive and ALT cells occurs with the same frequency. *EMBO Rep*. 2003;4(12):1138-1143. doi:10.1038/sj.embor.7400027

150. Alberti S. Phase separation in biology. *Curr Biol*. 2017;27(20):R1097-R1102. doi:10.1016/j.cub.2017.08.069

151. Lallemand-Breitenbach V, de The H. PML nuclear bodies: from architecture to function. *Curr Opin Cell Biol*. 2018;52:154-161. doi:10.1016/j.ceb.2018.03.011

152. Yeager TR, Neumann AA, Englezou A, Huschtscha LI, Noble JR, Reddel RR. Telomerase-negative immortalized human cells contain a novel type of promyelocytic leukemia (PML) body. *Cancer Res*. 1999;59(17):4175-4179.

153. Wu G, Jiang X, Lee W-H, Chen P-L. Assembly of functional ALT-associated promyelocytic leukemia bodies requires Nijmegen Breakage Syndrome 1. *Cancer Res*. 2003;63(10):2589-2595.

154. Grobelny J V, Godwin AK, Broccoli D. ALT-associated PML bodies are present in viable cells and are enriched in cells in the G(2)/M phase of the cell cycle. *J Cell Sci*. 2000;113 Pt 24:4577-4585.

155. Grudic A, Jul-Larsen A, Haring SJ, et al. Replication protein A prevents accumulation of single-stranded telomeric DNA in cells that use alternative lengthening of telomeres. *Nucleic Acids Res*. 2007;35(21):7267-7278. doi:10.1093/nar/gkm738

156. Cho NW, Dilley RL, Lampson MA, Greenberg RA. Interchromosomal homology searches drive directional ALT telomere movement and synapsis. *Cell*. 2014;159(1):108-121. doi:10.1016/j.cell.2014.08.030

157. Zeng S, Xiang T, Pandita TK, et al. Telomere recombination requires the MUS81 endonuclease. *Nat Cell Biol*. 2009;11(5):616-623. doi:10.1038/ncb1867

158. Nabetani A, Ishikawa F. Alternative lengthening of telomeres pathway: recombination-mediated telomere maintenance mechanism in human cells. *J Biochem*. 2011;149(1):5-14. doi:10.1093/jb/mvq119

159. Nabetani A, Yokoyama O, Ishikawa F. Localization of hRad9, hHus1, hRad1, and hRad17 and caffeine-sensitive DNA replication at the alternative lengthening of telomeres-associated promyelocytic leukemia body. *J Biol Chem*. 2004;279(24):25849-25857. doi:10.1074/jbc.M312652200

160. Dilley RL, Verma P, Cho NW, Winters HD, Wondisford AR, Greenberg RA. Break-induced

telomere synthesis underlies alternative telomere maintenance. *Nature*. 2016;539(7627):54-58. doi:10.1038/nature20099

161. Lu R, O'Rourke JJ, Sobinoff AP, et al. The FANCM-BLM-TOP3A-RMI complex suppresses alternative lengthening of telomeres (ALT). *Nat Commun*. 2019;10(1). doi:10.1038/s41467-019-10180-6
162. Osterwald S, Deeg KI, Chung I, et al. PML induces compaction, TRF2 depletion and DNA damage signaling at telomeres and promotes their alternative lengthening. *J Cell Sci*. 2015;128(10):1887-1900. doi:10.1242/jcs.148296
163. Zhang J-M, Yadav T, Ouyang J, Lan L, Zou L. Alternative Lengthening of Telomeres through Two Distinct Break-Induced Replication Pathways. *Cell Rep*. 2019;26(4):955-968.e3. doi:10.1016/j.celrep.2018.12.102
164. Sobinoff AP, Pickett HA. Alternative Lengthening of Telomeres: DNA Repair Pathways Converge. *Trends Genet*. 2017;33(12):921-932. doi:10.1016/j.tig.2017.09.003
165. Takubo K, Izumiyama-Shimomura N, Honma N, et al. Telomere lengths are characteristic in each human individual. *Exp Gerontol*. 2002;37(4):523-531. doi:https://doi.org/10.1016/S0531-5565(01)00218-2
166. Slagboom PE, Droog S, Boomsma DI. Genetic determination of telomere size in humans: A twin study of three age groups. *Am J Hum Genet*. 1994;55(5):876-882.
167. Borah S, Xi L, Zaug AJ, et al. Cancer. TERT promoter mutations and telomerase reactivation in urothelial cancer. *Science*. 2015;347(6225):1006-1010. doi:10.1126/science.1260200
168. Wu K-D, Orme LM, Shaughnessy J, Jacobson J, Barlogie B, Moore MAS. Telomerase and telomere length in multiple myeloma: correlations with disease heterogeneity, cytogenetic status, and overall survival. *Blood*. 2003;101(12):4982-4989. doi:10.1182/blood-2002-11-3451
169. Lee M, Hills M, Conomos D, et al. Telomere extension by telomerase and ALT generates variant repeats by mechanistically distinct processes. *Nucleic Acids Res*. 2014;42(3):1733-1746. doi:10.1093/nar/gkt1117
170. Bailey SM, Williams ES, Cornforth MN, Goodwin EH. Chromosome Orientation fluorescence in situ hybridization or strand-specific FISH. *Methods Mol Biol*. 2010;659:173-183. doi:10.1007/978-1-60761-789-1_12
171. Londono-Vallejo JA, Der-Sarkissian H, Cazes L, Bacchetti S, Reddel RR. Alternative lengthening of telomeres is characterized by high rates of telomeric exchange. *Cancer Res*. 2004;64(7):2324-2327.
172. Cerone MA, Autexier C, Londono-Vallejo JA, Bacchetti S. A human cell line that maintains telomeres in the absence of telomerase and of key markers of ALT. *Oncogene*. 2005;24(53):7893-7901. doi:10.1038/sj.onc.1208934
173. Cesare AJ, Griffith JD. Telomeric DNA in ALT cells is characterized by free telomeric circles

and heterogeneous t-loops. *Mol Cell Biol*. 2004;24(22):9948-9957. doi:10.1128/MCB.24.22.9948-9957.2004

174. Compton SA, Choi J-H, Cesare AJ, Özgür S, Griffith JD. Xrcc3 and Nbs1 Are Required for the Production of Extrachromosomal Telomeric Circles in Human Alternative Lengthening of Telomere Cells. *Cancer Res*. 2007;67(4):1513-1519. doi:10.1158/0008-5472.CAN-06-3672
175. Henson JD, Reddel RR. Assaying and investigating Alternative Lengthening of Telomeres activity in human cells and cancers. *FEBS Lett*. 2010;584(17):3800-3811. doi:10.1016/j.febslet.2010.06.009
176. Deng Z, Dheekollu J, Broccoli D, Dutta A, Lieberman PM. The origin recognition complex localizes to telomere repeats and prevents telomere-circle formation. *Curr Biol*. 2007;17(22):1989-1995. doi:10.1016/j.cub.2007.10.054
177. Regev A, Cohen S, Cohen E, Bar-Am I, Lavi S. Telomeric repeats on small polydisperse circular DNA (spcDNA) and genomic instability. *Oncogene*. 1998;17(26):3455-3461. doi:10.1038/sj.onc.1202250
178. Henson JD, Cao Y, Huschtscha LI, et al. DNA C-circles are specific and quantifiable markers of alternative-lengthening-of-telomeres activity. *Nat Biotechnol*. 2009;27(12):1181-1185. doi:10.1038/nbt.1587
179. Nabetani A, Ishikawa F. Unusual telomeric DNAs in human telomerase-negative immortalized cells. *Mol Cell Biol*. 2009;29(3):703-713. doi:10.1128/MCB.00603-08
180. Zhang T, Zhang Z, Shengzhao G, Li X, Liu H, Zhao Y. Strand break-induced replication fork collapse leads to C-circles, C-overhangs and telomeric recombination. *PLoS Genet*. 2019;15(2):e1007925. doi:10.1371/journal.pgen.1007925
181. Wu P, de Lange T. No overt nucleosome eviction at deprotected telomeres. *Mol Cell Biol*. 2008;28(18):5724-5735. doi:10.1128/MCB.01764-07
182. Kimura H, Cook PR. Kinetics of Core Histones in Living Human Cells. *J Cell Biol*. 2001;153(7):1341-1354. doi:10.1083/jcb.153.7.1341
183. Mattern KA, Swiggers SJJ, Nigg AL, Löwenberg B, Houtsmuller AB, Zijlmans JMJM. Dynamics of Protein Binding to Telomeres in Living Cells: Implications for Telomere Structure and Function. *Mol Cell Biol*. 2004;24(12):5587-5594. doi:10.1128/MCB.24.12.5587-5594.2004
184. Goldberg AD, Banaszynski LA, Noh K-M, et al. Distinct Factors Control Histone Variant H3.3 Localization at Specific Genomic Regions. *Cell*. 2010;140(5):678-691. doi:https://doi.org/10.1016/j.cell.2010.01.003
185. Voon HPJ, Collas P, Wong LH. Compromised telomeric heterochromatin promotes ALTernative lengthening of telomeres. *Trends in Cancer*. 2016;2(3):114-116. doi:10.1016/j.trecan.2016.02.003
186. Kim J, Sun C, Tran AD, et al. The macroH2A1.2 histone variant links ATRX loss to alternative

telomere lengthening. *Nat Struct Mol Biol*. 2019;26(3):213-219. doi:10.1038/s41594-019-0192-3

187. Montero JJ, Lopez-Silanes I, Megias D, F Fraga M, Castells-Garcia A, Blasco MA. TERRA recruitment of polycomb to telomeres is essential for histone trymethylation marks at telomeric heterochromatin. *Nat Commun*. 2018;9(1):1548. doi:10.1038/s41467-018-03916-3
188. Gauchier M, Kan S, Barral A, et al. SETDB1-dependent heterochromatin stimulates alternative lengthening of telomeres. *Sci Adv*. 2019;5(5). doi:10.1126/sciadv.aav3673
189. Arnoult N, Van Beneden A, Decottignies A. Telomere length regulates TERRA levels through increased trimethylation of telomeric H3K9 and HP1alpha. *Nat Struct Mol Biol*. 2012;19(9):948-956. doi:10.1038/nsmb.2364
190. Bettin N, Oss Pegorar C, Cusanelli E. The Emerging Roles of TERRA in Telomere Maintenance and Genome Stability. *Cells*. 2019;8(3):246. doi:10.3390/cells8030246
191. Lydeard JR, Jain S, Yamaguchi M, Haber JE. Break-induced replication and telomerase-independent telomere maintenance require Pol32. *Nature*. 2007;448(7155):820-823. doi:10.1038/nature06047
192. Roumelioti F-M, Sotiriou SK, Katsini V, Chiourea M, Halazonetis TD, Gagos S. Alternative lengthening of human telomeres is a conservative DNA replication process with features of break-induced replication. *EMBO Rep*. 2016;17(12):1731-1737. doi:10.15252/embr.201643169
193. Panier S, Maric M, Hewitt G, et al. SLX4IP Antagonizes Promiscuous BLM Activity during ALT Maintenance. *Mol Cell*. 2019:1-17. doi:10.1016/j.molcel.2019.07.010
194. Verma P, Dilley RL, Zhang T, Gyparaki MT, Li Y, Greenberg RA. RAD52 and SLX4 act nonepistatically to ensure telomere stability during alternative telomere lengthening. *Genes Dev*. 2019;33(3-4):221-235. doi:10.1101/gad.319723.118
195. Marzec P, Armenise C, Pérot G, et al. Nuclear-Receptor-Mediated Telomere Insertion Leads to Genome Instability in ALT Cancers. *Cell*. 2015;160(5):913-927. doi:10.1016/j.cell.2015.01.044
196. Perrem K, Bryan TM, Englezou A, Hackl T, Moy EL, Reddel RR. Repression of an alternative mechanism for lengthening of telomeres in somatic cell hybrids. *Oncogene*. 1999;18(22):3383-3390. doi:10.1038/sj.onc.1202752
197. Pickett HA, Reddel RR. Molecular mechanisms of activity and derepression of alternative lengthening of telomeres. *Nat Struct Mol Biol*. 2015;22(11):875-880. doi:10.1038/nsmb.3106
198. Napier CE, Huschtscha LI, Harvey A, et al. ATRX represses alternative lengthening of telomeres. *Oncotarget*. 2015;6(18):16543-16558. doi:10.18632/oncotarget.3846
199. Lovejoy CA, Li W, Reisenweber S, et al. Loss of ATRX, genome instability, and an altered DNA damage response are hallmarks of the alternative lengthening of telomeres pathway. *PLoS Genet*. 2012;8(7):e1002772. doi:10.1371/journal.pgen.1002772
200. O'Sullivan RJ, Arnoult N, Lackner DH, et al. Rapid induction of alternative lengthening of

telomeres by depletion of the histone chaperone ASF1. *Nat Struct Mol Biol*. 2014;21(2):167-174. doi:10.1038/nsmb.2754

201. Cox KE, Maréchal A, Flynn RL. SMARCAL1 Resolves Replication Stress at ALT Telomeres. *Cell Rep*. 2016;14(5):1032-1040. doi:10.1016/j.celrep.2016.01.011
202. Silva B, Pentz R, Figueira AM, et al. FANCM limits ALT activity by restricting telomeric replication stress induced by deregulated BLM and R-loops. *Nat Commun*. 2019;10(1):2253. doi:10.1038/s41467-019-10179-z
203. Hu Y, Shi G, Zhang L, et al. Switch telomerase to ALT mechanism by inducing telomeric DNA damages and dysfunction of ATRX and DAXX. *Sci Rep*. 2016;6:32280. doi:10.1038/srep32280
204. Flynn RL, Cox KE, Jeitany M, et al. Alternative lengthening of telomeres renders cancer cells hypersensitive to ATR inhibitors. *Science (80-)*. 2015;347(6219):273-277. doi:10.1126/science.1257216
205. Deeg KI, Chung I, Bauer C, Rippe K. Cancer Cells with Alternative Lengthening of Telomeres Do Not Display a General Hypersensitivity to ATR Inhibition. *Front Oncol*. 2016;6:186. doi:10.3389/fonc.2016.00186
206. Hu J, Hwang SS, Liesa M, et al. Antitelomerase therapy provokes ALT and mitochondrial adaptive mechanisms in cancer. *Cell*. 2012;148(4):651-663. doi:10.1016/j.cell.2011.12.028
207. Kaposi. Idiopathisches multiples Pigmentsarkom der Haut. *Arch Dermatol Syph*. 1872;4(2):265-273. doi:10.1007/BF01830024
208. Chang Y, Cesarman E, Pessin MS, et al. Identification of herpesvirus-like DNA sequences in AIDS-associated Kaposi{\textquoteright}s sarcoma. *Science (80-)*. 1994;266(5192):1865-1869. doi:10.1126/science.7997879
209. Cesarman E, Chang Y, Moore PS, Said JW, Knowles DM. Kaposi's sarcoma-associated herpesvirus-like DNA sequences in AIDS-related body-cavity-based lymphomas. *N Engl J Med*. 1995;332(18):1186-1191. doi:10.1056/NEJM199505043321802
210. Soulier J, Grollet L, Oksenhendler E, et al. Kaposi's sarcoma-associated herpesvirus-like DNA sequences in multicentric Castleman's disease. *Blood*. 1995;86(4):1276-1280.
211. Russo JJ, Bohenzky RA, Chien MC, et al. Nucleotide sequence of the Kaposi sarcoma-associated herpesvirus (HHV8). *Proc Natl Acad Sci U S A*. 1996;93(25):14862-14867. doi:10.1073/pnas.93.25.14862
212. Dalla Pria A, Pinato DJ, Bracchi M, Bower M. Recent advances in HIV-associated Kaposi sarcoma. *F1000Research*. 2019;8. doi:10.12688/f1000research.17401.1
213. Dedicoat M, Newton R. Review of the distribution of Kaposi's sarcoma-associated herpesvirus (KSHV) in Africa in relation to the incidence of Kaposi's sarcoma. *Br J Cancer*. 2003;88(1):1-3. doi:10.1038/sj.bjc.6600745
214. Schneider JW, Dittmer DP. Diagnosis and Treatment of Kaposi Sarcoma. *Am J Clin Dermatol*.

2017;18(4):529-539. doi:10.1007/s40257-017-0270-4

215. Chaabna K, Bray F, Wabinga HR, et al. Kaposi sarcoma trends in Uganda and Zimbabwe: a sustained decline in incidence? *Int J cancer*. 2013;133(5):1197-1203. doi:10.1002/ijc.28125
216. Hleyhel M, Belot A, Bouvier AM, et al. Risk of AIDS-defining cancers among HIV-1-infected patients in France between 1992 and 2009: results from the FHDH-ANRS CO4 cohort. *Clin Infect Dis*. 2013;57(11):1638-1647. doi:10.1093/cid/cit497
217. Etemad SA, Dewan AK. Kaposi Sarcoma Updates. *Dermatol Clin*. 2019;37(4):505-517. doi:10.1016/j.det.2019.05.008
218. Cesarman E, Damania B, Krown SE, Martin J, Bower M, Whitby D. Kaposi sarcoma. *Nat Rev Dis Prim*. 2019;5(1):9. doi:10.1038/s41572-019-0060-9
219. Lebbé C, Legendre C, Francès C. Kaposi sarcoma in transplantation. *Transplant Rev*. 2008;22(4):252-261. doi:https://doi.org/10.1016/j.trre.2008.05.004
220. Stasi E, De Santis S, Cavalcanti E, Armentano R. Iatrogenic Kaposi sarcoma of the terminal ileum following short-term treatment with immunomodulators for Crohn disease: A case report. *Medicine (Baltimore)*. 2019;98(20):e15714. doi:10.1097/MD.0000000000015714
221. Windon AL, Shroff SG. Iatrogenic Kaposi's Sarcoma in an HIV-Negative Young Male With Crohn's Disease and IgA Nephropathy: A Case Report and Brief Review of the Literature. *Int J Surg Pathol*. 2018;26(3):276-282. doi:10.1177/1066896917736610
222. Lebbe C, Garbe C, Stratigos AJ, et al. Diagnosis and treatment of Kaposi's sarcoma: European consensus-based interdisciplinary guideline (EDF/EADO/EORTC). *Eur J Cancer*. 2019;114:117-127. doi:10.1016/j.ejca.2018.12.036
223. Dupin N, Diss TL, Kellam P, et al. HHV-8 is associated with a plasmablastic variant of Castleman disease that is linked to HHV-8-positive plasmablastic lymphoma. *Blood*. 2000;95(4):1406-1412.
224. Oksenhendler E, Boutboul D, Galicier L. Kaposi sarcoma{\textendash}associated herpesvirus/human herpesvirus 8{\textendash}associated lymphoproliferative disorders. *Blood*. 2019;133(11):1186-1190. doi:10.1182/blood-2018-11-852442
225. Chadburn A, Said J, Gratzinger D, et al. HHV8/KSHV-Positive Lymphoproliferative Disorders and the Spectrum of Plasmablastic and Plasma Cell Neoplasms: 2015 SH/EAHP Workshop Report—Part 3. *Am J Clin Pathol*. 2017;147(2):171-187. doi:10.1093/ajcp/aqw218
226. Oksenhendler E, Boulanger E, Galicier L, et al. High incidence of Kaposi sarcoma-associated herpesvirus-related non-Hodgkin lymphoma in patients with HIV infection and multicentric Castleman disease. *Blood*. 2002;99(7):2331-2336. doi:10.1182/blood.v99.7.2331
227. Bower M, Powles T, Williams S, et al. Brief communication: rituximab in HIV-associated multicentric Castleman disease. *Ann Intern Med*. 2007;147(12):836-839. doi:10.7326/0003-4819-147-12-200712180-00003

228. Gerard L, Berezne A, Galicier L, et al. Prospective study of rituximab in chemotherapy-dependent human immunodeficiency virus associated multicentric Castleman's disease: ANRS 117 CastlemaB Trial. *J Clin Oncol*. 2007;25(22):3350-3356. doi:10.1200/JCO.2007.10.6732

229. Reddy D, Mitsuyasu R. HIV-associated multicentric Castleman disease. *Curr Opin Oncol*. 2011;23(5):475-481. doi:10.1097/CCO.0b013e328349c233

230. Horenstein MG, Nador RG, Chadburn A, et al. Epstein-Barr virus latent gene expression in primary effusion lymphomas containing Kaposi's sarcoma-associated herpesvirus/human herpesvirus-8. *Blood*. 1997;90(3):1186-1191.

231. Chadburn A, Hyjek E, Mathew S, Cesarman E, Said J, Knowles DM. KSHV-positive solid lymphomas represent an extra-cavitary variant of primary effusion lymphoma. *Am J Surg Pathol*. 2004;28(11):1401-1416. doi:10.1097/01.pas.0000138177.10829.5c

232. Nador RG, Cesarman E, Chadburn A, et al. Primary effusion lymphoma: a distinct clinicopathologic entity associated with the Kaposi's sarcoma-associated herpes virus. *Blood*. 1996;88(2):645-656.

233. Boulanger E, Gerard L, Gabarre J, et al. Prognostic factors and outcome of human herpesvirus 8-associated primary effusion lymphoma in patients with AIDS. *J Clin Oncol*. 2005;23(19):4372-4380. doi:10.1200/JCO.2005.07.084

234. Okada S, Goto H, Yotsumoto M. Current status of treatment for primary effusion lymphoma. *Intractable rare Dis Res*. 2014;3(3):65-74. doi:10.5582/irdr.2014.01010

235. Trus BL, Heymann JB, Nealon K, et al. Capsid structure of Kaposi's sarcoma-associated herpesvirus, a gammaherpesvirus, compared to those of an alphaherpesvirus, herpes simplex virus type 1, and a betaherpesvirus, cytomegalovirus. *J Virol*. 2001;75(6):2879-2890. doi:10.1128/JVI.75.6.2879-2890.2001

236. Kedes DH, Operskalski E, Busch M, Kohn R, Flood J, Ganem D. The seroepidemiology of human herpesvirus 8 (Kaposi's sarcoma-associated herpesvirus): distribution of infection in KS risk groups and evidence for sexual transmission. *Nat Med*. 1996;2(8):918-924.

237. Martin JN, Ganem DE, Osmond DH, Page-Shafer KA, Macrae D, Kedes DH. Sexual transmission and the natural history of human herpesvirus 8 infection. *N Engl J Med*. 1998;338(14):948-954. doi:10.1056/NEJM199804023381403

238. Malope BI, Pfeiffer RM, Mbisa G, et al. Transmission of Kaposi sarcoma-associated herpesvirus between mothers and children in a South African population. *J Acquir Immune Defic Syndr*. 2007;44(3):351-355. doi:10.1097/QAI.0b013e31802f12ea

239. Knipe DM, Howley P. *Fields Virology*. Wolters Kluwer Health; 2013. https://books.google.co.uk/books?id=dxIrrMrot3gC.

240. Akula SM, Pramod NP, Wang FZ, Chandran B. Human herpesvirus 8 envelope-associated

glycoprotein B interacts with heparan sulfate-like moieties. *Virology*. 2001;284(2):235-249. doi:10.1006/viro.2001.0921

241. Akula SM, Pramod NP, Wang FZ, Chandran B. Integrin alpha3beta1 (CD 49c/29) is a cellular receptor for Kaposi's sarcoma-associated herpesvirus (KSHV/HHV-8) entry into the target cells. *Cell*. 2002;108(3):407-419. doi:10.1016/s0092-8674(02)00628-1
242. Walker LR, Hussein HAM, Akula SM. Disintegrin-like domain of glycoprotein B regulates Kaposi's sarcoma-associated herpesvirus infection of cells. *J Gen Virol*. 2014;95(Pt 8):1770-1782. doi:10.1099/vir.0.066829-0
243. Veettil MV, Bandyopadhyay C, Dutta D, Chandran B. Interaction of KSHV with host cell surface receptors and cell entry. *Viruses*. 2014;6(10):4024-4046. doi:10.3390/v6104024
244. Arvin A, Campadelli-Fiume G, Mocarski E, et al., eds. *Human Herpesviruses: Biology, Therapy, and Immunoprophylaxis*. Cambridge; 2007.
245. Chakraborty S, ValiyaVeettil M, Sadagopan S, Paudel N, Chandran B. c-Cbl-Mediated Selective Virus-Receptor Translocations into Lipid Rafts Regulate Productive Kaposi{\textquoteright}s Sarcoma-Associated Herpesvirus Infection in Endothelial Cells. *J Virol*. 2011;85(23):12410-12430. doi:10.1128/JVI.05953-11
246. Chakraborty S, Veettil MV, Bottero V, Chandran B. Kaposi's sarcoma-associated herpesvirus interacts with EphrinA2 receptor to amplify signaling essential for productive infection. *Proc Natl Acad Sci*. 2012;109(19):E1163 LP-E1172. doi:10.1073/pnas.1119592109
247. Naranatt PP, Krishnan HH, Smith MS, Chandran B. Kaposi's sarcoma-associated herpesvirus modulates microtubule dynamics via RhoA-GTP-diaphanous 2 signaling and utilizes the dynein motors to deliver its DNA to the nucleus. *J Virol*. 2005;79(2):1191-1206. doi:10.1128/JVI.79.2.1191-1206.2005
248. Purushothaman P, Dabral P, Gupta N, Sarkar R, Verma SC. KSHV Genome Replication and Maintenance. *Front Microbiol*. 2016;7:54. doi:10.3389/fmicb.2016.00054
249. Dittmer D, Lagunoff M, Renne R, Staskus K, Haase A, Ganem D. A Cluster of Latently Expressed Genes in Kaposi{\textquoteright}s Sarcoma-Associated Herpesvirus. *J Virol*. 1998;72(10):8309-8315. https://jvi.asm.org/content/72/10/8309.
250. Renne R, Barry C, Dittmer D, Compitello N, Brown PO, Ganem D. Modulation of cellular and viral gene expression by the latency-associated nuclear antigen of Kaposi's sarcoma-associated herpesvirus. *J Virol*. 2001;75(1):458-468. doi:10.1128/JVI.75.1.458-468.2001
251. Sun Q, Matta H, Chaudhary PM. The human herpes virus 8-encoded viral FLICE inhibitory protein protects against growth factor withdrawal-induced apoptosis via NF-kappa B activation. *Blood*. 2003;101(5):1956-1961. doi:10.1182/blood-2002-07-2072
252. Guasparri I, Keller SA, Cesarman E. KSHV vFLIP is essential for the survival of infected lymphoma cells. *J Exp Med*. 2004;199(7):993-1003. doi:10.1084/jem.20031467

253. Briggs LC, Chan AWE, Davis CA, et al. IKKgamma-Mimetic Peptides Block the Resistance to Apoptosis Associated with Kaposi's Sarcoma-Associated Herpesvirus Infection. *J Virol*. 2017;91(23). doi:10.1128/JVI.01170-17

254. Yang Z, Honda T, Ueda K. vFLIP upregulates IKKepsilon, leading to spindle morphology formation through RelA activation. *Virology*. 2018;522:106-121. doi:10.1016/j.virol.2018.07.007

255. Xu Y, Ganem D. Induction of chemokine production by latent Kaposi's sarcoma-associated herpesvirus infection of endothelial cells. *J Gen Virol*. 2007;88(Pt 1):46-50. doi:10.1099/vir.0.82375-0

256. Olteanu G-E, Mihai I-M, Bojin F, Gavriliuc O, Paunescu V. The natural adaptive evolution of cancer: The metastatic ability of cancer cells. *Bosn J basic Med Sci*. February 2020:10.17305/bjbms.2019.4565. doi:10.17305/bjbms.2019.4565

257. Zhi H, Zahoor MA, Shudofsky AMD, Giam C-Z. KSHV vCyclin counters the senescence/G1 arrest response triggered by NF-kappaB hyperactivation. *Oncogene*. 2015;34(4):496-505. doi:10.1038/onc.2013.567

258. Mann DJ, Child ES, Swanton C, Laman H, Jones N. Modulation of p27(Kip1) levels by the cyclin encoded by Kaposi's sarcoma-associated herpesvirus. *EMBO J*. 1999;18(3):654-663. doi:10.1093/emboj/18.3.654

259. Laman H, Coverley D, Krude T, Laskey R, Jones N. Viral cyclin-cyclin-dependent kinase 6 complexes initiate nuclear DNA replication. *Mol Cell Biol*. 2001;21(2):624-635. doi:10.1128/MCB.21.2.624-635.2001

260. Ojala PM, Yamamoto K, Castãos-Vélez E, Biberfeld P, Korsmeyer SJ, Mäkelä TP. The apoptotic v-cyclin-CDK6 complex phosphorylates and inactives Bcl-2. *Nat Cell Biol*. 2000;2(11):819-825. doi:10.1038/35041064

261. Juillard F, Tan M, Li S, Kaye KM. Kaposi's Sarcoma Herpesvirus Genome Persistence. *Front Microbiol*. 2016;7:1149. doi:10.3389/fmicb.2016.01149

262. Grundhoff A, Ganem D. The latency-associated nuclear antigen of Kaposi's sarcoma-associated herpesvirus permits replication of terminal repeat-containing plasmids. *J Virol*. 2003;77(4):2779-2783. doi:10.1128/jvi.77.4.2779-2783.2003

263. Barbera AJ, Chodaparambil J V, Kelley-Clarke B, et al. The nucleosomal surface as a docking station for Kaposi's sarcoma herpesvirus LANA. *Science*. 2006;311(5762):856-861. doi:10.1126/science.1120541

264. Jha HC, Upadhyay SK, A J Prasad M, et al. H2AX phosphorylation is important for LANA-mediated Kaposi's sarcoma-associated herpesvirus episome persistence. *J Virol*. 2013;87(9):5255-5269. doi:10.1128/JVI.03575-12

265. Kang H, Wiedmer A, Yuan Y, Robertson E, Lieberman PM. Coordination of KSHV Latent and

Lytic Gene Control by CTCF-Cohesin Mediated Chromosome Conformation. *PLOS Pathog*. 2011;7(8):e1002140. https://doi.org/10.1371/journal.ppat.1002140.

266. Toth Z, Maglinte DT, Lee SH, et al. Epigenetic analysis of KSHV latent and lytic genomes. *PLoS Pathog*. 2010;6(7):e1001013. doi:10.1371/journal.ppat.1001013
267. Hu J, Yang Y, Turner PC, Jain V, McIntyre LM, Renne R. LANA binds to multiple active viral and cellular promoters and associates with the H3K4methyltransferase hSET1 complex. *PLoS Pathog*. 2014;10(7):e1004240. doi:10.1371/journal.ppat.1004240
268. Lim C, Lee D, Seo T, Choi C, Choe J. Latency-associated nuclear antigen of Kaposi's sarcoma-associated herpesvirus functionally interacts with heterochromatin protein 1. *J Biol Chem*. 2003;278(9):7397-7405. doi:10.1074/jbc.M211912200
269. Lu F, Stedman W, Yousef M, Renne R, Lieberman PM. Epigenetic Regulation of Kaposi{\textquoteright}s Sarcoma-Associated Herpesvirus Latency by Virus-Encoded MicroRNAs That Target Rta and the Cellular Rbl2-DNMT Pathway. *J Virol*. 2010;84(6):2697-2706. doi:10.1128/JVI.01997-09
270. Garber AC, Hu J, Renne R. Latency-associated nuclear antigen (LANA) cooperatively binds to two sites within the terminal repeat, and both sites contribute to the ability of LANA to suppress transcription and to facilitate DNA replication. *J Biol Chem*. 2002;277(30):27401-27411. doi:10.1074/jbc.M203489200
271. De Leo A, Deng Z, Vladimirova O, et al. LANA oligomeric architecture is essential for KSHV nuclear body formation and viral genome maintenance during latency. *PLoS Pathog*. 2019;15(1):e1007489. doi:10.1371/journal.ppat.1007489
272. Stedman W, Deng Z, Lu F, Lieberman PM. ORC, MCM, and Histone Hyperacetylation at the Kaposi{\textquoteright}s Sarcoma-Associated Herpesvirus Latent Replication Origin. *J Virol*. 2004;78(22):12566-12575. doi:10.1128/JVI.78.22.12566-12575.2004
273. Sun Q, Tsurimoto T, Juillard F, et al. Kaposi's sarcoma-associated herpesvirus LANA recruits the DNA polymerase clamp loader to mediate efficient replication and virus persistence. *Proc Natl Acad Sci U S A*. 2014;111(32):11816-11821. doi:10.1073/pnas.1404219111
274. Dabral P, Uppal T, Rossetto CC, Verma SC. Minichromosome Maintenance Proteins Cooperate with LANA during the G1/S Phase of the Cell Cycle To Support Viral DNA Replication. Longnecker RM, ed. *J Virol*. 2019;93(7). doi:10.1128/JVI.02256-18
275. Verma SC, Lu J, Cai Q, et al. Single molecule analysis of replicated DNA reveals the usage of multiple KSHV genome regions for latent replication. *PLoS Pathog*. 2011;7(11). doi:10.1371/journal.ppat.1002365
276. Dheekollu J, Chen H-S, Kaye KM, Lieberman PM. Timeless-Dependent DNA Replication-Coupled Recombination Promotes Kaposi{\textquoteright}s Sarcoma-Associated Herpesvirus Episome Maintenance and Terminal Repeat Stability. *J Virol*. 2013;87(7):3699-3709.

doi:10.1128/JVI.02211-12

277. Lee KY, Bang SW, Yoon SW, Lee S-H, Yoon J-B, Hwang DS. Phosphorylation of ORC2 protein dissociates origin recognition complex from chromatin and replication origins. *J Biol Chem*. 2012;287(15):11891-11898. doi:10.1074/jbc.M111.338467
278. Kuipers MA, Stasevich TJ, Sasaki T, et al. Highly stable loading of Mcm proteins onto chromatin in living cells requires replication to unload. *J Cell Biol*. 2011;192(1):29-41. doi:10.1083/jcb.201007111
279. Verma SC, Lan K, Choudhuri T, Cotter MA, Robertson ES. An Autonomous Replicating Element within the KSHV Genome. *Cell Host Microbe*. 2007;2(2):106-118. doi:10.1016/j.chom.2007.07.002
280. Lepone L, Rappocciolo G, Knowlton E, et al. Monofunctional and polyfunctional CD8+ T cell responses to human herpesvirus 8 lytic and latency proteins. *Clin Vaccine Immunol*. 2010;17(10):1507-1516. doi:10.1128/CVI.00189-10
281. Lambert M, Gannage M, Karras A, et al. Differences in the frequency and function of HHV8-specific CD8 T cells between asymptomatic HHV8 infection and Kaposi sarcoma. *Blood*. 2006;108(12):3871-3880. doi:10.1182/blood-2006-03-014225
282. Myoung J, Ganem D. Generation of a doxycycline-inducible KSHV producer cell line of endothelial origin: maintenance of tight latency with efficient reactivation upon induction. *J Virol Methods*. 2011;174(1-2):12-21. doi:10.1016/j.jviromet.2011.03.012
283. Gradoville L, Gerlach J, Grogan E, et al. Kaposi{\textquoteright}s Sarcoma-Associated Herpesvirus Open Reading Frame 50/Rta Protein Activates the Entire Viral Lytic Cycle in the HH-B2 Primary Effusion Lymphoma Cell Line. *J Virol*. 2000;74(13):6207-6212. doi:10.1128/JVI.74.13.6207-6212.2000
284. Lan K, Kuppers DA, Robertson ES. Kaposi's sarcoma-associated herpesvirus reactivation is regulated by interaction of latency-associated nuclear antigen with recombination signal sequence-binding protein Jkappa, the major downstream effector of the Notch signaling pathway. *J Virol*. 2005;79(6):3468-3478. doi:10.1128/JVI.79.6.3468-3478.2005
285. Wang Y, Yuan Y. Essential role of RBP-Jkappa in activation of the K8 delayed-early promoter of Kaposi's sarcoma-associated herpesvirus by ORF50/RTA. *Virology*. 2007;359(1):19-27. doi:10.1016/j.virol.2006.09.032
286. Mettenleiter TC. Herpesvirus Assembly and Egress. *J Virol*. 2002;76(4):1537-1547. doi:10.1128/JVI.76.4.1537-1547.2002
287. Luitweiler EM, Henson BW, Pryce EN, et al. Interactions of the Kaposi's Sarcoma-associated herpesvirus nuclear egress complex: ORF69 is a potent factor for remodeling cellular membranes. *J Virol*. 2013;87(7):3915-3929. doi:10.1128/JVI.03418-12
288. Aneja KK, Yuan Y. Reactivation and Lytic Replication of Kaposi's Sarcoma-Associated

Herpesvirus: An Update. *Front Microbiol*. 2017;8:613. doi:10.3389/fmicb.2017.00613

289. Rozen R, Sathish N, Li Y, Yuan Y. Virion-wide protein interactions of Kaposi's sarcoma-associated herpesvirus. *J Virol*. 2008;82(10):4742-4750. doi:10.1128/JVI.02745-07
290. Bortz E, Wang L, Jia Q, et al. Murine gammaherpesvirus 68 ORF52 encodes a tegument protein required for virion morphogenesis in the cytoplasm. *J Virol*. 2007;81(18):10137-10150. doi:10.1128/JVI.01233-06
291. Wang Y, Li H, Tang Q, Maul GG, Yuan Y. Kaposi's sarcoma-associated herpesvirus ori-Lyt-dependent DNA replication: involvement of host cellular factors. *J Virol*. 2008;82(6):2867-2882. doi:10.1128/JVI.01319-07
292. Wang SE, Wu FY, Fujimuro M, Zong J, Hayward SD, Hayward GS. Role of CCAAT/enhancer-binding protein alpha (C/EBPalpha) in activation of the Kaposi's sarcoma-associated herpesvirus (KSHV) lytic-cycle replication-associated protein (RAP) promoter in cooperation with the KSHV replication and transcription activator (R. *J Virol*. 2003;77(1):600-623. doi:10.1128/jvi.77.1.600-623.2003
293. Gonzalez-Molleda L, Wang Y, Yuan Y. Potent antiviral activity of topoisomerase I and II inhibitors against Kaposi's sarcoma-associated herpesvirus. *Antimicrob Agents Chemother*. 2012;56(2):893-902. doi:10.1128/AAC.05274-11
294. Gardella T, Medveczky P, Sairenji T, Mulder C. Detection of circular and linear herpesvirus DNA molecules in mammalian cells by gel electrophoresis. *J Virol*. 1984;50(1):248-254.
295. Gramolelli S, Ojala PM. Kaposi's sarcoma herpesvirus-induced endothelial cell reprogramming supports viral persistence and contributes to Kaposi's sarcoma tumorigenesis. *Curr Opin Virol*. 2017;26:156-162. doi:https://doi.org/10.1016/j.coviro.2017.09.002
296. Vart RJ, Nikitenko LL, Lagos D, et al. Kaposi's sarcoma-associated herpesvirus-encoded interleukin-6 and G-protein-coupled receptor regulate angiopoietin-2 expression in lymphatic endothelial cells. *Cancer Res*. 2007;67(9):4042-4051. doi:10.1158/0008-5472.CAN-06-3321
297. Lu J, Verma SC, Cai Q, Saha A, Dzeng RK, Robertson ES. The RBP-Jkappa binding sites within the RTA promoter regulate KSHV latent infection and cell proliferation. *PLoS Pathog*. 2012;8(1):e1002479. doi:10.1371/journal.ppat.1002479
298. Katano H, Sato Y, Kurata T, Mori S, Sata T. Expression and localization of human herpesvirus 8-encoded proteins in primary effusion lymphoma, Kaposi's sarcoma, and multicentric Castleman's disease. *Virology*. 2000;269(2):335-344. doi:10.1006/viro.2000.0196
299. Singh VV, Dutta D, Ansari MA, Dutta S, Chandran B. Kaposi{\textquoteright}s Sarcoma-Associated Herpesvirus Induces the ATM and H2AX DNA Damage Response Early during De Novo Infection of Primary Endothelial Cells, Which Play Roles in Latency Establishment. Longnecker R, ed. *J Virol*. 2014;88(5):2821-2834. doi:10.1128/JVI.03126-13

300. Xiao Y, Chen J, Liao Q, Wu Y, Peng C, Chen X. Lytic infection of Kaposi's sarcoma-associated herpesvirus induces DNA double-strand breaks and impairs non-homologous end joining. *J Gen Virol*. 2013;94(Pt 8):1870-1875. doi:10.1099/vir.0.053033-0

301. Jackson BR, Noerenberg M, Whitehouse A. A novel mechanism inducing genome instability in Kaposi's sarcoma-associated herpesvirus infected cells. *PLoS Pathog*. 2014;10(5):e1004098. doi:10.1371/journal.ppat.1004098

302. Hollingworth R, Skalka GL, Stewart GS, Hislop AD, Blackbourn DJ, Grand RJ. Activation of DNA Damage Response Pathways during Lytic Replication of KSHV. *Viruses*. 2015;7(6):2908-2927. doi:10.3390/v7062752

303. Davis ZH, Verschueren E, Jang GM, et al. Global mapping of herpesvirus-host protein complexes reveals a transcription strategy for late genes. *Mol Cell*. 2015;57(2):349-360. doi:10.1016/j.molcel.2014.11.026

304. Shamay M, Liu J, Li R, et al. A protein array screen for Kaposi's sarcoma-associated herpesvirus LANA interactors links LANA to TIP60, PP2A activity, and telomere shortening. *J Virol*. 2012;86(9):5179-5191. doi:10.1128/JVI.00169-12

305. Li T, Chen ZJ. The cGAS-cGAMP-STING pathway connects DNA damage to inflammation, senescence, and cancer. *J Exp Med*. 2018;215(5):1287-1299. doi:10.1084/jem.20180139

306. Ma Z, Jacobs SR, West JA, et al. Modulation of the cGAS-STING DNA sensing pathway by gammaherpesviruses. *Proc Natl Acad Sci U S A*. 2015;112(31):E4306-15. doi:10.1073/pnas.1503831112

307. Liu H, Zhang H, Wu X, et al. Nuclear cGAS suppresses DNA repair and promotes tumorigenesis. *Nature*. 2018;563(7729):131-136. doi:10.1038/s41586-018-0629-6

308. Harding SM, Benci JL, Irianto J, Discher DE, Minn AJ, Greenberg RA. Mitotic progression following DNA damage enables pattern recognition within micronuclei. *Nature*. 2017;548(7668):466-470. doi:10.1038/nature23470

309. Bakhoum SF, Ngo B, Laughney AM, et al. Chromosomal instability drives metastasis through a cytosolic DNA response. *Nature*. 2018;553(7689):467-472. doi:10.1038/nature25432

310. Zhang G, Chan B, Samarina N, et al. Cytoplasmic isoforms of Kaposi sarcoma herpesvirus LANA recruit and antagonize the innate immune DNA sensor cGAS. *Proc Natl Acad Sci U S A*. 2016;113(8):E1034-43. doi:10.1073/pnas.1516812113

311. Dunphy G, Flannery SM, Almine JF, et al. Non-canonical Activation of the DNA Sensing Adaptor STING by ATM and IFI16 Mediates NF-kappaB Signaling after Nuclear DNA Damage. *Mol Cell*. 2018;71(5):745-760.e5. doi:10.1016/j.molcel.2018.07.034

312. Roy A, Dutta D, Iqbal J, et al. Nuclear Innate Immune DNA Sensor IFI16 Is Degraded during Lytic Reactivation of Kaposi's Sarcoma-Associated Herpesvirus (KSHV): Role of IFI16 in Maintenance of KSHV Latency. *J Virol*. 2016;90(19):8822-8841. doi:10.1128/JVI.01003-16

313. Verma SC, Borah S, Robertson ES. Latency-associated nuclear antigen of Kaposi's sarcoma-associated herpesvirus up-regulates transcription of human telomerase reverse transcriptase promoter through interaction with transcription factor Sp1. *J Virol*. 2004;78(19):10348-10359. doi:10.1128/JVI.78.19.10348-10359.2004

314. UPHOFF CC, DREXLER HG. Comparative Pcr Analysis for Detection of Mycoplasma Infections in Continuous Cell Lines. *Vitr Cell Dev Biol - Anim*. 2002;38(2):79. doi:10.1290/1071-2690(2002)038<0079:cpafdo>2.0.co;2

315. Stürzl M, Gaus D, Dirks WG, Ganem D, Jochmann R. Kaposi's sarcoma-derived cell line SLK is not of endothelial origin, but is a contaminant from a known renal carcinoma cell line. *Int J cancer*. 2013;132(8):1954-1958. doi:10.1002/ijc.27849

316. Ahn K, Pan S, Beningo K, Hupe D. A permanent human cell line (EA.hy926) preserves the characteristics of endothelin converting enzyme from primary human umbilical vein endothelial cells. *Life Sci*. 1995;56(26):2331-2341. doi:10.1016/0024-3205(95)00227-w

317. Klein G, Lindahl T, Jondal M, et al. Continuous Lymphoid Cell Lines with Characteristics of B Cells (Bone-Marrow-Derived), Lacking the Epstein-Barr Virus Genome and Derived from Three Human Lymphomas. *Proc Natl Acad Sci*. 1974;71(8):3283 LP - 3286. doi:10.1073/pnas.71.8.3283

318. Ponten J, Saksela E. Two established in vitro cell lines from human mesenchymal tumours. *Int J Cancer*. 1967;2(5):434-447. doi:10.1002/ijc.2910020505

319. Baena-Del Valle JA, Zheng Q, Esopi DM, et al. MYC drives overexpression of telomerase RNA (hTR/TERC) in prostate cancer. *J Pathol*. 2018;244(1):11-24. doi:10.1002/path.4980

320. Pfeifer M, Brem R, Lippert TP, et al. SSB1/SSB2 Proteins Safeguard B Cell Development by Protecting the Genomes of B Cell Precursors. *J Immunol*. 2019;202(12):3423-3433. doi:10.4049/jimmunol.1801618

321. Déjardin J, Kingston RE. Purification of Proteins Associated with Specific Genomic Loci. *Cell*. 2009;136(1):175-186. doi:10.1016/j.cell.2008.11.045

322. Schindelin J, Arganda-Carreras I, Frise E, et al. Fiji: An open-source platform for biological-image analysis. *Nat Methods*. 2012;9(7):676-682. doi:10.1038/nmeth.2019

323. Carpenter AE, Jones TR, Lamprecht MR, et al. CellProfiler: image analysis software for identifying and quantifying cell phenotypes. *Genome Biol*. 2006;7(10):R100. doi:10.1186/gb-2006-7-10-r100

324. Otsu N. A Threshold Selection Method from Gray-Level Histograms. *IEEE Trans Syst Man Cybern*. 1979;9(1):62-66. doi:10.1109/TSMC.1979.4310076

325. Edelstein A, Amodaj N, Hoover K, Vale R, Stuurman N. Computer control of microscopes using manager. *Curr Protoc Mol Biol*. 2010;(SUPPL. 92). doi:10.1002/0471142727.mb1420s92

326. Myoung J, Ganem D. iSLK cell. *J Virol Methods*. 2011;174(1-2):12-21.

doi:10.1016/j.jviromet.2011.03.012

327. Vieira J, O'Hearn PM. Use of the red fluorescent protein as a marker of Kaposi's sarcoma-associated herpesvirus lytic gene expression. *Virology*. 2004;325(2):225-240. doi:https://doi.org/10.1016/j.virol.2004.03.049
328. Eng, Jimmy K., Ashley L. McCormack and JRY. An Approach to correlate Tandem Mass Spectral Data of Peptides with Amino Acid Sequences in a Protien Database. *J Am Soc Mass Spectrom*. 1994;5(11):976-989. https://link.springer.com/content/pdf/10.1016%2F1044-0305%2894%2980016-2.pdf%0Ahttps://link.springer.com/content/pdf/10.1016/1044-0305%2894%2980016-2.pdf.
329. Conomos D, Stutz MD, Hills M, et al. Variant repeats are interspersed throughout the telomeres and recruit nuclear receptors in ALT cells. *J Cell Biol*. 2012;199(6):893-906. doi:10.1083/jcb.201207189
330. Lanna A, Coutavas E, Levati L, et al. IFN-α Inhibits Telomerase in Human CD8 + T Cells by Both hTERT Downregulation and Induction of p38 MAPK Signaling . *J Immunol*. 2013;191(7):3744-3752. doi:10.4049/jimmunol.1301409
331. Kenoki Ohuchida, Kazuhiro Mizumoto, Yasuhiro Ogura, et al. Quantitative Assessment of Telomerase Activity and Human Telomerase Reverse Transcriptase Messenger RNA Levels in Pancreatic Juice Samples for the Diagnosis of Pancreatic Cancer. *Clin Cancer Res*. 2005;11:2285-2292.
332. Livak KJ, Schmittgen TD. Analysis of relative gene expression data using real-time quantitative PCR and the 2-ΔΔCT method. *Methods*. 2001;25(4):402-408. doi:10.1006/meth.2001.1262
333. Mender I, Shay JW. Telomerase Repeated Amplification Protocol (TRAP). *Bio-protocol*. 2015;5(22):e1657. https://www.ncbi.nlm.nih.gov/pubmed/27182535.
334. Whittington NC, Wray S. Suppression of Red Blood Cell Autofluorescence for Immunocytochemistry on Fixed Embryonic Mouse Tissue. *Curr Protoc Neurosci*. 2017;81:2.28.1-2.28.12. doi:10.1002/cpns.35
335. Coutts F, Palmos AB, Duarte RRR, et al. The polygenic nature of telomere length and the anti-ageing properties of lithium. *Neuropsychopharmacology*. 2019;44(4):757-765. doi:10.1038/s41386-018-0289-0
336. Patel S, Xiao P. Primary Effusion Lymphoma. *Arch Pathol Lab Med*. 2013;137(8):1152-1154. doi:10.5858/arpa.2012-0294-RS
337. Deng Z, Kim ET, Vladimirova O, et al. HSV-1 Remodels Host Telomeres to Facilitate Viral Replication. *Cell Rep*. 2014;9(6):2263-2278. doi:10.1016/j.celrep.2014.11.019
338. Chu H-P, Cifuentes-Rojas C, Kesner B, et al. TERRA RNA Antagonizes ATRX and Protects Telomeres. *Cell*. 2017;170(1):86-101.e16. doi:10.1016/j.cell.2017.06.017

339. Schoeftner S, Blasco MA. Developmentally regulated transcription of mammalian telomeres by DNA-dependent RNA polymerase II. *Nat Cell Biol*. 2007;10:228. https://doi.org/10.1038/ncb1685.

340. Redon S, Reichenbach P, Lingner J. The non-coding RNA TERRA is a natural ligand and direct inhibitor of human telomerase. *Nucleic Acids Res*. 2010;38(17):5797-5806. doi:10.1093/nar/gkq296

341. Kreilmeier T, Mejri D, Hauck M, Kleiter M, Holzmann K. Telomere Transcripts Target Telomerase in Human Cancer Cells. *Genes (Basel)*. 2016;7(8). doi:10.3390/genes7080046

342. Wu W, Togashi Y, Johmura Y, et al. HP1 regulates the localization of FANCJ at sites of DNA double-strand breaks. *Cancer Sci*. 2016;107(10):1406-1415. doi:10.1111/cas.13008

343. Toth Z, Papp B, Brulois K, Choi YJ, Gao S-J, Jung JU. LANA-Mediated Recruitment of Host Polycomb Repressive Complexes onto the KSHV Genome during De Novo Infection. *PLOS Pathog*. 2016;12(9):e1005878. https://doi.org/10.1371/journal.ppat.1005878.

344. Sun R, Liang D, Gao Y, Lan K. Kaposi's sarcoma-associated herpesvirus-encoded LANA interacts with host KAP1 to facilitate establishment of viral latency. *J Virol*. 2014;88(13):7331-7344. doi:10.1128/JVI.00596-14

345. Chodaparambil J V, Barbera AJ, Lu X, Kaye KM, Hansen JC, Luger K. A charged and contoured surface on the nucleosome regulates chromatin compaction. *Nat Struct Mol Biol*. 2007;14(11):1105-1107. doi:10.1038/nsmb1334

346. Kalashnikova AA, Porter-Goff ME, Muthurajan UM, Luger K, Hansen JC. The role of the nucleosome acidic patch in modulating higher order chromatin structure. *J R Soc Interface*. 2013;10(82):20121022. doi:10.1098/rsif.2012.1022

347. Shoaib M, Walter D, Gillespie PJ, et al. Histone H4K20 methylation mediated chromatin compaction threshold ensures genome integrity by limiting DNA replication licensing. *Nat Commun*. 2018;9(1):3704. doi:10.1038/s41467-018-06066-8

348. Burgess RC, Burman B, Kruhlak MJ, Misteli T. Activation of DNA damage response signaling by condensed chromatin. *Cell Rep*. 2014;9(5):1703-1717. doi:10.1016/j.celrep.2014.10.060

349. Toth Z, Brulois K, Lee H-R, et al. Biphasic Euchromatin-to-Heterochromatin Transition on the KSHV Genome Following De Novo Infection. *PLOS Pathog*. 2013;9(12):1-14. doi:10.1371/journal.ppat.1003813

350. Malkova A, Ira G. Break-induced replication: functions and molecular mechanism. *Curr Opin Genet Dev*. 2013;23(3):271-279. doi:10.1016/j.gde.2013.05.007

351. Madireddy A, Purushothaman P, Loosbroock CP, Robertson ES, Schildkraut CL, Verma SC. G-quadruplex-interacting compounds alter latent DNA replication and episomal persistence of KSHV. *Nucleic Acids Res*. 2016;44(8):3675-3694. doi:10.1093/nar/gkw038

352. Lagunoff M, Ganem D. The structure and coding organization of the genomic termini of

Kaposi's sarcoma-associated herpesvirus. *Virology*. 1997;236(1):147-154. doi:10.1006/viro.1997.8713

353. Grant MJ, Loftus MS, Stoja AP, Kedes DH, Smith MM. Superresolution microscopy reveals structural mechanisms driving the nanoarchitecture of a viral chromatin tether. *Proc Natl Acad Sci U S A*. 2018;115(19):4992-4997. doi:10.1073/pnas.1721638115
354. Wong L-Y, Wilson AC. Kaposi's sarcoma-associated herpesvirus latency-associated nuclear antigen induces a strong bend on binding to terminal repeat DNA. *J Virol*. 2005;79(21):13829-13836. doi:10.1128/JVI.79.21.13829-13836.2005
355. Juillard F, De Leon Vazquez E, Tan M, Li S, Kaye KM. Kaposi's Sarcoma-Associated Herpesvirus LANA-Adjacent Regions with Distinct Functions in Episome Segregation or Maintenance. *J Virol*. 2019;93(6). doi:10.1128/JVI.02158-18
356. Kamranvar SA, Masucci MG. The Epstein-Barr virus nuclear antigen-1 promotes telomere dysfunction via induction of oxidative stress. *Leukemia*. 2011;25(6):1017-1025. doi:10.1038/leu.2011.35
357. Kamranvar SA, Chen X, Masucci MG. Telomere dysfunction and activation of alternative lengthening of telomeres in B-lymphocytes infected by Epstein-Barr virus. *Oncogene*. 2013;32(49):5522-5530. doi:10.1038/onc.2013.189